Study on Non-Linear Distortion Compensation Methods for OFDM Based Wireless Communications Systems

by

Pornpawit Boonsrimuang, B.Eng., M.Eng.

Submitted in fulfillment of the requirements
for the Degree of Doctor of Engineering

Supervisor: Professor Hideo Kobayashi

Division of Systems Engineering
Graduate School of Engineering
Mie University
March 2013

三重大学

I declare that this thesis contains no material which has been accepted for a degree or diploma by the University or any other institution, except by way of background information and duly acknowledged in the thesis, and that, to the best of my knowledge and belief, this thesis contains no material previously published or written by another person, except where due acknowledgement is made in the text of the thesis.

Signed: P. Boonsrimuang

Pornpawit Boonsrimuang

Date: March 21, 2013

Signed: P. Boonsrimuang

Pornpawit Boonsrimuang

Date: March 21, 2023

ABSTRACT

The Orthogonal Frequency Division Multiplexing (OFDM) technique has been received a lot of attentions especially in the field of wireless communications because of its efficient usage of frequency bandwidth and robustness to the multi-path fading. From these advantages, the OFDM technique has already been adopted as the standard transmission technique in the wireless LAN systems and the terrestrial digital broadcasting systems including the Digital Audio Broadcasting (DAB) and the Digital Video Broadcasting (DVB). The OFDM technique is also employed as the standard transmission technique in the next generation of mobile communications systems (LTE).

One of the limitations of using OFDM technique is the larger Peak to Averaged Power Ratio (PAPR) of its time domain signal. The larger PAPR signal would cause the severe degradation of bit error rate (BER) performance and the undesirable frequency spectrum re-growth both due to the non-linear distortion occurring in the non-linear amplifier which is usually required at the transmitter in the wireless communications systems. The simple solution to overcome this problem is to operate the non-linear amplifier at the linear region with taking the enough larger input back-off (IBO). However, this approach leads the inefficient usage of non-linear power amplifier, and would lead a serious problem on battery consumption especially for the mobile handheld terminal and portable wireless LAN terminal. In order to maximize the usage of power efficiency, the non-linear amplifier is usually required to operate at the near its saturation region. However this approach will lead to the severe degradation of BER performance and undesirable frequency spectrum re-growth for the larger PAPR signal due to the occurring of inevitably higher non-linear distortion.

Many PAPR reduction techniques for OFDM signal have been proposed to overcome the PAPR problem up to today. These techniques can be categorized into two major methods as the distortion and distortion-less methods. The distortion technique includes the clipping and filtering method. Although this method can improve the PAPR performance relatively, it leads the degradation of BER performance and undesirable spectrum re-growth to the adjacent channel due to the non-linear clipping distortion. The mitigation method of Non-Linear Distortion is required at the receiver side to improve the BER performance. On the other hand, the distortion-less techniques include the coding, tone reservation (TR), tone injection (TI), active constellation extension (ACE), and multiple signal representation techniques such as partial transmit sequence (PTS) and selected mapping (SLM) methods. These techniques can achieve better PAPR performance without degradation of BER performance and undesirable spectrum re-growth. However these methods improve the PAPR performance at the cost of data rate loss, higher computational complexity, larger memory size, and requirement of separate channel for informing the side information to the receiver.

In this degree thesis, the following two types of methods are proposed to solve the above problems.

1) Non-linear distortion compensation method for OFDM signal

2) PAPR reduction methods for OFDM signal with lower computation complexity

As for the first method, this thesis proposes the Improved DAR (IDAR) method, which can mitigate both the clipping noise and inter-modulation noise. In the proposed IDAR method, the characteristics of non-linear amplifiers are required to be known at the receiver for mitigating the inter-modulation noise. This thesis also proposes the estimation method for AM-AM and AM-PM conversions characteristics of non-linear amplifiers by using low PAPR (Peak to Averaged Power Ratio) preamble symbols.

This thesis demonstrates the effectiveness of proposed IDAR method when applying the satellite communication systems. From the computer simulation results, it is concluded that the proposed IDAR method can achieve the higher transmission data rate and higher efficient usage of non-linear power amplifier with keeping the better BER performance even in the non-linear satellite channel.

As for the second method, this thesis proposes PAPR reduction methods based on PTS technique. The conventional PTS method requires the larger number of clusters and weighting factors to achieve the better PAPR performance which leads larger computation complexity. To reduce the computation complexity, DIF-PTS method is proposed which employs the intermediate signals within the IFFT and used radix-2, radix-4, Split-Radix and Extended Split-radix for decimation in the frequency domain (DIF) to obtain the PTS sub-blocks. Multiple IFFTs are then applied to the remaining stages. The PTS sub-blocking is performed in the middle stages of the N-point radix FFT DIF algorithm. The DIF-PTS method can reduce the computational complexity relatively while it shows almost the same PAPR reduction performance as that of the conventional PTS method. To improve the PAPR performance with low computation complexity, this thesis proposes a new weighting factor technique for the PTS method in conjunction with DIF-PTS sub-blocking based on radix-r, Split-Radix and Extended Split-Radix IFFT technique which can improve both the PAPR performance and computation complexity. The proposed method can achieve the better PAPR reduction performance than that for the DIF-PTS method without any increasing of size of side information.

In this thesis, a new PTS method by using the permutation of data sequence in the frequency domain is also proposed to improve the computation complexity. The proposed method employs the dummy and parity subcarriers as the embedded side information in the data subcarriers, which is used for the demodulation of data information at the receiver. The proposed method includes two types of permutation methods Type I and Type II. Type I is to perform the permutation only for the first M/2 subcarriers, while Type II is to perform the

permutation both for the first and the last part of M/2 subcarriers. Although the computation complexity for the Type II is larger than Type I, the improvement of PAPR performance for the Type II is better than Type I. The feature of proposed method is to detect the rotation number performed at the transmitter precisely at the receiver by using the very few dummy subcarriers which corresponds to the embedded side information. The propose method can achieve the higher transmission efficiency because the size of embedded side information in the proposed method is much smaller than that for the side information in the conventional PTS method. From the computer simulation results, this thesis confirmed that the proposed permutation of data sequence method can achieve the better PAPR performance and better BER performance in the non-linear channel with lower computation complexity.

In this thesis, the numerous computer simulations are conducted to confirm the effectiveness of all proposed method. Form the simulation results, it is confirmed that the proposed methods show the better PAPR performance with lower computation complexity. As a conclusion of researches in this thesis, the proposed PAPR reduction methods and mitigation methods of non-linear distortion noise could provide various practical solutions for the next generation of multimedia wireless communications systems employing the OFDM technique.

ACKNOWLEDGEMENTS

I would like to express gratitude to my supervisor Professor Dr. Hideo Kobayashi for his grand supports and magnificent encouragements during the whole time of my study at the Communications Laboratory, Division of Electrical and Electronics Engineering, Graduate School of Engineering, Mie University. His observations and comments helped me to establish the overall direction of the research and to move forward with investigation in depth. I sincerely appreciate his invaluable advises and professional recommendations on the research. The influence of his excellent personality and knowledge helped me to success the research and completed this thesis.

I address my best regards to Professor Dr. Kazuo Mori and Assistant Professor Dr. Katsuhiro Naito for their comments and recommendations during the discussions of the research results. I also would like to thank Mr. Yoshihiro Yamamoto for his permanent readiness to help on any technical problems.

I am greatly indebted to the Suan Sunandha Rajabhat University (SSRU) Scholarship for giving me the immense chance to study at Mie University and grand supports. I would like to thank to Associate Professor Dr. Chuangchote Bhuntuvech, President and Assistance Profressor Dr. Somkiat Korbuakaew Vice President of SSRU for their kindness supports.

I also would like to express gratitude to Professor Dr. Tawil Puangma President and Associate Professor Dr.Pisit Boonsrimuang Vice President of the King Moungkut's Institute of Technology Ladkrabang, Thailand who provided help, support and encouragement in various ways.

I would to express my warmest thanks to all students in the communications laboratory and Thai students at Mie University for their friendship and assistances.

Finally, I greatly appreciate for the constant love, understanding and patience of my family members. Without their moral support it would be impossible to concentrate on the research and completed this thesis.

TABLE OF CONTENTS

LIST OF TABLES

LIST OF FIGURES

LIST OF FIGURES

LIST OF FIGURES

CHAPTER 1

INTRODUCTION

This chapter presents a basic overview of Orthogonal Frequency Division Multiplexing (OFDM) technique, the general structure of an OFDM system and standardized system of using the OFDM technique in the wireless communications systems. Section 1.2 explains FFT and IFFT Algorithm. Section 1.3 explains about definitions of PAPR. Section 1.4 explains the PAPR problems and several solutions for PAPR problems proposed up to today. Section 1.5 explains about the channel models. Section 1.6 is overview of research background and motivate on PAPR problems of OFDM signals. Finally, it describes the organization of thesis contents in Section 1.7.

1.1 Overview of Orthogonal Frequency Division Multiplexing (OFDM)

Multicarrier transmission is known as the Orthogonal Frequency-Division Multiplexing (OFDM) or Discrete Multi-tone (DMT). The basic principle of OFDM is to split a high rate data stream into multiple parallel lower rate data streams, which are block-wise transmitted simultaneously over a number of frequency-spaced subcarriers. As the symbol duration for each of the lower rate subcarriers is increased, the relative dispersion in time caused by multipath delay spread is decreased. The longer symbol duration and the introduction of a guard time for every OFDM symbol can eliminate almost completely inter symbol interference. The cyclic extension of the OFDM symbol into the guard time ensures the minimization of inter-carrier interference. The process of generating an OFDM signal and the reasoning behind each step will be described in the following sections.

1.1.1 OFDM Basics

An OFDM signal consists of a sum of subcarriers that are modulated by using phase shift keying (PSK), Quadrature Amplitude modulation (QAM) and other modulation techniques could also be used. A multicarrier signal is the sum of many independent signals modulated onto sub-channels of equal bandwidth. Let us denote the collection of all data symbols, $X_n, n=0,1,\cdots,N-1$, as a vector $X=[X_0,X_1,\cdots,X_{N-1}]^T$ that will be termed data sub-carriers. The complex baseband representation of a multicarrier signal consisting of N sub-carriers is given by

$$x(t)=\frac{1}{\sqrt{N}}\sum_{n=0}^{N-1}X_n\cdot e^{j2\pi n\Delta ft} \quad ,0\le t<NT \tag{1.1}$$

where $j=\sqrt{-1}$, Δf is the sub-carriers spacing and NT denotes the useful data block period. In OFDM the sub-carriers are chosen to be orthogonal (i.e., $\Delta f=1/NT$). The Nyquist rate sampled OFDM signal is given by

$$x_k=\frac{1}{\sqrt{N}}\sum_{n=0}^{N-1}X_n\cdot e^{j2\pi kn/N} \tag{1.2}$$

The OFDM signal has the inter symbol inference (ISI) when passing the signal thought a time dispersive channel, it also makes that orthogonality of the subcarrier is lost, resulting inter carrier interference (ICI). The cyclic prefix (CP) or guard interval (GI) is used to overcome these problems. A cyclic prefix is a copy of the last part of OFDM symbols that is

shown in figure 1. The CP is removed at the receiver before the demodulation. The cyclic prefix should be at least as long as the significant part of the impulse response experienced by the transmitted signal. The cyclic prefix has the two benefits. First, it avoids ISI because it acts as a guard space between successive symbols. Second, it also converts the linear convolution with the channel impulse response into a cyclic convolution. As a cyclic convolution in the time domain translated into a scalar multiplication in the frequency domain, the sub-carriers remain orthogonal and there is no ICI. The length of the cyclic prefix should be made longer than the experienced impulse to avoid ISI and ICI. However, the transmitted energy increases with the length of the cyclic prefix. There is loss power due to the insertion of the CP.

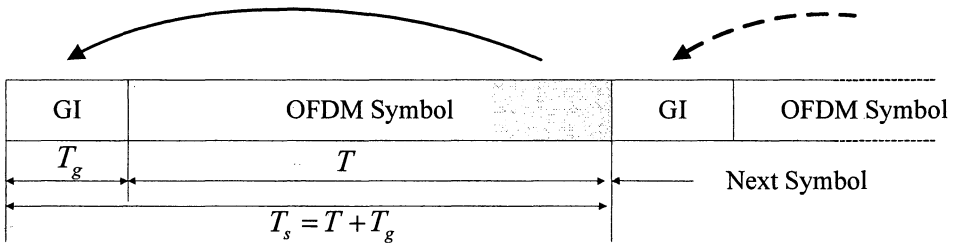

Fig. 1.1. OFDM symbol in the time domain.

The sharp phase transition at the symbol boundaries cause the out-of-band spectrum re-grown. To reduce the spectrum re-grown, the windowing is applied to individual OFDM symbols. Windowing essentially smooth the phase transition between OFDM symbols. A commonly used window type is the raised cosine window, which is shown in figure 1.2.

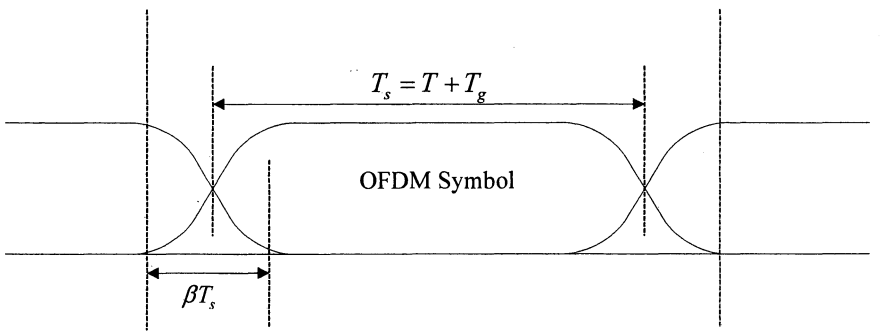

Fig. 1.2. Raised cosine window for OFDM symbol.

The OFDM signal is multiplied by raised cosine window to where to reduce the power of out-of-band frequencies. The OFDM symbol is added to the output of the previous OFDM symbol with a delay of T_s, such that there is an overlap of βT_s, β is the roll-off factor of the raised cosine window. As orthogonallity between sub-carriers require that amplitude and phase of the sub-carriers stay constant during the FFT integration interval of length T, the

roll-off region of the window thus decrease the effective guard time by βT_s. Therefore, there is a tradeoff between having a large roll-off factor, which will suppress the out-of-band spectrum and a decreased delay spread tolerance.

Summary of conventional OFDM transmitter as shown in figure 1.3(a), the modulated signal is passing to serial-to-parallel (S/P) before input to *IFFT* processing and passed parallel-to-serial (P/S). The time domain sampled OFDM signal after adding the guard interval (GI) to will be converted to the analogue signal by the digital-analogue converter (D/A) with the analogue band pass filter (BPF) and then converted to the radio frequency (RF) by the frequency up-converter (U/C) as shown in figure 1.3(a). Here the analogue filter is used to reject the aliasing and spectrum re-grown occurring at the output of D/A converter. The output signal of U/C is inputted to the non-linear amplifier and transmitted to the channel as shown in figure 1.3(a).

For the receiver path, the receiver receives the received signal $r(t)$. The received signal performs the inverse operations. The received RF signal is first down converted (D/C) to the base band signal and digitized by A/D converter. The receiver then applies a *FFT* after removes the guard interval (GI). Finally, the original data can get from demodulation as shown in figure 1.3(b).

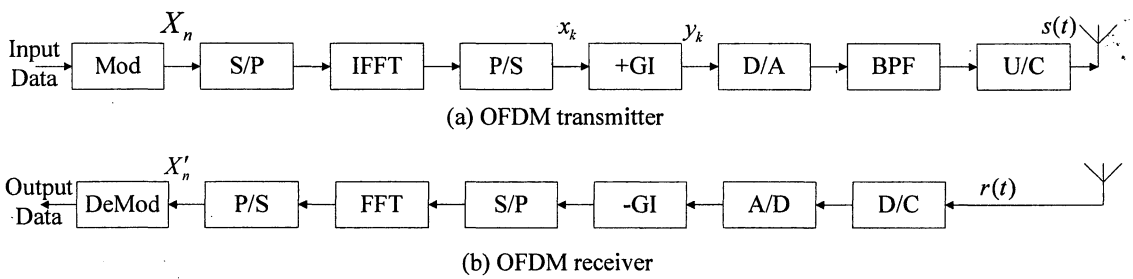

Fig. 1.3. Structure of conventional OFDM transceiver.

1.1.2 OFDM Standards

OFDM is used as the transmission technique in digital audio and television broadcasting applications, and in wireless LAN applications. This section describes the main applications of OFDM in the wireless communications systems.

(A) Digital Audio Broadcasting (DAB)

Digital audio broadcasting (DAB) was specified between 1988 and 1992, with its introduction in Europe scheduled for the late 1990s. Many DAB field trials were carried out by broadcasters in Europe, including DAB single frequency operations in Munich, Germany,

DAB test operation in trials in L-band, and so on. In addition to these, a lot of DAB measurements were also carried out, on electromagnetic field strength, channel rate, and so on. Table 1.1 shows the three modes defined in EUREKA 147 DAB.

(B) Terrestrial Digital Video Broadcasting

In Europe, based on the successful results from DAB field trials and measurements, terrestrial digital video broadcasting (DVB-T), with use of OFDM, was standardized by the European Telecommunication Standards Institute (ETSI) in 1996. Table 1.2 shows the two modes defined in the DVB-T. In 1998, the DVB-T was first adopted in the United Kingdom, with multi-frequency network (MFN) use, 2k mode, 64QAM, 7μsec guard interval $R_c = 2/3$ convolutional code and 24.13 Mbps information transmission rate.

(C) Wireless LAN Standards

In 1998, the IEEE 802.11 standardization group decided to select OFDM as a basic for its new 5GHz wireless LAN standard, which supports data transmission rate from 6 to 56 Mbps. In the DVB-T, OFDM is used in continuous transmission mode for the purpose of broadcasting. This new standard, called "IEEE 802.11a," is the first to use OFDM in packet transmission mode.

Following the IEEE 802.11 decision, ETSI adopted OFDM in the standard of HIPERLAN/2, as well as ARIB in the standard of MMAC. Since then, the three bodies have worked in close cooperating to ensure that differences between the three standards are kept to a minimum, enabling the manufacturing of equipment that can be used worldwide.

The main differences between IEEE 802.11a and HIPERLAN type 2 are in the medium access control (MAC). The IEEE 802.11a uses distributed MAC based on carrier sense multiple access with collision avoidance (CSMA/CA), whereas the HIPERLAN type 2 uses a centralized and scheduled MAC based on time division multiple access with dynamic slot assignment (TDMA/DSA). The MMAC support both of these MACs. In terms of the physical layer (PHY), there are only a few minor differences among the three standards. Table 1.3 shows the system parameter for the IEEE 802.11a, HIPERLAN type 2 and the MMAC.

Table 1.1 DAB parameters.

Parameter Mode	Mode I	Mode II	Mode III
Bandwidth	1.536 MHz	1.536 MHz	1.536 MHz
Number of sub-carriers	1,546	768	384
Modulation	DQPSK		
Useful symbol length (t_s)	1 msec	250 μsec	125 μsec
Sub-carriers separation (Δf)	3.968 kHz	1.984 kHz	0.992 kHz
Guard interval length (ΔG)	$t_s/4$ (250 μsec)	$t_s/4$ (62.5 μsec)	$t_s/4$ (31.25 μsec)
FEC	Convolution code		
Information transmission rate	2.4 Mbps		

Table 1.2 DVB-T parameters.

Parameter Mode	2k				8k			
Bandwidth	7.61 MHz				7.61 MHz			
Number of sub-carriers	1,705				6,817			
Modulation	QPSK 16QAM 64QAM							
Useful symbol length (t_s)	224 μsec				896 μsec			
Sub-carriers separation (Δf)	4.464 kHz				1.116 kHz			
Guard interval length (ΔG)	$t_s/4$ 56 μsec	$t_s/8$ 28 μsec	$t_s/16$ 14 μsec	$t_s/32$ 7 μsec	$t_s/4$ 224 μsec	$t_s/8$ 112 μsec	$t_s/16$ 56 μsec	$t_s/32$ 28 μsec
FEC (inner code)	Convolution code (R=1/2, 2/3, 3/4, 5/6, 7/8)							
FEC (Outer code)	Reed-Solomon code (204, 188)							
Interleaving	Time-frequency domain bit interleaving							
Information transmission rate	4.98 – 31.67 Mbps							
Required C/N	3.1dB – 20.1 dB							

Table 1.3 IEEE 802.11a, HIPERLAN/2 and MMAC.

Standard	IEEE 802.11a	HIPERLAN/2
Channel spacing	20 MHz	
Bandwidth	16.56 MHz (-3dB)	
Number of sub-carriers	52	
Number of pilot sub-carriers	4	
Useful symbol length (t_s)	3.2 μsec	
Sub-carriers separation (Δf)	312.5 kHz	
Guard interval length (ΔG)	800 nsec	
FEC	Convolution code	
Interleaving	Frequency domain bit interleaving (Within on OFDM symbol)	
Information transmission rate	6 Mbps (BPSK, $R_c = 1/2$)	
Modulation/coding rate	9 Mbps (BPSK, $R_c = 3/4$) 12 Mbps (QPSK, $R_c = 1/2$) 18 Mbps (QPSK, $R_c = 3/4$) 24 Mbps (16QAM, $R_c = 1/2$) 36 Mbps (16QAM, $R_c = 3/4$) 48 Mbps (64QAM, $R_c = 1/2$) 54 Mbps (64QAM, $R_c = 3/4$)	
Multiple access method	CSMA/CA	TDMA/DSA

1.2 Fast Fourier Transform (FFT) Algorithm

1.2.1 Radix-2 DIT-FFT Algorithm

This algorithm is based on decomposing an N-point sequence (assuming $N=2^l$, l = integer) into two N=-2point sequences (one of even samples and another of odd samples) and obtaining the N-point DFT in terms of the DFTs of these two sequences. This operation by itself results in some savings of the arithmetic operations. Further savings can be achieved by decomposing each of the two N=-2point sequences into two N=-4point sequences (one of even samples and another of odd samples) and obtaining the N=-2point DFTs in terms of the corresponding two N=-4point DFTs. This process is repeated till two-point sequences are obtained.

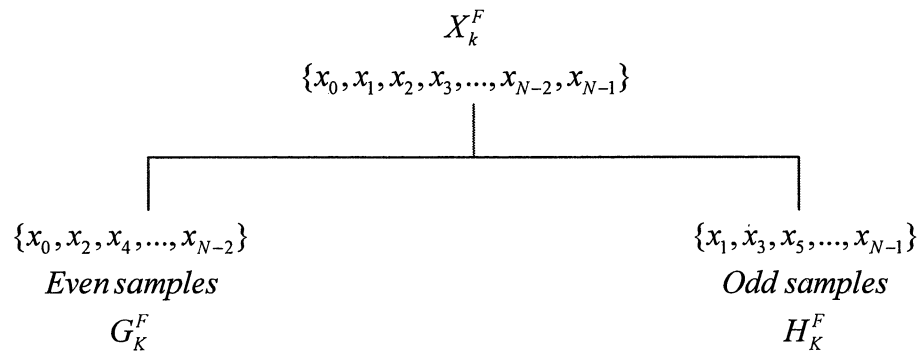

(1.3)

Length N DFT

$$X^F(k) = \sum_{n=0}^{N-1} x(n) W_N^{nk}, \quad k = 0,1,..,N-1$$
$$= \sum_{r=0}^{(N/2)-1} x(2r) W_N^{2rk} + \sum_{r=0}^{(N/2)-1} x(2r+1) W_N^{(2r+1)k}$$
$$= \sum_{r=0}^{(N/2)-1} x(2r)(W_N^2)^{rk} + W_N^k \sum_{r=0}^{(N/2)-1} x(2r+1)(W_N^2)^{rk} \tag{1.4}$$

Note that

$$W_N^2 = \exp\left[\frac{-j2(2\pi)}{N}\right] = \exp\left(\frac{-j2\pi}{N/2}\right) = W_{N/2} \tag{1.5}$$

$$X^F(k) = \sum_{r=0}^{(N/2)-1} x(2r) W_{N/2}^{rk} + W_N^k \sum_{r=0}^{(N/2)-1} x(2r+1) W_{N/2}^{rk}$$
$$= G^F(k) + W_N^k H^F(k), \quad k = 0,1,\ldots,\tfrac{N}{2}-1 \tag{1.6}$$

Here $X^F(k)$ the N-point DFT of $x(n)$ is expressed in terms of $N/2$-point DFTs, $G^F(k)$ and $H^F(k)$ which are DFTs of even samples and odd samples of $x(n)$ respectively.

$X^F(k)$: periodic with period $N, X^F(k) = X^F(k+N)$.

$G^F(k), H^F(k)$: periodic with period $\frac{N}{2}, G^F(k) = G^F(k+\frac{N}{2})$ and $H^F(k) = H^F(k+\frac{N}{2})$

$$X^F(k) = G^F(k) + W_N^k H^F(k), \quad k = 0,1,...,\tfrac{N}{2}-1 \tag{1.7}$$
$$X^F(k+N/2) = G^F(k) + W_N^{k+N/2} H^F(k)$$
$$W_N^{N/2} = \exp\left(\frac{-j2\pi}{N}\frac{N}{2}\right) = \exp(-j\pi) = -1$$

Since $W_N^{k+N/2} = \exp\left[\frac{-j2\pi}{N}\left(k+\frac{N}{2}\right)\right] = W_N^k W_N^{N/2} = -W_N^k$, it follows that

$$X^F(k+\tfrac{N}{2}) = G^F(k) - W_N^k H^F(k), \quad k = 0,1,...,\tfrac{N}{2}-1 \tag{1.8}$$

Equation (1.7(and (1.8) are shown below as a butterfly (Figure.1 .4)

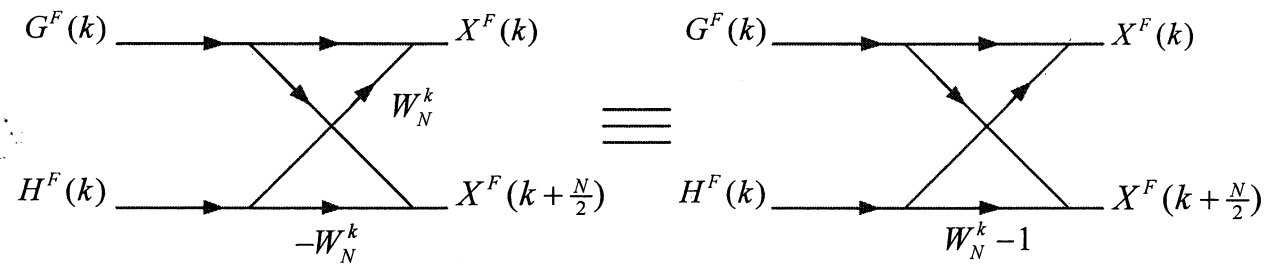

Fig. 1.4. Butterfly to compute Eq. 1.7 and Eq. 1.8.

For each k in Figure 11.4(a) requires two multiplies and two adds whereas Figure 1.4(b) requires one multiply and two adds. Repeat these processes iteratively till two-point DFTs are obtained, i.e., $G^F(k)$ the $N/2$-point DFT of $\{x_0, x_2, x_4, ..., x_{N-2}\}$ can be implemented using two $N/4$-point DFT. Similarly for $H^F(k)$

$G^F(k)$ and $H^F(k)$ require $(N/2)^2$ complex addition and $(N/2)^2$ complex multiplies. $X^F(k)$ N-point DFT requires N^2 complex addition and multiplies.

Let $N = 16$ Direct computation of a 16-point DFT requires $N^2 = 256$ adds and multiplies. Through $G^F(k)$ and $H^F(k)$, it requires only $128+16=144$ adds and multiplies, resulting in saving of 112 adds and multiplies. Additional savings can be achieved by decomposing the eight-point DFTs into two four-point DFTs and finally into four two-point DFTs. $G^F(k)$ and $H^F(k)$ are eight-point DFT Each requires 64 adds and multiplies. The algorithm based on this technique is called radix- 2DIT-FFT.

1.2.2 Radix-2 DIF-FFT Algorithm

Similar to radix-2 DIT-FFT radix-2 DIF-FFT can be developed as follows:

$$X^F(k)=\sum_{n=0}^{N-1}x(n)W_N^{nk},\ k=0,1,...,N-1 \tag{1.9}$$

here N is an integer power of two.

$$X^F(k)=\sum_{n=0}^{(N/2)-1}x(n)W_N^{nk}+\sum_{n=N/2}^{N-1}x(n)W_N^{nk}=I+II \tag{1.10}$$

Equation (1.10) summation changes to (let $n=m+N/2$)

$$\sum_{m=0}^{(N/2)-1}x(m+\frac{N}{2})W_N^{(m+N/2)k}=\sum_{m=0}^{(N/2)-1}x(n+\frac{N}{2})W_N^{(N/2)k}W_N^{nk} \tag{1.11}$$

Hence (1.11) becomes

$$X^F(k)=\sum_{n=0}^{(N/2)-1}x(n)W_N^{nk}+W_N^{(N/2)k}\sum_{n=0}^{(N/2)-1}x(n+\frac{N}{2})W_N^{nk} \tag{1.12}$$

$$X^F(k)=\sum_{n=0}^{(N/2)-1}\left[x(n)+(-1)^k x(n+\frac{N}{2})\right]W_N^{nk} \tag{1.13}$$

Since $W_N^{N/2}=-1$, for k even integer$=2r$ and for k odd integer$=2r+1$ (1.14) reduces to

$$X^F(2r)=\sum_{n=0}^{(N/2)-1}\left[x(n)+x(n+\frac{N}{2})\right]W_N^{2nr} \tag{1.14}$$

$$X^F(2r+1)=\sum_{n=0}^{(N/2)-1}\left[x(n)-x(n+\frac{N}{2})\right]W_N^{n}W_N^{2nr} \tag{1.15}$$

Since $W_N^{2nr}=\exp\left(\frac{-j2\pi 2nr}{N}\right)=\exp\left(\frac{-j2\pi nr}{N/2}\right)=W_{N/2}^{nr}$

$$X^F(2r)=\sum_{n=0}^{(N/2)-1}\left[x(n)+x(n+\frac{N}{2})\right]W_{N/2}^{nr} \tag{1.16}$$

and $X^F(2r)$ is $N/2-$point DFT

$$\left[x(n)+x(n+\frac{N}{2})\right]\ \text{By}\ r,n=0,1,...,\tfrac{N}{2}-1 \tag{1.17}$$

Similarly $X^F(2r+1)$ is $N/2-$point DFT of

$$\left[x(n)-x(n+\frac{N}{2})\right]W_N^n\ \text{when}\ \ r,n=0,1,...,\tfrac{N}{2}-1 \tag{1.18}$$

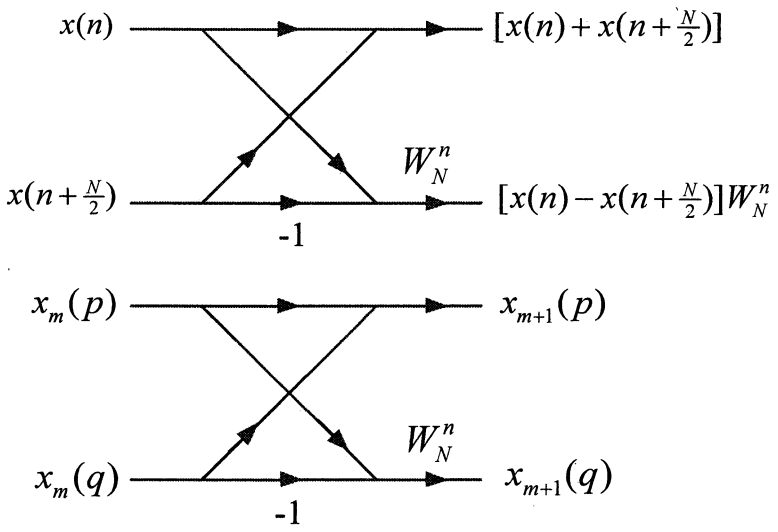

Fig. 1.5. Butterfly to compute Eq.1.18 and Eq.1.19 for $n = 0,1,...,\frac{N}{2}-1$ [40].

From Figure 1.8 $N-$point DFT can be executed from the two $N/2-$point DFTs as described in (1.18) and (1.19). This results in reduction of computational complexity as in the case of DIT-FFT algorithm. Further savings can be achieved by successively repeating this decomposition (i.e. first half of the samples and second half of the samples). The DIF-FFT algorithm is illustrated for N = 8.

For DIF-FFT $N=8$

DFT

$$X^F(k)=\sum_{n=0}^{7}x(n)W_8^{nk}, \qquad k=0,1,...,7 \tag{1.19}$$

IDFT

$$x(n)=\frac{1}{8}\sum_{n=0}^{7}X^F(k)W_8^{-kn}, \qquad n=0,1,...,7 \tag{1.20}$$

For $N=8$, becomes

$$X^F(2r)=\sum_{n=0}^{3}\left[x(n)+x(n+\frac{N}{2})\right]W_4^{nr}, \quad r=0,1,2,3 \tag{1.21}$$

$$X^F(2r+1)=\sum_{n=0}^{3}\left[x(n)-x(n+\frac{N}{2})\right]W_8^{n}W_4^{2nr}, \quad r=0,1,2,3 \tag{1.22}$$

Equation (1.20) and (1.21) can be explicitly described as follows:

When $X^F(2r), \ r=0,1,2,3$ is a four-point DFT

$$\{x(0)+x(4),x(1)+x(5),x(2)+x(6),x(3)+x(7)\}.$$
$$X^F(0)=[x(0)+x(4)]+[x(1)+x(5)]+[x(2)+x(6)]+[x(3)+x(7)]$$
$$X^F(2)=[x(0)+x(4)]+[x(1)+x(5)]W_4^1+[x(2)+x(6)]W_4^2+[x(3)+x(7)]W_4^3$$
$$X^F(4)=[x(0)+x(4)]+[x(1)+x(5)]W_4^2+[x(2)+x(6)]W_4^4+[x(3)+x(7)]W_4^6$$
$$X^F(6)=[x(0)+x(4)]+[x(1)+x(5)]W_4^3+[x(2)+x(6)]W_4^6+[x(3)+x(7)]W_4^9 \quad (1.23)$$

And when $X^F(2r+1), r=0,1,2,3$ is a four-point DFT of

$$\{x(0)-x(4),[x(1)-x(5)]W_8^1,[x(2)-x(6)]W_8^2,[x(3)+x(7)]W_8^3\}.$$
$$X^F(1)=(x(0)-x(4))+(x(1)-x(5))W_8^1+(x(2)-x(6))W_8^2$$
$$+[(x(3)-x(7))W_8^3]W_4^2$$
$$X^F(3)=(x(0)-x(4))+[(x(1)-x(5))W_8^1]W_4^1+[(x(2)-x(6))W_8^2]W_4^2$$
$$+[(x(3)-x(7))W_8^3]W_4^3$$
$$X^F(5)=(x(0)-x(4))+[(x(1)-x(5))W_8^1]W_4^2+[(x(2)-x(6))W_8^2]W_4^4$$
$$+[(x(3)-x(7))W_8^3]W_4^6$$
$$X^F(7)=(x(0)-x(4))+[(x(1)-x(5))W_8^1]W_4^3+[(x(2)-x(6))W_8^2]W_4^6$$
$$+[(x(3)-x(7))W_8^3]W_4^9 \quad (1.24)$$

Each of the four-point DFTs it can be implemented by using two-point DFTs. Hence the eight-point DIF-FFT is obtained in three stages i.e., Figure 1.6

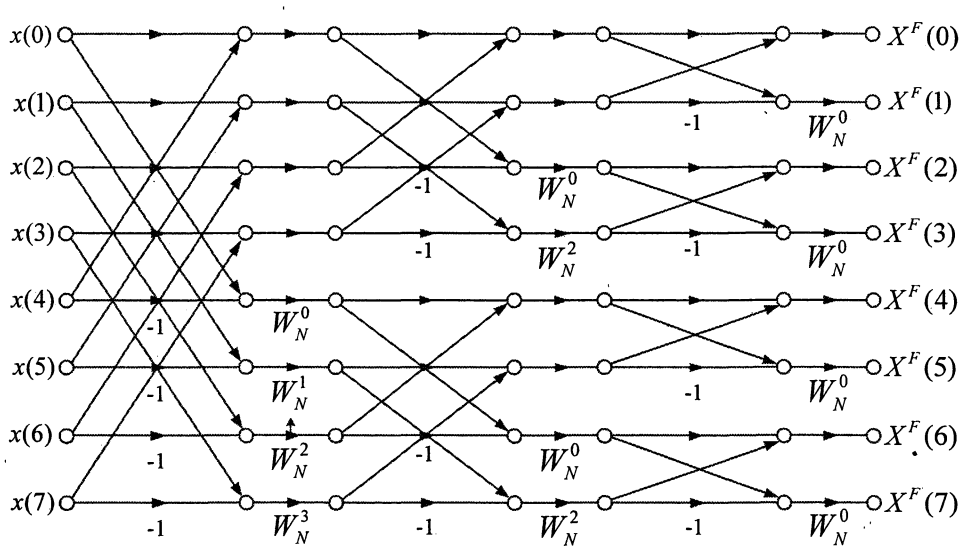

Fig. 1.6. Butterfly to compute Fast Fourier transform Radix-2 , 8 Points $(W_N=W_8)$ [40].

1.3 Peak-to-Average Power Ratio (PAPR) of OFDM signal

OFDM signal is the result of adding up a number of independently modulated subcarriers, it can have a very large instantaneous power compared to the average power of the signal.

1.3.1 Over Sampling

The zero padding is usually required in the actual hardware of OFDM system to avoid the aliasing occurring at the output of D/A converter. The meaning of aliasing occurring at the output of D/A converter is that the same OFDM signal will be appeared repeatedly at the outside of allocated frequency bandwidth as shown in the following figure 1.7. The analogue filter located after D/A converter is usually used to reject these aliasing as shown in figure 1.7. From figure 1.7, it can be seen that the required number of zero padding is dependent on the achievable sharpness of employed analogue filter. If the number of zero padding is larger, it is possible to use the simple and dull analogue filter, which can be realized easily, to reject the aliasing occurred at the output of D/A converter although the number of *IFFT* points becomes larger.

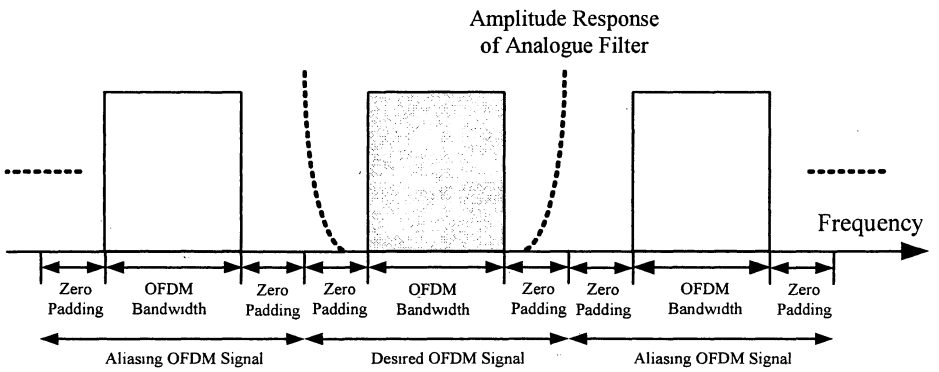

Fig. 1.7. OFDM Signal at Output of D/A Converter.

However, the time domain analogue signal at the output of analogue filter always has the same signal waveform if the over sampling ratio for the time domain signal is higher than the Nyquist sampling ratio. Here the Nyquist sampling ratio means that the number of *IFFT* points is equal to the number of sub-carriers (over sampling ratio is 1) which corresponds to no usage of zero padding. In other words, the time domain analogue signal in the practical OFDM system always has the same signal waveform with regardless of the number of zero padding if the over sampling ratio is higher than the Nyquist sampling ratio, which is obvious from the Nyquist sampling theory. Here, it should be noted that if assuming the Nyquist sampling ratio with no zero padding, the analogue filter must be realized by the ideal brick wall type filter to reject the aliasing perfectly. However it is impossible to realize such ideal

analogue filter in practical. This is the reason that the zero padding is required in the actual hardware of OFDM system.

The ratio for the number of *IFFT* points to the sub-carriers is usually taken by 1.2 to 1.5 in the actual OFDM system. This means that the number of zero padding is 10 to 22 when the number of sub-carriers is 64. As an example, the radio LAN system standardized by IEEE802.11a employs the OFDM signal in which the number of *IFFT* points is 64 and the number of sub-carriers is 48. This means that the ratio is 1.3 and the number of zero padding is 16.

However any PAPR reduction method on the basis of digital processing technique including our proposed method is required to evaluate the PAPR performance by using the sampled time domain signal. When using the sampled time domain signal, the accuracy of evaluated PAPR performance will depend on the number of zero padding which corresponds to the over sampling ratio of OFDM signal. This is from that the maximum amplitude level in the sampled time domain OFDM signal would be varied when changing the over sampling ratio. Figure 1.8 shows the relationships between the sampled time domain signal of the Nyquist sampling ratio and its composite signal, which corresponds to the analogue signal including all impulse responses. From the figure, it is cleared that the amplitude of composite signal (analogue signal) has a possibility to become larger than the level obtained at the Nyquist sampling points.

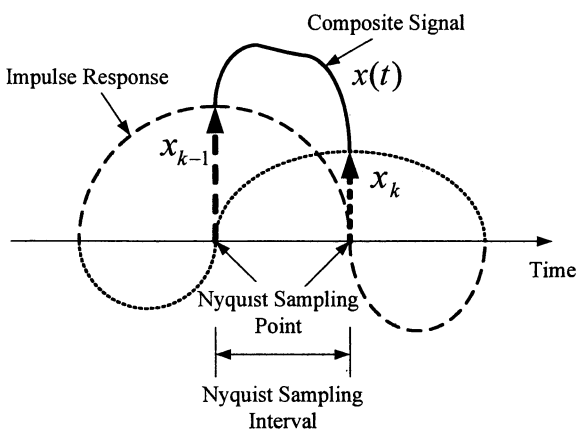

Fig. 1.8. Relationships between sampled time domain and analogue signals.

From the above fact, the following relations between the sampled and analogue time domain signals are always satisfied.

$$\max_{k=0-N-1}\left[\left|x_k\right|\right] \le \max_{0\le t\le T}\left[\left|x(t)\right|\right] \tag{1.22}$$

where N is the number of samples in one OFDM symbol, T is the time duration of OFDM symbol, x_k and $x(t)$ represent the sampled time domain and analogue signals, respectively.

Since the following relations on the averaged signal power for the sampled and analogue time domain signals is satisfied,

$$E\left[|x_k|^2\right] = E\left[|x(t)|^2\right] \tag{1.23}$$

The relationship of PAPR performance between them is given by,

$$PAPR(sampled) \leq PAPR(analogue) \tag{1.24}$$

where $E[\ ]$ represents the averaged signal power and the PAPR for the sampled signal and analogue signal are expressed by the following equations, respectively.

$$PAPR(sampled) = 10\log\left(\frac{\max\limits_{k=0\sim N-1}|x_k|^2}{E\left[|x_k|^2\right]}\right) \tag{1.25}$$

$$PAPR(analogue) = 10\log\left(\frac{\max\limits_{0\leq t\leq T}|x(t)|^2}{E\left[|x(t)|^2\right]}\right) \tag{1.26}$$

where x_k and $x(t)$ represent the sampled time domain and analogue signals, respectively.

Since the following relations on the averaged signal power for the sampled and analogue time domain signals is satisfied.

1.3.2 Mathematical Definition of PAPR

The mathematically the Peak-to-Average Power Ratio (PAPR) of the transmitted signal can be defined as following equation.

$$PAPR = \frac{\max\limits_{0\leq t<NT}|x(t)|^2}{1/NT\int_0^{NT}|x(t)|^2\,dt} \tag{1.27}$$

where $x(t)$ is time domain OFDM signal. In the remaining part of this thesis, an approximation will be made in that only NL equidistant samples of $x(t)$ will be considered where L is an integer that is larger than or equal to 1. These "L-times oversampled" time-domain signal samples are represented as a vector $x = [x_0, x_1, \ldots x_{NL-1}]^T$ and obtained as,

$$x_k = x(kT/L) = \frac{1}{\sqrt{N}}\sum_{n=0}^{N-1} X_n \cdot e^{j2\pi n\Delta fT/L} \quad ,k = 0,1,\ldots,NL-1 \tag{1.28}$$

It can be seen that the sequence $\{x_k\}$ can be interpreted as the inverse discrete Fourier transform (IDFT) of data block X with $(L-1)N$ zero padding. It is well known that the

PAPR of the continuous-time signal cannot be obtained precisely by the use of Nyquist rate sampling, which corresponds to the case of $L = 1$. The $L = 4$ can provide sufficiently accurate PAPR results. The PAPR computed from the L times oversampled time domain signal samples is given by,

$$PAPR = \frac{\max_{0 \le k < NL-1} |x_k|^2}{E\left[|x_k|^2\right]} \tag{1.29}$$

where $E[\ ]$ denotes average OFDM signal.

1.3.3 Distribution of PAPR

The cumulative distribution function (CDF) of the PAPR is one of the most frequently used performance measures for PAPR reduction techniques. The complementary CDF (CCDF) is commonly used instead of the CDF itself. The CCDF of the PAPR denotes the probability that the PAPR of a data block exceeds a given threshold. A simple approximate expression is derived for the CCDF of the PAPR of a multicarrier signal with Nyquist rate sampling. From the central limit theorem, the real and imaginary parts of the time domain signal samples follow Gaussian distributions, each with a mean of zero and a variance of 0.5 for a multicarrier signal with a large number of subcarriers. Hence, the amplitude of a multicarrier signal has a Rayleigh distribution, while the power distribution becomes a central chi-square distribution with two degrees of freedom. The CDF of the amplitude of a signal sample is given by,

$$F(PAPR_0) = 1 - e^{PAPR_0} \tag{1.30}$$

The CCDF of the PAPR of a data block with Nyquist rate sampling is derived as

$$\begin{aligned} P(PAPR > PAPR_0) &= 1 - P(PAPR \le PAPR_0) \\ &= 1 - F(PAPR_0)^N \\ &= 1 - (1 - e^{(-PAPR_0)})^N \end{aligned} \tag{1.31}$$

This expression assumes that the N time domain signal samples are mutually independent and uncorrelated. This is not true, however, when oversampling is applied. Also, this expression is not accurate for a small number of subcarriers since a Gaussian assumption does not hold in this case. Therefore, there have been many attempts to derive more accurate distribution of PAPR. Refer to [50–52] for more results on this topic. Figure 1.9 shows the example calculation results of PAPR performance for the conventional OFDM when changing the over sampling ratio. From the figure, it can be observed that the Nyquist sampling (over sampling ratio is 1) shows the better PAPR performance than that the over

sampling ratio is higher than 2. It can be also observed that the PAPR performances of the conventional OFDM become the same when the over sampling ratio is higher than 4. This means that the over sampling ratios are required by higher than 4 to achieve the accurate evaluation of PAPR performance which can be considered as the analogue signal.

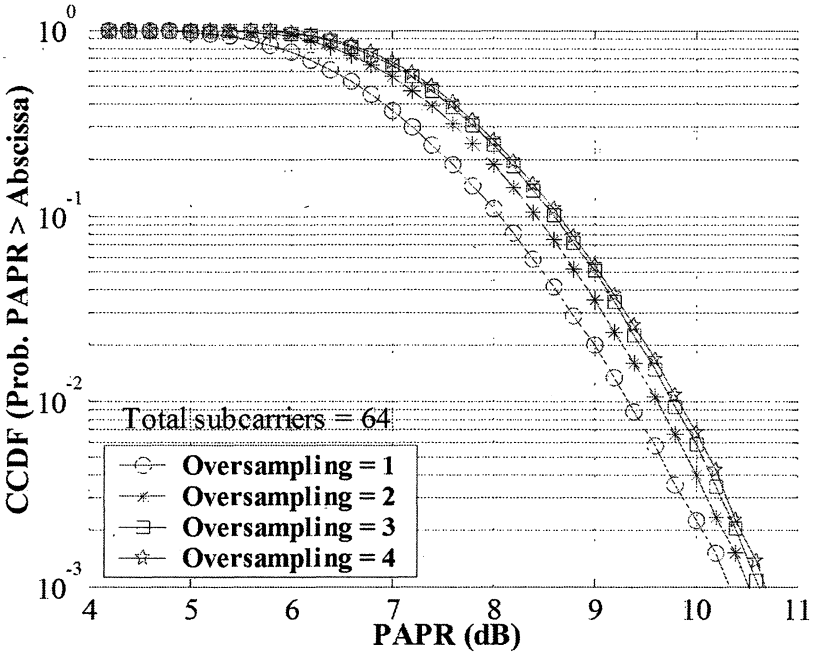

Fig. 1.9. PAPR performance when changing over sampling ratio.

The OFDM complex baseband signal for N sub-carriers from equation (1.1) can be rewritten as,

$$x(t) = \sum_{n=0}^{N-1} a_n \cos \omega_n t + j b_n \sin \omega_n t \tag{1.32}$$

The a_n and b_n are the in-phase and quadrature modulating symbols. If each carrier has amplitude A, the maximum PAPR will be given by

$$\begin{aligned} max(PAPR) &= \frac{(NA)^2}{[N(A^2/2)]} \\ &= 2N \end{aligned} \tag{1.33}$$

When the number of subcarriers N is small, a PAPR of $2N$ has reasonable chances of occurring. However, if N is large enough so that the central limit theorem applies, the amplitude distribution of the OFDM signal is better approximated by a Rayleigh distribution since a PAPR of $2N$ has exceedingly small probability of occurring. In [53], it is shown that the cumulative distribution function for the peak power per OFDM symbol is shown by following equation.

$$F(max\|x(t)\le z\|)=\left(1-e^{\left(-\frac{1}{2}\frac{z}{\sigma^2}\right)}\right)^N \tag{1.34}$$

The complementary CDF for the peak power per OFDM symbol can write as following equation.

$$P(max\|x(t)\le z\|)=1-\left(1-e^{\left(-\frac{1}{2}\frac{z}{\sigma^2}\right)}\right)^N \tag{1.35}$$

Figure 1.10 shows the PAPR performance of conventional OFDM signal when the numbers of sub-carriers are increasing. The number of subcarrier is taken by 64, 256 and 1024 sub-carriers, respectively. From figure, its cans observed that the PAPR performance is increasing as increased the number of N subcarriers.

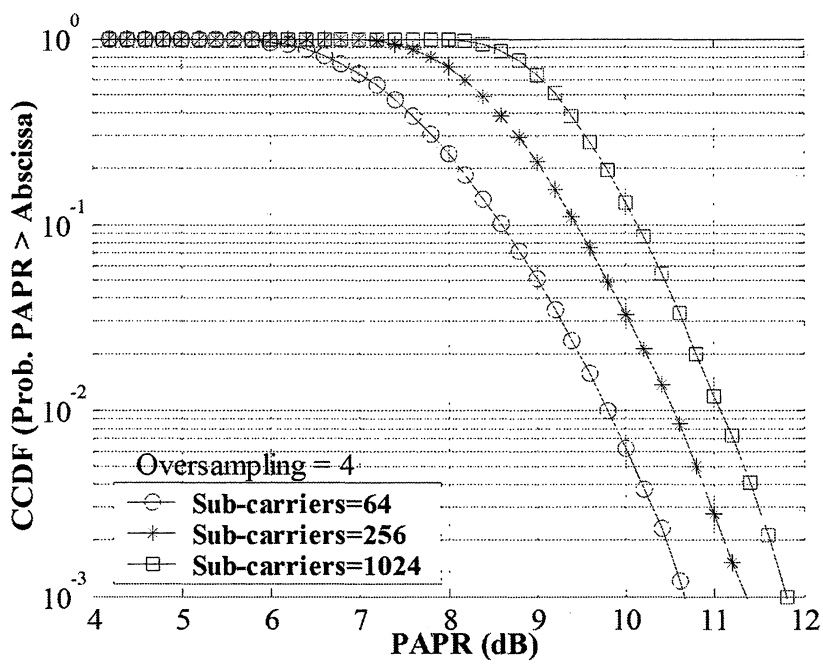

Fig. 1.10. PAPR performance when changing the number of sub-carriers.

1.4 Solutions for PAPR Problems

1.4.1 Clipping and Filtering Method

The simplest technique for PAPR reduction might be amplitude clipping. Amplitude clipping limits the peak envelope of the input signal to a predetermined value or otherwise passes the input signal through unperturbed, that is,

$$C(x)=\begin{cases} x, & |x|\le A_c \\ A_c e^{j\phi(x)}, & |x|\le A_c \end{cases} \tag{1.36}$$

where $C(x)$ is the phase of x and A_c. The distortion caused by amplitude clipping can be viewed as another source of noise. The noise caused by amplitude clipping falls both in-band and out-of- band. In-band distortion cannot be reduced by filtering and results error performance degradation, while out-of-band radiation reduces spectral efficiency. Filtering after clipping can reduce out-of-band radiation but may also cause some peak regrowth so that the signal after clipping and filtering will exceed the clipping level at some points. To reduce overall peak regrowth, a repeated clipping-and-filtering operation can be used. Generally, repeated clipping-and-filtering takes many iterations to reach a desired amplitude level. When repeated clipping-and-filtering is used in conjunction with other PAPR reduction techniques described below, the deleterious effects may be significantly reduced.

There are a few techniques proposed to mitigate the harmful effects of the amplitude clipping. The iteratively reconstruct method the signal before clipping is proposed. This method is based on the fact that the effect of clipping noise is mitigated when decisions are made in the frequency domain. When the decisions are converted back to the time domain, the signal is recovered somewhat from the harmful effects of clipping, although this may not be perfect. An improvement can be made by repeating the above procedures. Another way to compensate for the performance degradation from clipping is to reconstruct the clipped samples based on the other samples in the oversampled signals. In [44] oversampled signal reconstruction is used to compensate for signal-to-noise ratio (SNR) degradation due to clipping for low values of clipping threshold. In [45] iterative estimation and cancellation of clipping noise is proposed. This technique exploits the fact that clipping noise is generated by a known process that can be recreated at the receiver and subsequently removed.

1.4.2 Partial Transmit Sequence Method (PTS)

In the PTS technique, an input data block of N symbols is partitioned into disjoint sub-blocks. The subcarriers in each sub-block are weighted by a phase factor for that sub-block. The phase factors are selected such that the PAPR of the combined signal is minimized.

Figure 1.11 shows the block diagram of the PTS technique. In the ordinary PTS technique input data block X is partitioned into V disjoint sub-blocks $X^v = [X_0^v, X_1^v, \ldots, X_{N-1}^v]^T$, $v = 1,2,\ldots,V$ such that $\sum_{v=1}^{V} X^v = X$ and the sub-blocks are combined to minimize the PAPR in the time domain. The L -times oversampled time domain signal of $X^v, v = 1,2,\ldots,V$ is denoted by $x^v = [x_0^v, x_1^v, \ldots, x_{NL-1}^v]^T$. $x^v, v = 1,2,\ldots,V$ is obtained by taking an *IFFT* of length NL on X^v concatenated with $(L-1)N$ zeros. Complex phase factors, $b^v = e^{j\phi_v}$, $v = 1,2,\ldots,V$ are introduced to combine the PTSs. The set of phase factors is denoted as a vector $b = [b_1, b_2, \ldots, b_V]^T$. The time domain signal after combining is given by

$$x'(b) = \sum_{v=1}^{V} b^v \cdot x^v \tag{1.37}$$

where $x'(b) = [x'_0(b), x'_1(b), \ldots, x'_{NL-1}(b)]^T$. The objective is to find the set of phase factors that minimizes the PAPR. Minimization of PAPR is related to the minimization of

$$\max_{0 \le k \le NL-1} |x'_k(b)|. \tag{1.38}$$

In general, the selection of the phase factors is limited to a set with a finite number of elements to reduce the search complexity. The set of allowed phase factors is written in $e^{j\phi_v}, \phi = \frac{2\pi i}{W} \mid i = 0,1,\ldots,W-1$, where W is the number of allowed phase factors. In addition, we can set $b_1 = 1$ without any loss of performance. So, we should perform an exhaustive search for $(M-1)$ phase factors. Hence, W^{M-1} sets of phase factors are searched to find the optimum set of phase factors. The search complexity increases exponentially with the number of sub-blocks M. PTS needs M *IFFT* operations for each data block, and the number of required side information bits is $\log_2 W^{M-1}$. The amount of PAPR reduction depends on the number of sub-blocks M and the number of allowed phase factors W. Another factor that may affect the PAPR reduction performance in PTS is the sub-block partitioning, which is the method of division of the subcarriers into multiple disjoint sub-blocks. There are three kinds of sub-block partitioning schemes: adjacent, interleaved, and pseudo-random partitioning. In this thesis, the conventional PTS method is only defined by using the adjacent sub-block partitioning.

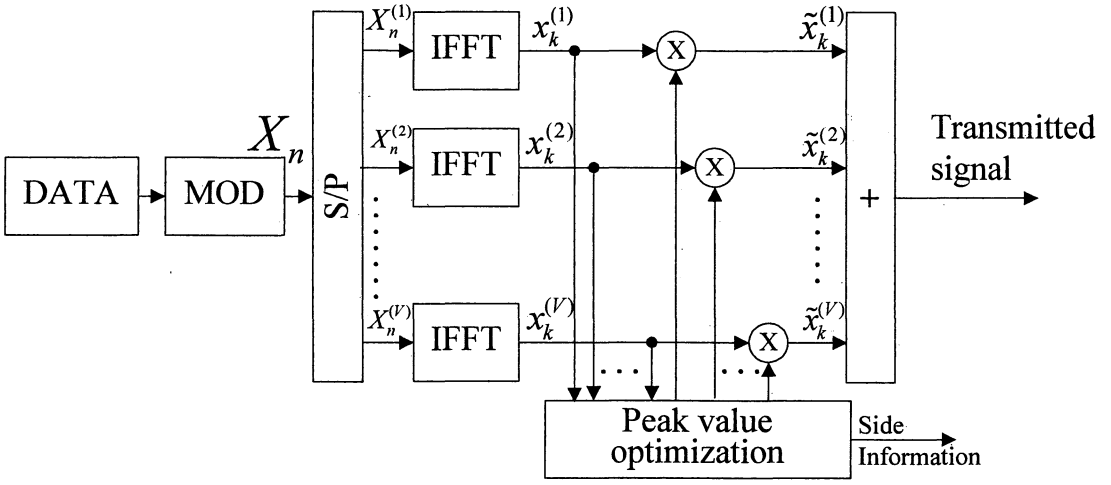

Fig. 1.11. A block diagram of PTS technique.

1.4.3 Selected Mapping method (SLM)

In the SLM technique, the transmitter generates a set of sufficiently different candidate data blocks, all representing the same information as the original data block, and selects the most favorable for transmission. A block diagram of the SLM technique is shown in figure 1.12. Each data block is multiplied by U different phase sequences, each of length N, $B^{(U)} = [b_0^u, b_1^u, \ldots, b_{N-1}^u]^T$, $u = 1, 2, \ldots, U$, resulting in U modified data blocks. To include the unmodified data block in the set of modified data blocks, which $B^{(1)}$ is the all-one vector of length N. Let us denote the modified data block for the *u-th* phase sequence $X^{(U)} = [X_0 b_0^u, X_1 b_1^u, \ldots, X_{N-1} b_{N-1}^u]^T$, $u = 1, 2, \ldots, U$. After applying SLM to X, the multi-carrier signal becomes

$$x^{(U)}(t) = \frac{1}{\sqrt{N}} \sum_{n=0}^{N-1} X_n b_{u,n} \cdot e^{j2\pi n \Delta f t}, \quad 0 \le t < NT, \quad u = 1, 2, \ldots, U. \tag{1.39}$$

Among the modified data blocks $X^{(u)}, u = 1, 2, \ldots, U$, the one with the lowest PAPR is selected for transmission. Information about the selected phase sequence should be transmitted to the receiver as side information. At the receiver, the reverse operation is performed to recover the original data block. For implementation, the SLM technique needs U *IFFT* operations, and the number of required side information bits is $\log_2 U$ for each data block. This approach is applicable with all types of modulation and any number of subcarriers. The amount of PAPR reduction for SLM depends on the number of phase sequences U and the design of the phase sequences.

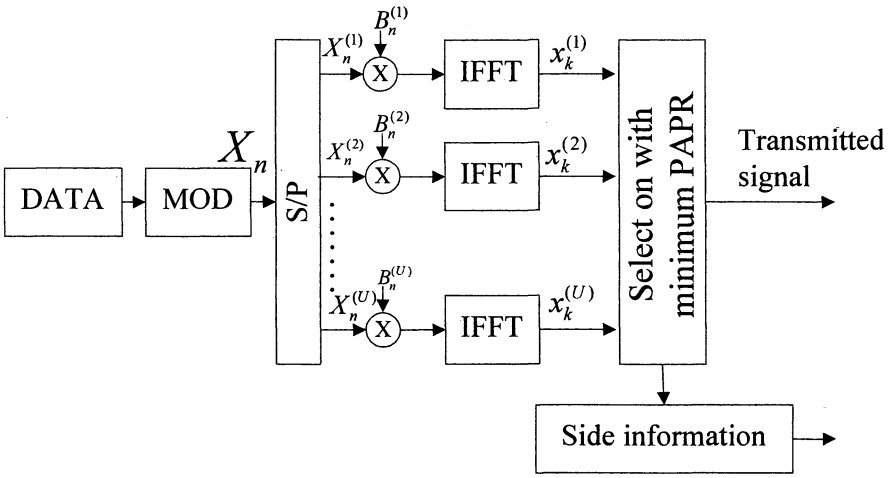

Fig. 1.12. A block diagram of SLM technique.

1.4.4 Other Solutions

The mitigation methods of non-linear distortions are described from above mention, which relate to this research and some proposed methods use the basic concept. There are various other proposed methods to mitigate the non-linear distortions for OFDM wireless communications systems. These techniques include coding, tone reservation (TR), tone injection (TI), active constellation extension (ACE) and etc. However, it's not given the detail in this thesis.

1.5 Channel models

This section presents the mathematical models of communication channels. It initially describes the basic radio channel. Then this section explains the non-linear amplifier characteristics and effect of nonlinearity. Finally, satellite communications system and satellite system channel model.

1.5.1 Radio Channel Model

In the radio channel, the signal quality is not only be distorted by multipath fading but also corrupted by thermal noise. The radio channel model shows in figure 1.13. The received signal through the channel can write the following equation.

$$r(t) = \int_{-\infty}^{\infty} h(\tau;t)s(t-\tau)d\tau + w(t) \tag{1.40}$$

where $h(\tau,t)$ is the impulse response of the channel and $w(t)$ is an additive white Gaussian noise (AWGN). If the channel impulse response is a time-invariant constant given by

$$h(\tau,t) = h\delta(\tau) \tag{1.41}$$

where h is a complex-valued channel gain, then we can ignore the effect of fading and there is only AWGN in the channel. We call " AWGN Channel". On the other hand, there is fading and AWGN in the channel. We call "Fading Channel". The BER performance of a modulation/demodulation scheme largely depends on the received signal to noise power ration (SNR) or carrier to noise ratio (C/N).

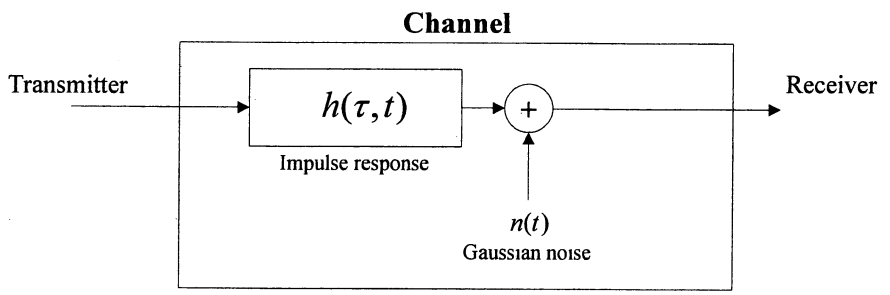

Fig. 1.13. Radio channel model.

1.5.2 Non-linear Channel

To determine the impact of the PAPR on system performance, power amplifier models must be defined. Two models commonly used in the research literature are the solid-state power amplifier (SSPA) model and the traveling-wave tube amplifier (TWTA) model. The details of these non-linear amplifier models are explained as following.

1.5 Channel Models

Typically, most the non-linear behavior in the continuous time domain is caused by the high power amplifier (HPA). For most non-linear HPA, it is convenient to represent the input signal in polar coordinates as

$$\begin{aligned} x &= |x| e^{j \arg\{x\}} \\ &= \rho e^{j\phi} \end{aligned} \tag{1.42}$$

Here, the complex envelope of the output signal can be expressed by

$$g(x) = F[\rho] e^{[j(\phi + \Phi[\rho])]} \tag{1.43}$$

where $F[\rho]$ and $\Phi[\ ]$ represent the AM/AM and AM/PM conversion characteristics of the memory-less. In the particular, some of the most commonly used models for non-linear amplifiers are solid-state power amplifier (SSPA) and Traveling-wave tube amplifier (TWTA). The mathematic models for both models can describe as following.

➢ Solid State Power Amplifier (SSPA)

In general, modeling nonlinear power amplifiers is complicated. A common simplification is to assume that the HPA is a memory-less nonlinearity, and therefore has a frequency-nonselective response.

The Solid State Power Amplifier (SSPA) modeled by Rapp's. The AM-AM and AM-PM conversions characteristics of SSPA are given by the following equations, respectively.

$$F_{SSPA}(\rho) = \frac{v\rho}{[1 + (\frac{v\rho}{A_0})^{2p}]^{1/2p}} \tag{1.44}$$

$$\Phi_{SSPA}(\rho) = \alpha_\phi \left(\frac{v\rho}{A_0} \right)^4 \tag{1.45}$$

where, ρ is the amplitude of input signal, v is the gain factor, A_0 is the saturated output level, p is the parameter to decide the non-linear level and α_ϕ is phase displacement.

For example, the values for these parameters are assumed by $A_0 = 1$, $v = 1$, $p = 6$ and $\alpha_\phi = 0.025$. Figure 1.14 shows the AM-AM and AM-PM conversion characteristics of SSPA when assuming the above values for the parameters.

➢ Traveling Wave Tube Amplifier (TWTA)

The non-linear amplifier located at the satellite station is assumed by the Traveling Wave Tube Power Amplifier (TWTA), which is modeled by Saleh. The AM-AM and AM-PM

conversions characteristics of TWTA modeled by Saleh are given by the following equations, respectively.

$$F_{TWTA}(\gamma) = \frac{\alpha_a \gamma}{(1+\beta_a \gamma^2)} \tag{1.46}$$

$$\Phi_{TWTA}(\gamma) = \frac{\alpha_\theta \gamma^2}{(1+\beta_\theta \gamma^2)} \tag{1.47}$$

where, γ is the amplitude of input signal, α_a and β_a are the parameters to decide the non-linear level of power amplifier, and α_θ and β_θ are phase displacements. The values for these parameters are assumed by $\alpha_a = 2$, $\beta_a = 1$, $\alpha_\theta = 2$ and $\beta_\theta = 1$ which can approximate the standard TWTA. For these parameters, figure 1.14 shows the AM-AM and AM-PM conversion characteristics of TWTA when assuming the above values for the parameters.

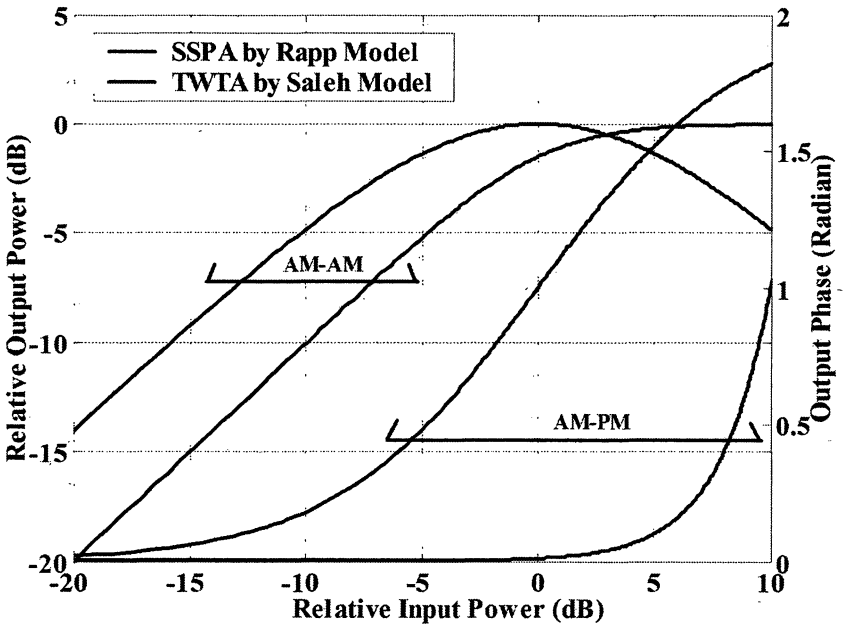

Fig. 1.14. Input and output relationships for SSPA and TWTA.

1.5.3 Satellite Channel

Basic concepts of satellite communications system are illustrated in figure 1.15. Form figure 1.15, satellite communication system is broadly divided into a space segment consisting of a space station (satellite) and a ground segment consisting of earth stations. The earth stations consist of transmitter and receiver earth stations.

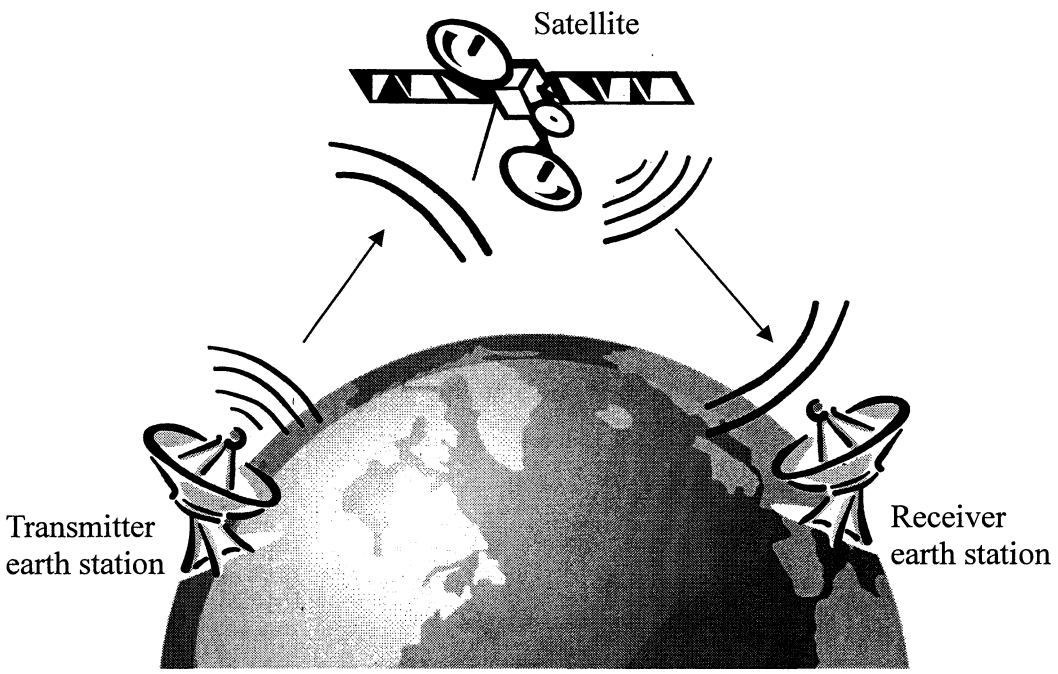

Fig. 1.15. Satellite communications system.

Figure 1.16 shows the typical satellite system model assumed in the following evaluations in this thesis. The increasing of transmitted signal power, the transmitter uses the high power amplifier (HPA) for amplifier the signal power. The transmitters at the earth station and the satellite station have the HPA. Therefore, the satellite communication system can be modeled as following.

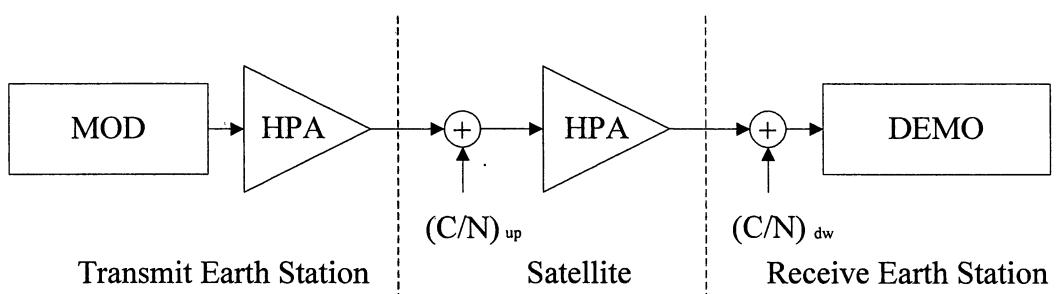

Fig. 1.16. Satellite system model.

1.5.4 Effect of Non-linear Amplifier

When the transceiver suffers from non-linear distortion, the system experiences two main problems, namely, PSD degradation and BER increase. To reduce nonlinear distortion in the amplified OFDM signal, The operation point of non-linear amplifier should operates in the linear region, which it is required to take enough input power back-off (IBO) The operation point of non-linear amplifier is defined by the Input Back-Off (IBO), which is given by the following equation.

$$IBO = 10\log\frac{P_{in}}{P_0} \tag{1.48}$$

where P_{in} is the average power of input signal to the non-linear amplifier and P_0 is the input saturation power.

Figure 1.17(a) and 1.17(b) show the BER performance of conventional OFDM system for 16QAM and 64QAM modulation. Form the figure, it can be observed that the BER performance is degraded when the IBO is taken by high IBO or non-linear region. It is also observed that the 64QAM modulation requires the lower IBO or linear region to achieve the good BER performance.

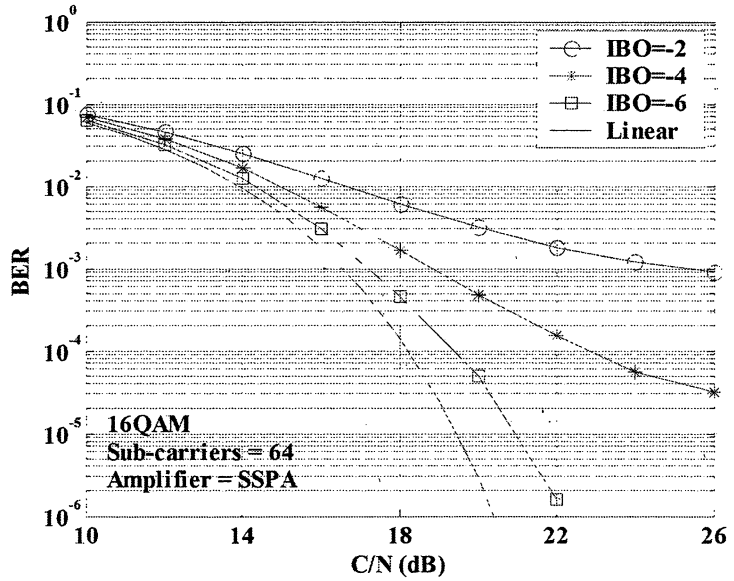

(a) 16QAM

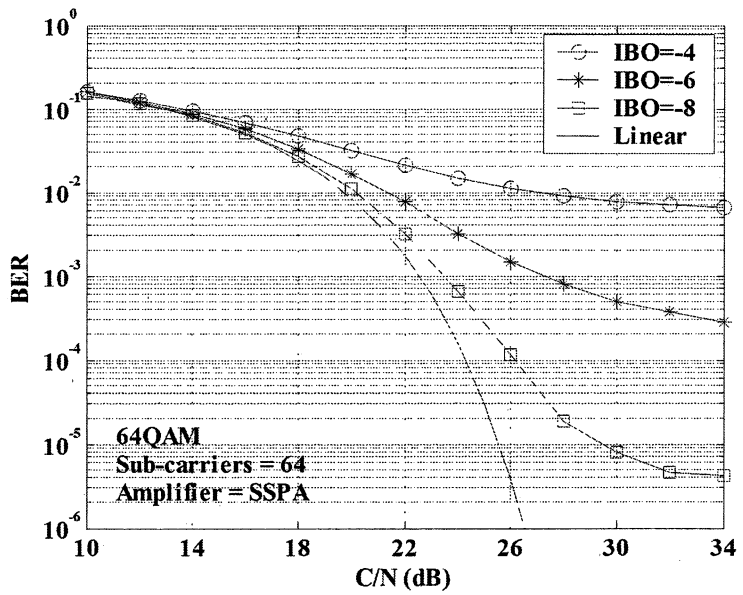

(b) 64QAM

Fig. 1.17. BER performance versus C/N in non-linear channel.

1.6 Research Background

The future wireless communications systems including the fixed, mobile and broadcasting systems are required to support the higher transmission data rate for providing the multimedia services. In the next generation of wireless communications systems, the transmission data rate for outdoor users with higher mobility and indoor users with lower mobility are required up to 100Mbps and 1Gbps, respectively. To realize such higher transmission data rate by using the conventional single carrier transmission scheme, it is requested to employ the efficient modulation method such as multi-level QAM. However, the single carrier transmission scheme with multi-level QAM would cause the fatal degradation of signal quality due to the inter-modulation noise incurred at the non-linear channel.

The Orthogonal Frequency Division Multiplexing (OFDM) technique has been received a lot of attentions especially in the field of wireless communications because of its efficient usage of frequency bandwidth and robustness to the multi-path fading. From these advantages, the OFDM technique has already been adopted as the standard transmission technique in the wireless LAN systems and the terrestrial digital broadcasting systems including the Digital Audio Broadcasting (DAB) and the Digital Video Broadcasting (DVB). The OFDM technique is also employed as the standard transmission technique in the next generation of mobile communications systems (LTE).

One of the limitations of using OFDM technique is the larger Peak to Averaged Power Ratio (PAPR) of its time domain signal. The larger PAPR signal would cause the severe degradation of bit error rate (BER) performance and the undesirable frequency spectrum re-growth both due to the non-linear distortion occurring in the non-linear amplifier which is usually required at the transmitter in the wireless communications systems. The simple solution to overcome this problem is to operate the non-linear amplifier at the linear region with taking the enough larger input back-off (IBO). However, this approach leads the inefficient usage of non-linear power amplifier, and would lead a serious problem on battery consumption especially for the mobile handheld terminal and portable wireless LAN terminal. In order to maximize the usage of power efficiency, the non-linear amplifier is usually required to operate at the near its saturation region. However this approach will lead to the severe degradation of BER performance and undesirable frequency spectrum re-growth for the larger PAPR signal due to the occurring of inevitably higher non-linear distortion.

In this degree thesis, the following two types of methods are proposed to solve the above problems.

1) Non-linear distortion compensation method for OFDM signal
2) PAPR reduction methods for OFDM signal with lower computation complexity

As for the first method, this thesis proposes the Improved DAR (IDAR) method, which can mitigate both the clipping noise and inter-modulation noise. In the proposed IDAR method, the characteristics of non-linear amplifiers are required to be known at the receiver for mitigating the inter-modulation noise. This thesis also proposes the estimation method for AM-AM and AM-PM conversions characteristics of non-linear amplifiers by using low PAPR (Peak to Averaged Power Ratio) preamble symbols.

This thesis demonstrates the effectiveness of proposed IDAR method when applying the satellite communication systems. From the computer simulation results, it is concluded that the proposed IDAR method can achieve the higher transmission data rate and higher efficient usage of non-linear power amplifier with keeping the better BER performance even in the non-linear satellite channel.

As for the second method, this thesis proposes PAPR reduction methods based on PTS technique. The conventional PTS method requires the larger number of clusters and weighting factors to achieve the better PAPR performance which leads larger computation complexity. To reduce the computation complexity, DIF-PTS method is proposed which employs the intermediate signals within the IFFT and used radix-2, radix-4, Split-Radix and Extended Split-radix for decimation in the frequency domain (DIF) to obtain the PTS sub-blocks. Multiple IFFTs are then applied to the remaining stages. The PTS sub-blocking is performed in the middle stages of the N-point radix FFT DIF algorithm. The DIF-PTS method can reduce the computational complexity relatively while it shows almost the same PAPR reduction performance as that of the conventional PTS method. To improve the PAPR performance with low computation complexity, this thesis proposes a new weighting factor technique for the PTS method in conjunction with DIF-PTS sub-blocking based on radix-r, Split-Radix and Extended Split-Radix IFFT technique which can improve both the PAPR performance and computation complexity. The proposed method can achieve the better PAPR reduction performance than that for the DIF-PTS method without any increasing of size of side information.

In this thesis, a new PTS method by using the permutation of data sequence in the frequency domain is also proposed to improve the computation complexity. The proposed method employs the dummy and parity subcarriers as the embedded side information in the data subcarriers, which is used for the demodulation of data information at the receiver. The proposed method includes two types of permutation methods Type I and Type II. Type I is to perform the permutation only for the first M/2 subcarriers, while Type II is to perform the permutation both for the first and the last part of M/2 subcarriers. Although the computation complexity for the Type II is larger than Type I, the improvement of PAPR performance for the Type II is better than Type I. The feature of proposed method is to detect the rotation number performed at the transmitter precisely at the receiver by using the very few dummy

subcarriers which corresponds to the embedded side information. The propose method can achieve the higher transmission efficiency because the size of embedded side information in the proposed method is much smaller than that for the side information in the conventional PTS method. From the computer simulation results, this thesis confirmed that the proposed permutation of data sequence method can achieve the better PAPR performance and better BER performance in the non-linear channel with lower computation complexity

In this thesis, the numerous computer simulations are conducted to confirm the effectiveness of all proposed method. Form the simulation results, it is confirmed that the proposed methods show the better PAPR performance with lower computation complexity. As a conclusion of researches in this thesis, the proposed PAPR reduction methods and mitigation methods of non-linear distortion noise could provide various practical solutions for the next generation of multimedia wireless communications systems employing the OFDM technique.

1.7 Thesis Structure

The remainder of this thesis is organized as follows.

Chapter 2 presets non-linear distortion compensation method. Section 2.1 introduces the basic background and problems of conventional method. Section 2.2 presets clipping and inter-modulation noise mitigation method for OFDM signal in non-linear channel. Section 2.2 explains structure of OFDM transmitter, Improved DAR (IDAR) method, generation of low PAPR preamble symbol and mitigation of clipping and inter-modulation noise. Section 2.3 presets satellite system model. Section 2.4 presets OFDM-IDAR Method for satellite channel. Section 2.5 presets estimation method of non-linear amplifier. Section 2.6 presets QAM-OFDM system with IDAR method designed for satellite channel. Section 2.7 describes the evaluation of proposed method. Section 2.6 is conclusions.

Chapter 3 presets a new weighting factor of PTS OFDM with low complexity. Section 3.1 introduces the basic background and problems of computation complexity of conventional PTS method. Section 3.2 presets PAPR Distribution and PAPR characteristics of OFDM signal. Section 3.3 presets conventional weighting factor of PTS method. Section 3.4 describes proposal of new weighting factor of PTS method. Section 3.5 describes the evaluation of proposed method. Section 3.6 is conclusions.

Chapter 4 presets a new weighting factor of PTS OFDM with low complexity base on radix-R IFFT. Section 4.1 introduces the basic background partial transmit sequence (PTS) and improved partial transmit sequence (IPTS) methods base on radix-R IFFT. Section 4.3 presets proposal of new weighting factor based on radix-R such as Radix-2, Radix-4 and Extended Split-Radix. Section 4.4 describes the evaluation of proposed method. Section 4.5 is conclusions.

Chapter 5 presets proposal of new PAPR reduction method for OFDM signal by using permutation sequences. Section 5.1 introduces the basic background and problems of conventional non-distortion PAPR reduction method. Section 5.2 describes system model. Section 5.3 describes proposal of permutation sequences method including Type I and Type II. Section 5.4 describes embedded side information at the transmitter side and detection method for embedded side information at the receiver side. Section 5.5 describes the evaluation of proposed method. Section 5.6 is conclusions.

Finally, the overall conclusion of this thesis is given in Chapter 6.

CHAPTER 2

NON-LINEAR DISTORTION COMPENSATION METHOD

The future satellite communication systems are required to support the higher transmission data rate for providing multimedia services by employing the efficient modulation method such as multi-level QAM. However, the employment of conventional single carrier transmission method with multi-level QAM which has larger PAPR (Peak to Averaged Power Ratio) would cause the fatal degradation of signal quality due to the non-linear amplifiers located at the earth station and satellite. To overcome this problem, this chapter proposes broadband satellite communication systems by using the multi-level QAM-OFDM technique with IDAR (Improved Decision Aided Reconstruction) method, which is designed for satellite channel. In the IDAR method, the characteristics of non-linear amplifiers are required to be known at the receiver for mitigating the inter-modulation noise. The chapter also explains the estimation method for AM-AM and AM-PM conversion characteristics of non-linear amplifiers by using low PAPR preamble symbols. The various computer simulations are conducted in section 2.5 and 2.6 to verify the effectiveness of proposed system in the non-linear satellite channel.

2.1 Introduction

The future satellite communications including the fixed, mobile and broadcasting systems are required to support the higher transmission data rate for providing the multimedia services, which are already available in the terrestrial network [57]-[62]. To realize the higher data rate transmission in the satellite channel, it is requested to employ the efficient modulation method such as multi-level QAM. However, the employment of conventional single carrier transmission method with multi-level QAM which has larger PAPR would cause the fatal degradation of signal quality due to the inter-modulation noise incurred at the non-linear amplifiers located at the transmit earth station and satellite [13]-[17]. From this reason, the modulation method used in the current satellite communications is usually limited by low transmission data rate of using QPSK method, which has the robustness to the non-linear distortion fairly because of its better PAPR performance as compared with that for the multi-level QAM modulation method.

On the other hand, the Orthogonal Frequency Division Multiplexing (OFDM) technique has been received a lot of attentions especially in the field of terrestrial wireless communications because of its efficient usage of frequency bandwidth, robustness to the multi-path fading and enabling the employment of multi-level QAM with less complexity of receiver[16]-[19]. One of the disadvantages of using the OFDM signal is that its time domain signal has the larger PAPR, which causes the degradation of BER performance in the non-linear amplifier. From this reason, the OFDM has been considered as unsuitable transmission technique for the satellite channel although it has a potential capability to improve the transmission data rate by employing the multi-level QAM with less complexity structures of transmitter and receiver. To solve the problem of performance degradation due to the non-linear distortion for the OFDM signal, we have already proposed the OFDM technique with IDAR method designed for terrestrial wireless communication systems, which includes one non-linear amplifier at the transmitter such as wireless LAN system [67]. The proposed IDAR method can mitigate the non-linear distortion by using the decision data at the receiver and achieve the higher transmission data rate with keeping the better BER performance even in the non-linear channel. In the IDAR method, however the input and output relationships of non-linear amplifier characteristics are required at the receiver. The evaluation of proposed OFDM-IDAR method in [67] was assumed that the ideal input and output relationships of amplifier characteristics are known at the receiver.

In this chapter, we propose the broadband satellite communication systems by using multi-level QAM-OFDM technique with IDAR method designed for the non-linear satellite channel, which includes two non-linear amplifiers located at the transmit earth station and

satellite[67]. The proposed method could achieve the higher transmission data rate in the non-linear satellite channel with keeping the better BER performance than that for the conventional single carrier transmission technique of using multi-level QAM method. This chapter also proposes the estimation method for non-linear amplifier characteristics, which is required for the IDAR method, by using the low PAPR preamble symbols inserted at the start of every frame. The proposed estimation method for non-linear amplifier characteristics could achieve the better accuracy even when the characteristics of non-linear amplifiers located at the earth station and satellite are changed frequently due to the aging or operation environments.

In this chapter, Section 2.2 firstly presents clipping and inter-modulation noise mitigation method for OFDM signal in non-linear channel. Section 2.3 presents the satellite system model. Section 2.4 proposes the OFDM-IDAR method designed for satellite channel, and Section 2.5 proposes the estimation method of non-linear amplifier characteristics, which are required in the IDAR method. Section 2.6 presents QAM-OFDM system with IDAR method designed for satellite channel and presents the various computer simulation results to verify the effectiveness of OFDM-IDAR technique with the proposed estimation method, and Section 2.7 draws some conclusions.

2.2 Clipping and Inter-Modulation Noise Mitigation Method for OFDM Signal in Non-Linear Channel

2.2.1 Structure of OFDM Transmitter

Figure 2.1 shows the structure of OFDM transmitter with clipping method. In the figure, transmission data is first modulated in the frequency domain by using the certain modulation technique. The frequency domain signal X_n after adding the zero padding is converted to the time domain signal x_k by *IFFT*. Here, the zero padding is usually required to enable the usage of simple analogue filter to reject the aliasing occurring at the D/A converter. The insertion of zero padding results the over sampling of time domain OFDM signal. The over sampled time domain signal x_k can be given by the following equation (1.1) and (1.2). Then the guard interval (GI) is added to (2.1) to avoid the inter symbol interference (ISI) in the multi-path fading channel. The time domain signal with GI is clipped by the following equation so as to improve the PAPR performance.

$$y_k = \begin{cases} x_k & |x_k| \le A_c \\ A_c e^{j\{\arg(x_k)\}} & |x_k| > A_c \end{cases} \tag{2.1}$$

where y_k is the clipped signal with the maximum amplitude of A_c. In this chapter, the clipping level (*CL*) is defined by the following equation.

$$CL(dB) = 10\log(A_c^2 / E_s) \tag{2.2}$$

where E_s is the averaged power of transmitted signal.

Since the clipping operation given by (2.1) is the non-linear operation, the clipping noise would fall both in-band and out-band of OFDM desired signal bandwidth, which cause the degradation of BER performance and the undesirable spectrum re-growth, respectively. Although the undesirable spectrum re-growth can be reduced by using the pre-filter as shown in Fig.2.1, the PAPR performance at the output of pre-filter might be degraded slightly due to the band limitation of pre-filter. The PAPR performance for the clipped signal with pre-filter is evaluated in Section 2.6. The employment of pre-filter is also problematic on the usage of conventional DAR method proposed in [44]. In the DAR method, the clipping noise is reconstructed by using the received time domain signal, which is distorted by the band limitation of pre-filter. To solve this problem, we proposed the modified DAR method by using the in-band frequency domain signal, which is not affected by the pre-filter because the bandwidth of pre-filter is wider than the desired OFDM signal bandwidth.

The transmission data symbols at the output of pre-filter are formed by the burst frame as shown in Fig.2.2. The burst frame consists of two preamble symbols and L data symbols. Two preamble symbols will be used for the synchronization both for the symbol timing and carrier frequency, and the estimation of channel frequency response at the receiver. This chapter considers the wireless LAN system operating in the indoor environments as the application field of proposed method. In the indoor environment, the multi-path fading can be modeled by the quasi-static condition that is, the time variance of channel frequency response due to the multi-path fading is sufficiently slow over one burst frame duration because the moving speed of terminal is usually static or very slow. From this fact, the channel frequency response estimated by using the preamble symbols inserted at the start of every burst frame as shown in Fig.2.2 can be used in the frequency domain equalization for the data symbols transmitted after the preamble symbols. The time domain signal formatted by the burst frame is converted to the analogue signal by D/A converter and reject the aliasing by using analogue filter as shown in Fig.2.1.Then, the analogue signal is up converted (U/C) to the radio frequency (RF) and input to the non-linear amplifier. The RF signal at the output of non-linear amplifier can be given by the following equation.

$$s(t) = F\left[\left|z(t)\right|\right] \cdot e^{j \cdot arg\{z(t)\}} \tag{2.3}$$

where, $z(t)$ is the up converted RF signal, and $F[\ ]$ represents the AM/AM conversion characteristics of non-linear amplifier which is modeled by the following equation [14], the values for these parameters are assumed by $A_0 = 1, v = 1, p = 2$ and $\alpha_\phi = 0$. Fig. 1.14 shows the input-output relative power characteristics.

The non-linear amplifier shown in Fig.1.14 is well known as the non-linear amplifier model of SSPA. The OFDM signal at the output of amplifier including the original signal $x(t)$, clipping noise $c(t)$, band limitation noise $b(t)$ and the inter-modulation noise $p(t)$ can be given by the following equation.

$$s(t) = x(t) + c(t) + b(t) + p(t) \tag{2.4}$$

where all kind of noises which lead the degradation of BER performance at the receiver are assumed to be added to the original desired signal $x(t)$ linearly. However, it should be noted that these noises at the output of non-linear amplifier are unable to express separately because these noises are strongly related to the original signal $x(t)$. However, the IDAR method proposed in the next section estimates the summation of these noises not separately by subtracting the decision data from the received composite signal in the time domain. Although

it is inappropriate to express these noises separately, equation (2.4) is given only for the purpose of easy explaining for the following proposed algorithm.

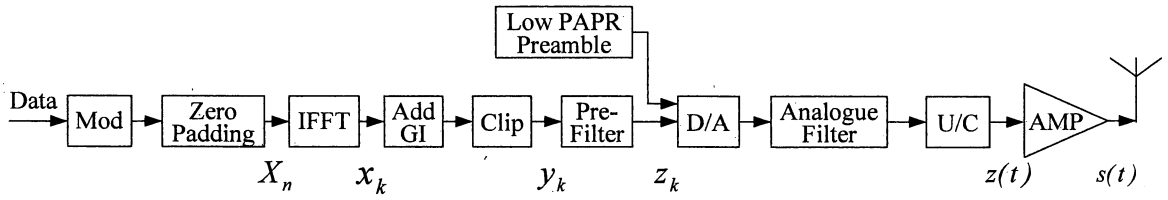

Fig. 2.1 Structure of OFDM transmitter with clipping.

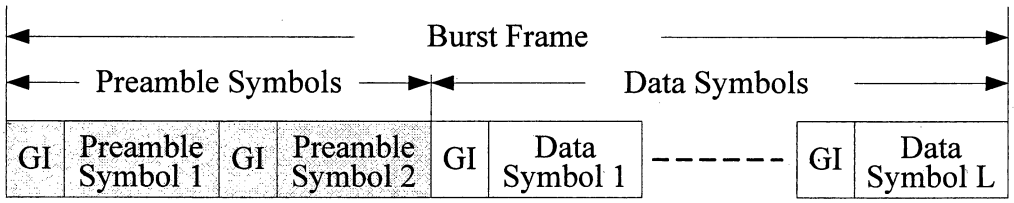

Fig. 2.2 Structure of burst frame format.

In this chapter, we propose the improved DAR (IDAR) method in which the clipping noise as well as inter-modulation noise due to the non-linear amplifier could be mitigated on the basis of modified DAR method in [44]. The salient feature of proposed method is to enable the efficient usage of non-linear amplifier at the transmitter with keeping the better PAPR and BER performances. This chapter also presents the method for generating the low PAPR preamble symbol, which can achieve the accurate estimation of multi-path fading channel response in the non-linear channel.

In this section will explains the improved DAR method, which can mitigate the clipping noise, band limitation noise and inter-modulation noise all of which are occurred at the transmitter as shown in Fig.2.1.

2.2.2 Structure of Proposed IDAR Receiver

Figure 2.4 shows the structure of proposed IDAR receiver. In the figure, the received RF signal $r(t)$ is first down converted (D/C) to the base band signal and digitized by A/D converter. The time domain sampled signal r_k after removing the GI can be expressed by the following equation.

$$r_k = (x_k + c_k + b_k + p_k) \otimes h_k + w_k \tag{2.5}$$

where x_k and w_k represent the original signal and additive noise in the sampled time domain, respectively. c_k, b_k, and p_k represent the clipping noise, band limitation noise, and inter-modulation noise, respectively all of which are induced at the transmitter as shown in Fig.1. h_k and $\otimes$ denotes the time domain channel impulse response of multi-path fading and the operation of convolution, respectively. Then, the received sampled time domain signal is converted to the frequency domain signal by *FFT*, which is given by the following equation.

$$R_n = (X_n + C_n + P_n) \cdot H_n + W_n \tag{2.6}$$

In (2.6), the capital letter represents the frequency domain signal, which corresponds to its small letter given in (2.5). As comparing with the time domain signal given by (2.5), it can be seen the difference from (2.6) that the frequency domain signal includes no band limitation noise over the desired frequency bandwidth because the bandwidth of pre-filter is usually taken wider than the desired signal bandwidth of OFDM signal. The frequency domain channel response affected by multi-path fading can be estimated by using the preamble symbols inserted at the starting of every burst frame as shown in Fig.2.2. Although the preamble symbols are inserted after the clipping circuit as shown in Fig.2.1, the estimation accuracy of channel frequency response would be degraded due to the non-linear amplifier if the preamble symbols is generated by using the random pilot data pattern similar to the data symbol with larger PAPR. To solve this problem, it is requested to use the low PAPR preamble symbols for achieving the accurate estimation of channel response in the non-linear channel.

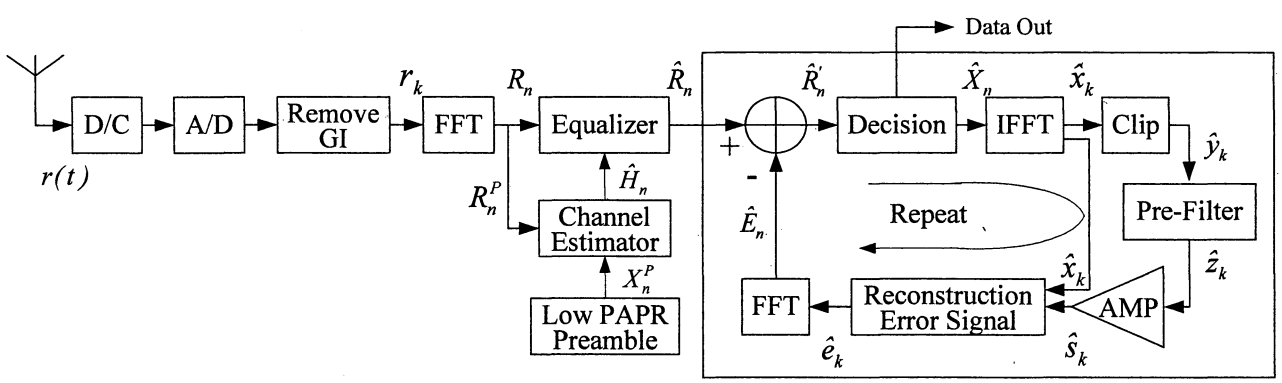

Fig. 2.3 Structure of proposed IDAR receiver.

2.2.3 Generation of Low PAPR Preamble Symbol

In the generation of low PAPR preamble symbol, this chapter employs the Time-Frequency domains swapping algorithm, which was proposed in [36][37]. This algorithm is proposed to provide the multi-tone signal with low crest factor, which can be used for the measurement of frequency response for the non-linear circuit. By using this algorithm, the phase value for each frequency domain OFDM sub-carrier with keeping the constant amplitude can be optimized so as to minimize the PAPR performance in the time domain signal. Fig.2.4 shows the envelopes of preamble symbol in the time domain with and without the Time-Frequency domains swapping algorithm. The results of PAPR performances for Fig.2.4 (a) and (b) are 8dB and 1.4dB, respectively.

From the figure and the results of PAPR performance, it can be concluded that the low PAPR preamble symbol can be used for the accurate estimation of multi-path fading channel response in the non-linear channel.

From the facts that the low PAPR preamble symbol is added at the output of pre-filter as shown in Fig.2.1 and its envelope of time domain signal is almost constant as shown in Fig.2.4(b), the received low PAPR preamble symbol in the frequency domain can be given by the following equation.

$$R_n^P = X_n^P \cdot H_n + W_n^P \tag{2.7}$$

As comparing with (2.6) for the received data symbol, the clipping noise and inter-modulation noise can be ignored in (2.7). By using (2.7), the channel frequency response affected by the multi-path fading can be estimated by the following equation from the fact that X_n^P transmitted in the low PAPR preamble symbol is known at the receiver.

$$\begin{aligned} \hat{H}_n &= R_n^P / X_n^P \\ &= H_n + W_n^P / X_n^P \end{aligned} \tag{2.8}$$

By using (2.8), the data symbol can be equalized by the following equation in the frequency domain.

$$\begin{aligned} \hat{R}_n &= R_n / \hat{H}_n \\ &= X_n^{'} + C_n^{'} + P_n^{'} + W_n^{'} \end{aligned} \tag{2.9}$$

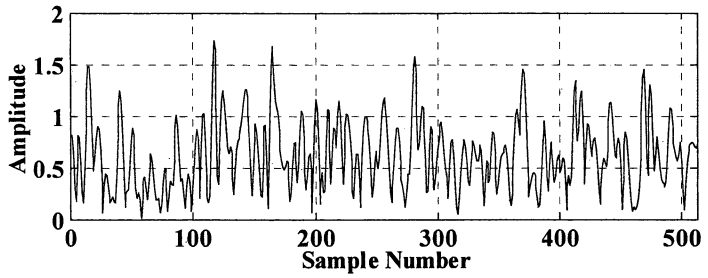

(a) Conventional Preamble Symbol

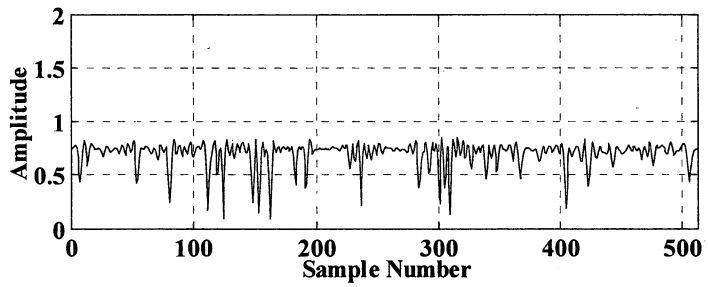

(b) Low PAPR Preamble Symbol

Fig. 2.4 Envelope of time domain preamble symbol.

2.2.4 Mitigation of Clipping and Inter-Modulation Noise

In the conventional modified DAR method in [44], the clipping noise introduced at the transmitter is reconstructed in the frequency domain by using the decision data at the receiver, and subtract the reconstructed clipping noise from the received signal so as to improve the BER performance. However, the modified DAR method can compensate only the clipping noise, and not for the inter-modulation noise in the non-linear channel. This chapter proposes the Improved DAR (IDAR) method, which can mitigate both the clipping noise and inter-modulation noise from the fact that the operation of non-linear amplifier given in (2.3) is very similar to the clipping operation given in (2.1). This means that the inter-modulation noise could be also mitigated by using the modified DAR method.

By using (2.9), the decision for the information data is made for each sub-carrier on the basis of the following equation.

$$\hat{X}_n = \min_X \left| \hat{R}_n - X \right| \tag{2.10}$$

By using (2.10), the signal distances between the received signal point and all candidates transmitted signal points are calculated, and then find the signal point with the minimum signal distance, which corresponds to the most likely the transmitted data information. Here, it should be noted that (2.10) is given only for the purpose of theoretical analysis. The actual hardware usually employs the quantized decision boundary method in the demodulation of

data information, which can achieve the same performance as that for (2.10) with less complexity.

If there are decision errors in (2.10), the decision data including the errors can be given by the following equation.

$$\hat{X}_n = X_n + F_n \quad (n = 0 \sim N-1)$$
$$F_n = \begin{cases} 0 & if\ \hat{X}_n = X_n \\ \hat{X}_n - X_n & if\ \hat{X}_n \neq X_n \end{cases} \tag{2.11}$$

where, F_n represents the error data at the n-th sub-carrier. By using (2.11) in the frequency domain, the time domain signal after *IFFT* can be given by the following equation.

$$\begin{aligned} \hat{x}_k &= \sum_{n=0}^{N-1} X_n \cdot e^{j\frac{2\pi nk}{N}} + \sum_{n=0}^{N-1} F_n \cdot e^{j\frac{2\pi nk}{N}} \\ &= x_k + f_k \end{aligned} \tag{2.12}$$

From (2.12) in the time domain, it can be observed that the error data in the frequency domain F_n is spread over the OFDM symbol time duration where the amplitude level of f_k at k-th sapling time becomes smaller because the total power of error data in the frequency domain is spread over all the sampling points of the OFDM symbol time duration. From this fact, it can be expected that if the number of error data are few after the decision of data information, (2.12) can be approximated by the original signal $x(t)$. This means that the time domain signal which is converted by *IFFT* from the frequency domain decision data can be used for the reconstruction of error signal including the clipping, band limitation and inter-modulation noises by using the same manner as processed in the transmitter. Here, all the characteristics of clipping operation, pre-filter operation and AM/AM conversion operation of non-linear amplifier used in the following process are assumed to be the same as those for the transmitter as shown in Fig.2.1. The clipped signal can be given by the following equation.

$$\hat{y}_k = \begin{cases} \hat{x}_k & |\hat{x}_k| \leq A_c \\ A_c e^{j\{\arg(\hat{x}_k)\}} & |\hat{x}_k| > A_c \end{cases} \tag{2.13}$$

The clipped signal is also processed for the same operation of pre-filter and non-linear amplifier at the transmitter. The output signal after the non-linear amplifier operation is given by the following equation.

$$\hat{s}_k = F\left[|\hat{z}_k|\right] \cdot e^{j\arg(\hat{z}_k)} \tag{2.14}$$

where $\hat{z}_k$ is the time domain signal at the output of pre-filter as shown in Fig. 2.3. Here, it should be noted that the operation of non-linear amplifier in (2.14) is performed for the digital sampled data by assuming the same AM/AM conversion characteristics as that operated in the radio frequency at the transmitter. Since the time domain signal given by (2.14) includes the clipping noise, band limitation noise and inter-modulation noise, (2.14) can be approximated by the following equation.

$$\hat{s}_k = \hat{x}_k + \hat{c}_k + \hat{b}_k + \hat{p}_k \tag{2.15}$$

By using (2.15), the error signal including all types of noises can be given by the following equation.

$$\begin{aligned} \hat{e}_k &= \hat{s}_k - \hat{x}_k \\ &= \hat{c}_k + \hat{b}_k + \hat{p}_k \end{aligned} \tag{2.16}$$

The error signal is then converted to the frequency domain signal by *FFT*, which is given by the following equation.

$$\hat{E}_n = \hat{C}_n + \hat{P}_n \tag{2.17}$$

In (2.17), the band limitation noise in the frequency domain is not existed in the desired frequency bandwidth of OFDM signal because the bandwidth of pre-filter is taken wider than the desired OFDM signal bandwidth. By subtracting (2.17) from (2.9), the frequency domain signal coped with both the clipping noise and inter-modulation noise can be obtained by the following equation.

$$\begin{aligned} \hat{R}_n' &= \hat{R}_n - \hat{E}_n \\ &= X_n' + (C_n' - \hat{C}_n) + (P_n' - \hat{P}_n) + W_n' \\ &\approx X_n' + W_n' \end{aligned} \tag{2.18}$$

If the BER performance of (2.18) is better than that for (2.9), the BER performance could be improved further by repeating the above procedures from (2.11) to (2.19) as shown in Fig.2.3. From the fact as mentioned above that the time domain signal given in (2.12) can be approximated by the original signal even when the BER performance of (2.18) is worse than that for (2.9), the divergence of BER performance would not occur during the iteration of above procedures. This will be also confirmed by the performance evaluation in the next section. The proposed IDAR method on the basis of above procedures could provide the better BER performance even when the non-linear amplifier is operated at the saturation region.

2.3 Satellite System Model

Figure 1.16 shows the typical satellite system model assumed in the following evaluations. The non-linear amplifier located at the earth station is assumed by the Solid State Power Amplifier (SSPA), which is modeled by Rapp [13]. The AM-AM and AM-PM conversion characteristics of SSPA modeled by Rapp are given by the following equations (1.44) and (1.45), respectively. In the following evaluations, the values for these parameters are assumed by $A_0 = 1$, $v = 1$, $p = 6$ and $\alpha_\phi = 0.01$ which can approximate the standard characteristics of SSPA

The output signal of SSPA, which corresponds to the uplink signal in the radio frequency, can be given by the following equation

$$s_{up}(t) = F_E\left[|s(t)|\right] e^{j\{\arg[s(t)]+\Phi_E[|s(t)|]\}} \tag{2.19}$$

where $s(t)$ is the OFDM signal at the input of earth station amplifier SSPA. The signal given by (2.19) is transmitted to the satellite and then input to the satellite non-linear amplifier after converting from the uplink to down link radio frequency. The non-linear amplifier located at the satellite station is assumed by the Traveling Wave Tube Power Amplifier (TWTA), which is modeled by Saleh [14]. The AM-AM and AM-PM conversion characteristics of TWTA modeled by Saleh are given by the following equations (1.46) and (1.47), respectively. The values for these parameters are assumed by $\alpha_a = 2$, $\beta_a = 1$, $\alpha_\theta = 2$ and $\beta_\theta = 1$ which can approximate the standard TWTA.

Figure 1.14 shows the input and output relationships of AM-AM and AM-PM conversion characteristics for both SSPA and TWTA when the parameters are given by the above values. In this chapter, we assume the higher non-linearity for the satellite amplifier (TWTA) than that for the earth station amplifier (SSPA) as shown in Fig.1.14. By using (2.19), the output signal of TWTA, which corresponds to the downlink signal in the radio frequency, is given by the following equation.

$$s_{dw}(t) = F_S\left[|s_{up}(t)|\right] e^{j\{\arg[s_{up}(t)]+\Phi_S[|s_{up}(t)|]\}} \tag{2.20}$$

The output signal of TWTA given in (2.20) includes the inter-modulation noises incurred at the SSPA and TWTA.

2.4 OFDM-IDAR Method for Satellite Channel

This chapter proposes OFDM-IDAR method designed for satellite channel, which included two high non-linear amplifiers located at the transmit earth station and satellite. To apply the OFDM technique to non-linear satellite channel, it is requested to mitigate the non-linear distortion occurred at the transmit earth station and satellite. The OFDM-IDAR method proposed in this section could compensate the non-linear distortion at the receiver by using the feature of OFDM signal in the time and frequency domains.

Figure 2.3 shows the structure of receiver for the proposed OFDM-IDAR method designed for satellite channel. The received downlink radio frequency signal affected by the non-linear amplifiers at the transmit earth station and satellite amplifiers is given by the following equation.

$$r(t) = s_{dw}(t) + w(t) \tag{2.21}$$

where $s_{dw}(t)$ is the downlink signal given in (2.20), and $w(t)$ is the additive white Gaussian noise (AWGN). The received RF signal $r(t)$ is first down converted (D/C) to the base band signal and digitized by A/D converter. The time domain sampled signal $r'(m,k)$ after compensating the phase rotation due to the AM-PM conversions of SSPA and TWTA and removing the OFDM guard interval (GI), can be expressed by the following equation.

$$\begin{aligned} r'(m,k) &= r(m,k)\cdot e^{-j\Phi^{c}_{ref}} \\ &= s(m,k) + i(m,k) + w(m,k) \end{aligned} \tag{2.22}$$

where, $s(m,k)$, $i(m,k)$ and $w(m,k)$ represent the original signal, composite inter-modulation noises incurred at the SSPA and TWTA, and AWGN on the k-th time domain sampled signal of m-th OFDM symbol, respectively. The phase rotation of Φ^{c}_{ref} due to the SSPA and TWTA at the operation points that is input back-off (IBO) can be estimated by using the low PAPR preamble symbols of which estimation method is proposed in Section 2.5.

The received time domain sampled signal given (2.22) is converted to the frequency domain signal by FFT, which is given by the following equation.

$$R'(m,n) = S(m,n) + I(m,n) + W(m,n) \tag{2.23}$$

In (2.23), the capital letter represents the frequency domain signal on n-th subcarrier of m-th OFDM symbol, which corresponds to its small letter given by (2.22) in the time domain. By using (2.23), the decision for the information data $\hat{S}(m,n)$ can be made for each sub-carrier in the frequency domain.

In the IDAR method, the time domain signal $\hat{s}(m,k)$, which is converted from the above decision data $\hat{S}(m,n)$ in the frequency domain, is used for the reconstruction of inter-

modulation noise. This is based on the fact that the OFDM time domain signal converted from the decision data in the frequency domain, which includes even some decision errors, would be almost the same as the original time domain signal without error.

The decision data $\hat{S}(m,n)$ in the frequency domain can be expressed by the following equation

$$R'(m,n) = S(m,n) + I(m,n) + W(m,n) \tag{2.24}$$

where $F(m,n)$ is the decision error, which can be expressed by the following equation.

$$F(m,n) = \begin{cases} 0 & if \ \hat{S}(m,n) = S(m,n) \\ \hat{S}(m,n) - S(m,n) & if \ \hat{S}(m,n) \neq S(m,n) \end{cases} \tag{2.25}$$

The time domain signal, which is converted from the frequency domain signal of (2.25), is given by the following equation.

$$\begin{aligned} \hat{s}(m,k) &= \sum_{n=0}^{N-1} \hat{S}(m,n) \cdot e^{j\frac{2\pi nk}{N}} \\ &= \sum_{n=0}^{N-1} S(m,n) \cdot e^{j\frac{2\pi nk}{N}} + \sum_{n=0}^{N-1} F(m,n) \cdot e^{j\frac{2\pi nk}{N}} \\ &= s(m,k) + f(m,k) \end{aligned} \tag{2.26}$$

where $s(m,k)$ shows the original time domain signal without decision error and $f(m,k)$ shows the time domain signal for the decision error occurred in the frequency domain. From (2.26), it can be seen that the decision error occurred in the frequency domain is spread over the N sample time domain signal and level of $f(m,k)$ would be relatively small as compared with $s(m,k)$. From this fact, it can be concluded that the time domain signal $\hat{s}(m,k)$ which is converted from the frequency domain signal $\hat{S}(m,n)$ including decision error, can be approximated by the original signal $s(m,k)$. Figure 2.6 (b) shows an example of relationships between $\hat{s}(m,k)$ and $s(m,k)$ when the number of decision errors occurred in the frequency domain is 5 as shown in Fig. 2.6 (a). From Fig.2.6 (b), it can be observed that the time domain signal for the decision error is much smaller than the original signal and the time domain signal $\hat{s}(m,k)$, which included 5 decision errors in the frequency domain is almost the same as the original signal without decision error. From this fact, the inter-modulation noise can be reconstructed in the time domain by using the decision data even including error in the frequency domain.

In the reconstruction of inter-modulation noise, the operation of non-linear amplifier is performed to the time domain signal, which is converted from the decision data in the frequency domain. Here, it should be noted that the operations of non-linear amplifiers in the IDAR method are performed on the digital sampled data by assuming the same AM-AM and

AM-PM conversion characteristics as that operated in the radio frequency at the earth station (SSPA) and satellite (TWTA). The estimation method for non-linear amplifiers characteristics of SSPA and TWTA is proposed in Section 2.6. The time domain signal at the output of AMP as shown in Fig.2.6 is given by the following equation.

$$\begin{aligned} r'(m,k) &= r(m,k)\cdot e^{-j\Phi^{c}_{ref}} \\ &= s(m,k)+i(m,k)+w(m,k) \end{aligned} \tag{2.27}$$

where, $\hat{s}(m,k)$ is the time domain signal converted from the frequency domain decision data $\hat{S}(m,n)$, and F_P and Φ_P are the AM-AM and AM-PM conversion characteristics for AMP which is the composite characteristics of SSPA and TWTA. By using (2.27), the inter-modulation noises incurred at the SSPA and TWTA could be estimated by the following equation.

$$\begin{aligned} \hat{e}(m,k) &= \hat{s}^{*}_{dw}(m,k)\cdot e^{-j\Phi^{c}_{ref}} - \hat{s}(m,k) \\ &\approx \hat{s}(m,k)+\hat{i}(m,k)-\hat{s}(m,k) \\ &\approx \hat{i}(m,k) \end{aligned} \tag{2.28}$$

where, the phase rotation of Φ^{c}_{ref} due to SSPA and TWTA is given in Section 2.4. The inter-modulation noise given by (2.28) is then converted to the frequency domain signal by FFT. By subtracting the reconstructed inter-modulation noise $\hat{E}(m,n)$ in the frequency domain from (2.28) as shown in Fig. 2.6, the frequency domain signal coped with the inter-modulation noise can be obtained by the following equation.

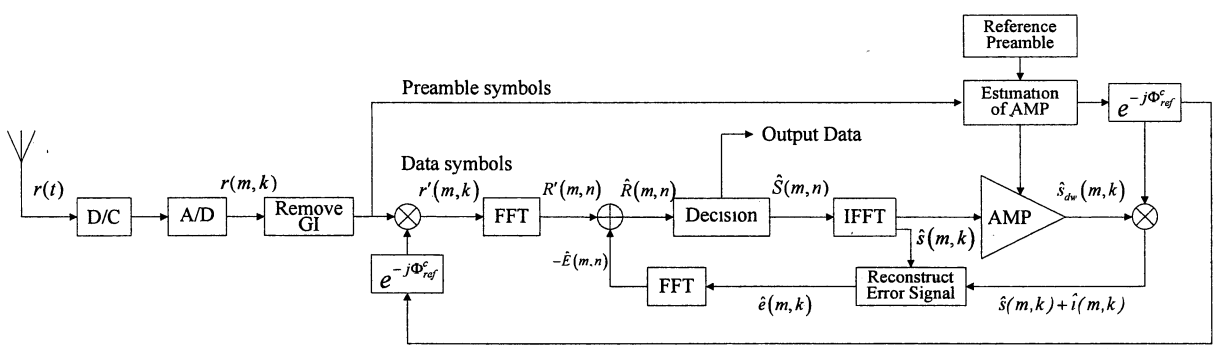

Fig. 2.5 Structure of proposed OFDM-IDAR receiver.

$$\begin{aligned} \hat{R}(m,n) &= R'(m,n)-\hat{E}(m,n) \\ &= S(m,n)+\left\{I(m,n)-\hat{I}(m,n)\right\}+W(m,n) \\ &\approx S(m,n)+W(m,n) \end{aligned} \tag{2.29}$$

If the BER performance for the decision data on (2.29) is better than that for (2.22), the BER performance could be improved further by repeating the above procedures from (2.22) to (2.29).

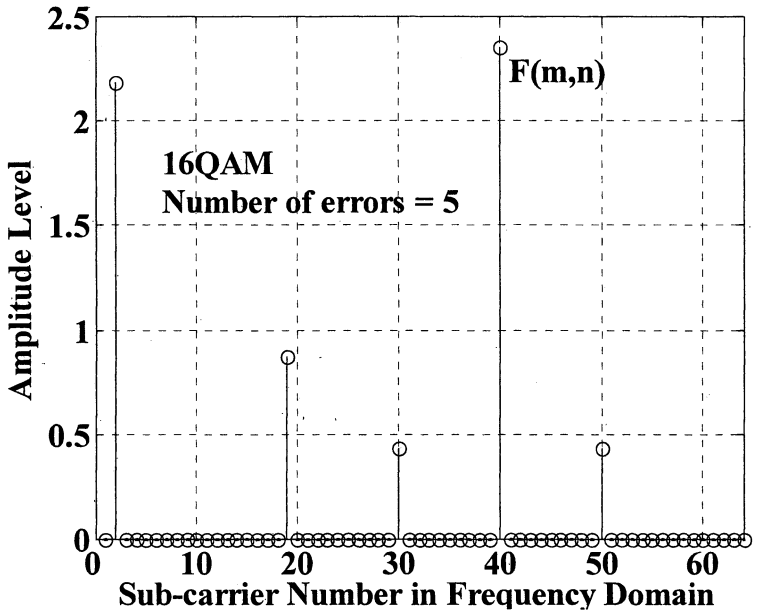

(a) Frequency domain signal.

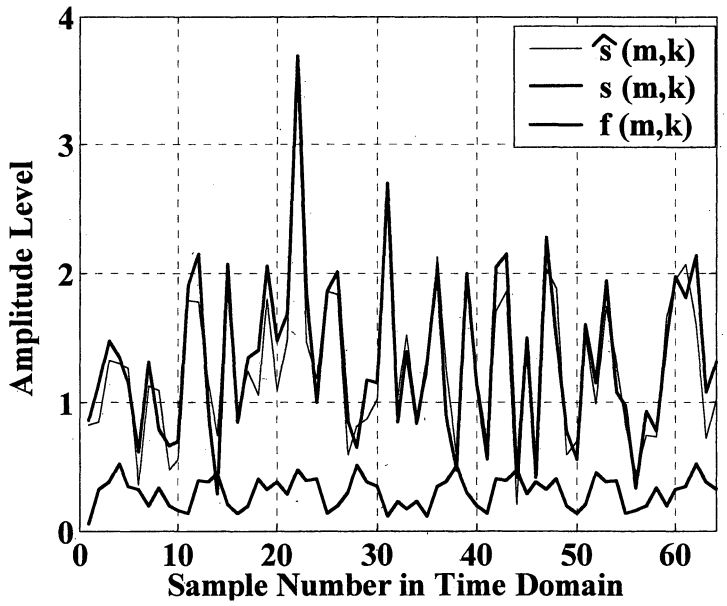

(b) Time domain signal.

Fig. 2.6. Decision error signal in frequency and time domains.

2.5 Estimation Method of Non-Linear Amplifier

In the OFDM-IDAR method proposed in Section 2.2, it is required for the input and output relationships of AMP, which includes the output power as a function of input power (AM-AM) and the output phase as a function of input power (AM-PM). These AM-AM and AM-PM conversion characteristics are also required to update at the receiver frequently because they may be changed due to the aging or the operation environments of earth station and satellite. The actual operation point (IBO: Input Back off) of satellite TWTA would be also changed because the signal power in the uplink would be fluctuated due to the rain attenuation.

The non-linear amplifier characteristics are usually measured by changing the power level of continuous waves (pure tone signal), of which signal envelope is the constant in the time domain. However, the pure tone signal has the line spectrum at the operating radio frequency with larger power level and this line spectrum would cause very large co-channel interference to other satellite systems employing the same frequency band.

Taking into account these conditions, we propose the estimation method for characteristics of non-linear amplifiers by using low PAPR preamble symbols. Fig. 2.7 shows the proposed frame structure for the estimation of non-linear amplifier, which consists of K low PAPR preamble symbols and L data symbols. As shown in Fig. 2.7, K low PAPR preamble symbols with increasing their power levels are transmitted to the receive earth station before transmitting the data symbols.

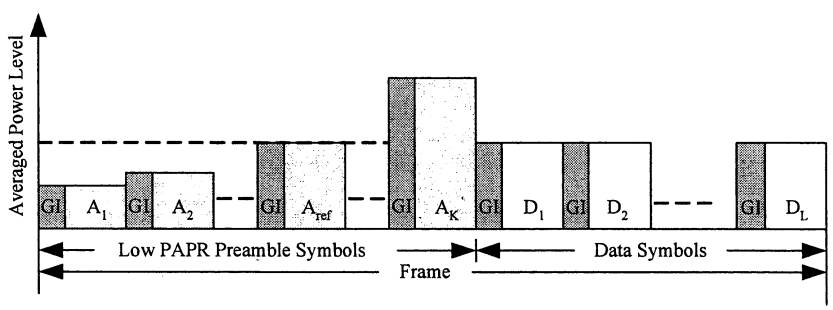

Fig. 2.7. Structure of proposed frame format.

In the generation of low PAPR preamble symbol, we employed the time-frequency domain-swapping algorithm [37], which can optimize the phase value for each OFDM sub-carrier so as to minimize the PAPR. In the optimization of phase value for preamble symbol, the amplitude of all sub-carriers in the preamble symbol is kept by the constant value. From this fact, the frequency spectrum of low PAPR preamble symbol becomes flat over the whole allocated bandwidth. Fig. 2.8 shows an example of time domain signals both for low PAPR preamble symbol and conventional OFDM symbol. From the figure, it can be observed that the low PAPR preamble symbol has the similar feature of pure tone signal with the constant

envelope in the time domain, while its frequency spectrum density is flat over the whole occupied bandwidth. From these features of low PAPR preamble symbol, it is possible to measure the input and output relationships of non-linear amplifier precisely and not to interfere to other systems using the same frequency band.

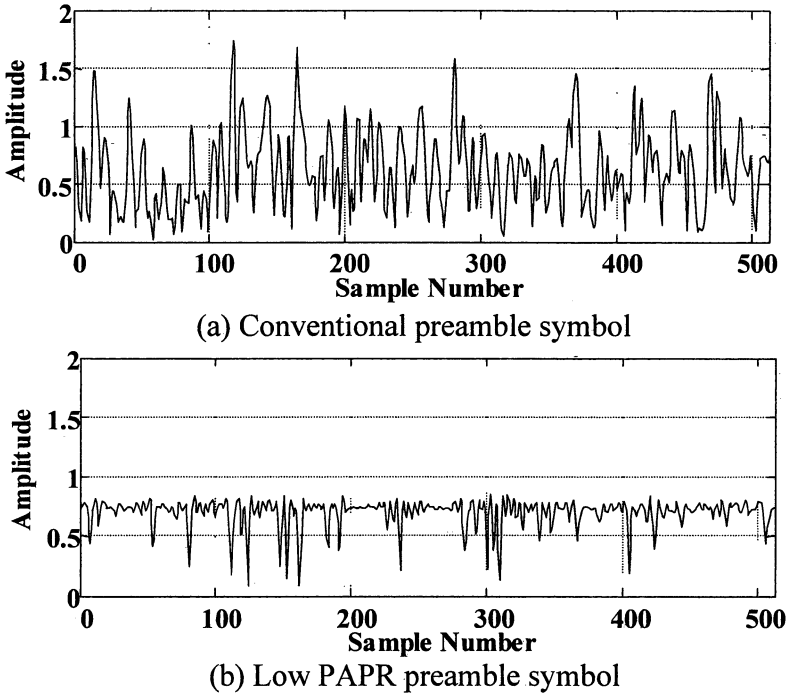

(a) Conventional preamble symbol

(b) Low PAPR preamble symbol

Fig. 2.8. Envelope of preamble symbol in the time domain.

From the proposed frame structure as shown in Fig. 2.7, it can be seen that the power levels of preamble symbols has the certain dynamic range at the center of reference preamble symbol of which power level is taken as the same as that for the data symbols. Therefore, the relative non-linear amplifier characteristics, which are normalized by the power level of reference preamble symbol can be estimated by measuring the received power level and phase difference of received low PAPR preamble symbols.

2.5.1 Estimation of AM-AM Conversion Characteristics

The input power level for the composite non-linear amplifier can be expressed in the values relative to the transmission power level of reference preamble symbol as shown in Fig. 2.7, because the relative transmission power levels between the preamble symbols are known at the receiver. If the input power level of reference preamble symbol is assumed by 0dB, the relative input power levels for all preamble symbols can be given by the following equation.

$$P_m^{input} = 10\log_{10}\left(\frac{P_m^t}{P_{ref}^t}\right) \quad (m = 1 \sim K) \tag{2.30}$$

where, P_m^t and P_{ref}^t are the transmission power levels at the m-th preamble symbol and reference preamble symbol, respectively. The output power level as a function of input power level given by (2.30) can be estimated by measuring the received power level for the preamble symbols at the receive earth station. The received power level for the preamble symbol m can be measured in the time domain by using the following equation.

$$P_m^r = \frac{1}{N}\sum_{k=0}^{N-1}|r(m,k)|^2 \tag{2.31}$$

where, N is the number of sample points in one OFDM symbol. By using the all measured power levels for preamble symbols, the preamble symbol with the maximum power level can be detected by the following equation.

$$P_{\max}^r = \underset{m=1\sim K}{Max}\left[P_m^r\right] \tag{2.32}$$

By using (2.32), the relative output power level of composite AMP at the corresponding relative input power level of (2.30) can be given by the following equation.

$$P_m^{output} = 10\log_{10}\left(\frac{P_m^r}{P_{max}^r}\right) \quad (m=1\sim K) \tag{2.33}$$

By using (2.30) and (2.33), the relative combined AM-AM conversion characteristics for SSPA and TWTA can be estimated as a function of the input power levels for K preamble symbols. The AM-AM conversion characteristics between measurement results of two consecutive preamble symbols can be estimated by using the interpolation method.

2.5.2 Estimation of AM-PM Conversion Characteristics

The output phase as a function of input power level (AM-PM) for the composite characteristics of SSPA and TWTA can be estimated by measuring the phase differences in the frequency domain between the transmitted and received sub-carriers for the preamble symbols. The received preamble symbol in the frequency domain can be given by the following equation.

$$R(m,n) = S(m,n)\cdot e^{j\left\{\Phi_E\left(\sqrt{P_m^e}\right)+\Phi_S\left(\sqrt{P_m^s}\right)\right\}} \tag{2.34}$$

where, $S(m,n)$ is the transmitted data on n-th sub-carrier of m-th symbol, P_m^e and P_m^s are power levels of m-th preamble symbol at the input of SSPA and TWTA, respectively. Since the transmitted data $S(m,n)$ in the preamble symbols are known at the receiver, the averaged phase rotation due to both SSPA and TWTA can be estimated by the following equation.

$$\begin{aligned}\Phi_m^c &= \frac{1}{N}\sum_{n=0}^{N-1} Arg\left[\frac{R(m,n)}{S(m,n)}\right] \\ &= \Phi_E\left(\sqrt{P_m^e}\right)+\Phi_S\left(\sqrt{P_m^s}\right)\end{aligned} \tag{2.35}$$

By using (2.30) and (2.35), the output phase as a function of input power level (AM-PM) can be estimated for the composite characteristics of SSPA and TWTA. The AM-PM conversion characteristics between two measurement results of two consecutive preamble symbols can be estimated by using the interpolation method.

The averaged phase rotation obtained at the reference preamble symbol will be used for the compensation of phase rotation for the data symbols as used in (2.22) and (2.28), because the averaged power level of reference preamble symbol is taken as the same as that for the data symbols as shown in Fig. 2.7.

The required dynamic range of power level between the first and *K*-th preamble symbols can be decided on the basis of averaged power level of transmission data symbol and possible dynamic range of power level for OFDM data symbol in the time domain. The dynamic range of power level for OFDM signal is usually around 30dB from -20dB to 10dB at the center of averaged power level of 0dB. From these facts, the required dynamic range of power level over the preamble symbols can be set from -10dB to +10dB in which the power level of reference symbol is set by 0dB. Here, the input and output relationships of non-linear amplifier from -20dB to -10dB can be estimated precisely by using the extrapolation method, because these regions of non-linear amplifier can be assumed as the linear characteristics.

Figure 2.9 shows the actual and estimated input and output relationships of non-linear amplifier characteristics when the input power level of reference preamble symbol is -4dB. Here, the input level of reference preamble symbol is corresponding to the IBO of data symbols. To simplify the explanation, the non-linear amplifier is assumed only to use TWTA. From Fig.2.9 (a), it can be seen that the input level of non-linear amplifier for 11 low PAPR preamble symbols is changed from -14dB to 6dB by 2dB step at the center of reference preamble symbol of which level is -4dB. By using the proposed estimation method described above, the estimated input and output relationships of non-linear amplifier characteristics can be given as shown in Fig.2.9 (b). In Fig.2.9 (b), it should be noted that the estimated characteristics of non-linear amplifier is obtained only by the relative input and output relationships, which is normalized by the power level of reference preamble symbol. Since the inter-modulation noise is reconstructed by using the decision data, which has the same power level as the reference preamble symbol, the relative input and output relationships of non-linear amplifier can be used in the IDAR method as described in the previous section.

By using the proposed estimation method, the higher estimation accuracy can be achieved even when the characteristics of non-linear amplifiers located at the earth station and

satellite are changed frequently due to the aging or operation environments including the uplink rain attenuation, because the characteristics of non-linear amplifier can be estimated every frame by using the low PAPR preamble symbols. The accuracy of proposed estimation method with the interpolation and extrapolation methods would depend on the number of employed preamble symbols and power allocation method of preamble symbols over K preamble symbols. The detailed evaluation on the estimation accuracy of proposed estimation method is presented in the next section.

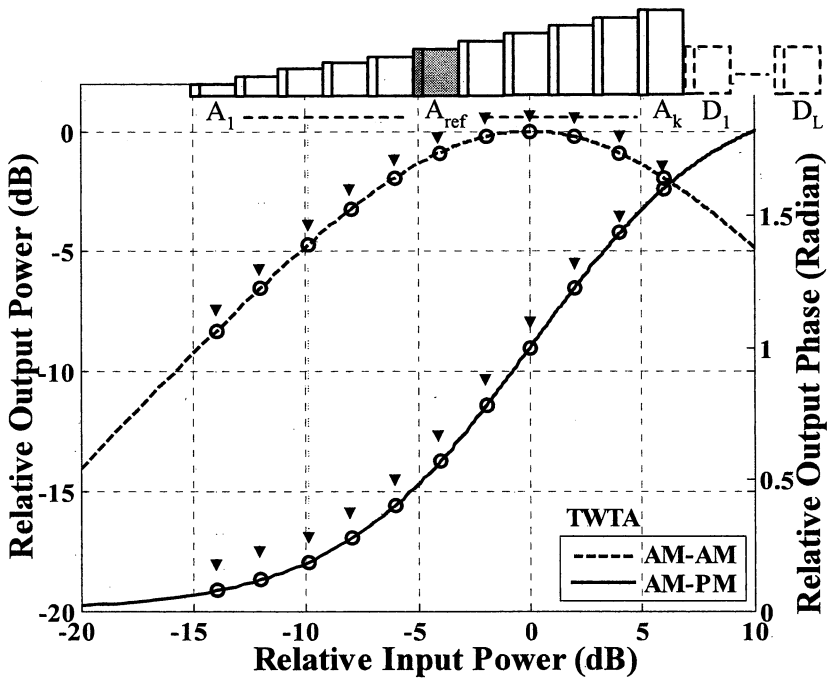

(a) Actual input and output relationships of non-linear amplifier.

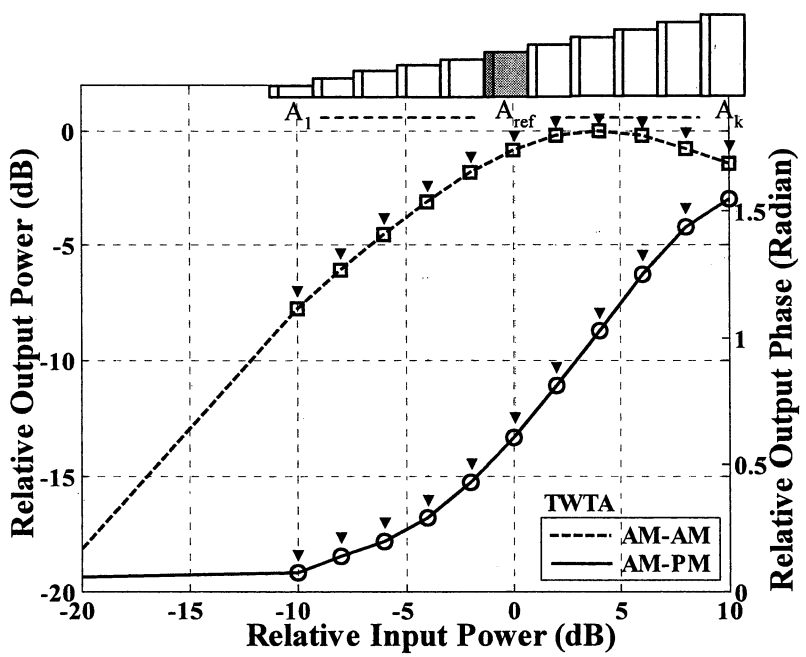

(b) Estimated input and output relationships of non-linear amplifier.

Fig. 2.9. Schematic figure of proposed estimation method.

2.6 Performance Evaluations

This section presents the various computer simulation results to verify the performance of OFDM-IDAR method with the proposed estimation method. Table 2.1 shows the simulation parameters to be used in the following evaluations. The modulation method is assumed by 16QAM with coherent detection method and the channel model is AWGN channel, which corresponds to the fixed and broadcasting satellite systems. The achievable transmission data rate for the proposed OFDM-IDAR method is 90.1Mbit/s by using the frequency bandwidth 25MHz out of 27MHz which is taken into account the interference to adjacent channel. In the table, the parameters for conventional single carrier (SC) transmission with 16QAM are also shown as the purpose of comparison with the proposed OFDM-IDAR method. The frame length for the proposed method is assumed by 22.73ms including 11 low PAPR preamble symbols and 1000 data symbols. Assuming this frame structure, the non-linear amplifier characteristics both for SSPA and TWTA can be estimated every 22.73ms, which would be enough small cycle to cope with the fluctuation of amplifier characteristics due to the aging or operation conditions including the rain attenuation in the uplink.

Table 2.1 Simulation parameters.

Allocated occupied bandwidth	26MHz
Modulation method	16QAM
Earth station amplifier	SSPA
Satellite amplifier	TWTA
Conventional Single Carrier Transmission (SC) Method	
Number of sample points/data symbol	4
Number of data symbols / frame	128
Type of Tx and Rx filters	Root Nyquist
Roll-off factor	0.4
Transmission data rate	104 Mbit/s
Proposed OFDM-IDAR Method	
Number of FFT points	512
Number of sub-carriers	128
Symbol duration	4.92 us
Guard interval	0.1 us
Number of preamble symbols / frame	11
Number of data symbols / frame	1000
Frame duration	5.08 ms
Transmission data rate	100.8 Mbit/s

2.6.1 Accuracy of Proposed Estimation Method

The estimation accuracy for the characteristics of composite AMP would be much dependent on the design of low PAPR preamble symbols including the number of preamble symbols and power allocation method for them. Table 2.2 shows three cases of preamble symbol designs for the evaluation of proposed estimation method. All cases are taken by 20dB as the dynamic range from -10dB to 10dB. The number of preamble symbols for Cases 1, 2 and 3 are taken by 21, 11 and 5, respectively. In Table 2.2, the Ideal means that the characteristics of non-linear amplifiers both for SSPA and TWTA are given by equations (1), (2), (4) and (5). Table 2.2 shows the computer simulation results on the required C/N to achieve BER=10^{-4} for all cases. In the simulation, only the downlink noise $(C/N)_{dw}$ is considered as 20dB and IBO for the earth station SSPA and satellite TWTA are taken by -3dB and -4dB, respectively. From the table, it can be observed that Cases 1 and 2 show the same required C/N to achieve BER=10^{-4} with 1.2dB degradation from the Ideal case, although the number of preamble symbols for Case 1 is larger than that for Case 2 by almost 2 times. Case 3 with fewer number of preamble symbols shows 2.8dB degradation from the Ideal case. From these results, it can be concluded that Case 2 using 11 preamble symbols of which power levels are increasing by 2 dB step from -10dB to +10dB is the best design for preamble symbols. In the following evaluation, Case 2 is used for the estimation of composite characteristics of AMP.

Figures 2.9 (a) and (b) show the estimated composite characteristics of AMP when IBO of SSPA is taken by -3dB and -10dB, respectively. In the simulation, Case 2 is used as the preamble design, and the downlink $(C/N)_{dw}$ is 20dB. The ideal characteristics of composite AMP when using the equations are also shown in the figures. From the figure, it can be observed that proposed method can estimate almost the same AMP characteristics as the Ideal case. Here it should be noted that the composite characteristics of AMP shown in Fig.2.8 (b) is almost the same as that for the satellite amplifier of TWTA when the IBO of earth station amplifier of SSPA is -10dB. This fact is come from that the non-linear characteristics of SSPA can be considered as the linear because of taking enough IBO at the transmit earth station.

Figure 2.10 shows the BER performances of OFDM-IDAR with proposed estimation method when changing the number of iterations of IDAR method. In the figure, BER performance when assuming the ideal characteristics of SSPA and TWTA are also shown as comparing with the proposed estimation method using Case 2. The IBO for the SSPA and TWTA are taken by -3dB and -4dB, respectively. From the figure, it can be observed that the BER performance of OFDM-IDAR with the proposed estimation method is slightly degraded as compared with the ideal case. It can be also observed that the BER performances for the proposed methods at $(C/N)_{dw}$ =20dB are converged when the number of iterations is taken

larger than 6. From these results, the following simulations for OFDM-IDAR method are assumed to use 6 as the iteration number for the IDAR method

Table 2.2 List of power allocation methods.

	Power allocation of preamble symbols	No. of preamble symbols	Required C/N at BER=10^{-4}
Ideal	*NA*	*NA*	19 dB
Case 1	-10dB to +10dB by 1dB step	*21*	20.2 dB
Case 2	-10dB to +10dB by 2dB step	*11*	20.2 dB
Case 3	-10dB to +10dB by 5dB step	*5*	21.8 dB

Figure 2.11 shows the BER performances at the downlink $(C/N)_{dw}$=20dB both for the conventional SC transmission method and OFDM-IDAR method when changing IBO of satellite TWTA. The IBO of transmit earth station SSPA is fixed by -3dB. In the figure, BER performances when assuming the ideal characteristics of SSPA and TWTA for IDAR method are also shown.

Here, the downlink $(C/N)_{dw}$ is defined by using the desired signal power at the output of satellite TWTA of which IBO is 0dB. In this definition of $(C/N)_{dw}$, the actual received C/N at the receive earth station would be changed from the given $(C/N)_{dw}$ according to the IBO of TWTA. The power of inter-modulation noise could be improved as decreasing IBO of TWTA while the desired signal power at the output of TWTA would be reduced. In other words, there is the trade-off between the inter-modulation noise power and the desired signal power according to the value of TWTA IBO. Therefore, the best BER performance could be achieved at the optimum value of TWTA IBO, which is compromised of them. The definition of C/N assumed here is based on the actual satellite communications systems, which are taken into account the desired signal power at the output of non-linear amplifier, and can evaluate the usage of power efficiency of non-linear amplifier.

From the figure, it can be observed that the OFDM-IDAR with proposed estimation method has the optimum TWTA IBO at -4dB, which can achieve the best BER performance, while the optimum TWTA IBO for the conventional SC transmission method is around -8dB. It can be also seen that the proposed method at the optimum TWTA IBO shows much better BER performance than that for the conventional SC method. In other words, the proposed OFDM-IDAR method can operate at the higher TWTA IBO with keeping the better BER performance than that for the conventional SC modulation method. From these results, it can be concluded that the proposed OFDM-IDAR method can achieve the higher usage of non-linear amplifier with keeping the better BER performance.

Figure 2.12 shows the BER performances both for the conventional SC and OFDM-IDAR methods when changing the downlink $(C/N)_{dw}$. In the simulation, the optimum IBO for satellite TWTA are taken by -4dB and -8dB for the proposed and conventional SC methods, respectively based on the results of Fig.2.11. The IBO of earth station SSPA is fixed by -3dB. From the figure, it can be observed that the OFDM-IDAR with the proposed estimation method shows slightly higher BER performance than that for the ideal estimation method. However, the proposed method can achieve much better BER performance than that for the conventional SC transmission method. From these results, it can be concluded that the proposed OFDM-IDAR with the estimation method for non-linear amplifier characteristics can achieve the higher transmission data rate with keeping the better BER performance than that for the conventional SC transmission method in the non-linear satellite channel.

2.6.2 BER Performance of OFDM-IDAR Method

Figure 2.11 shows the BER performances of OFDM-IDAR with proposed estimation method when changing the number of iterations of IDAR method. In the figure, BER performance when assuming the ideal characteristics of SSPA and TWTA are also shown as comparing with the proposed estimation method using Case 2. The IBO for the SSPA and TWTA are taken by -3dB and -4dB, respectively. From the figure, it can be observed that the BER performance of OFDM-IDAR with the proposed estimation method is slightly degraded as compared with the ideal case. It can be also observed that the BER performances for the proposed methods at $(C/N)_{dw}$ =20dB are converged when the number of iterations is taken larger than 6. From these results, the following simulations for OFDM-IDAR method are assumed to use 6 as the iteration number for the IDAR method.

Figure 2.12 shows the BER performances at the downlink $(C/N)_{dw}$ =20dB both for the conventional SC transmission method and OFDM-IDAR method when changing IBO of satellite TWTA. The IBO of transmit earth station SSPA is fixed by -3dB. In the figure, BER performances when assuming the ideal characteristics of SSPA and TWTA for IDAR method are also shown.

Here, the downlink $(C/N)_{dw}$ is defined by using the desired signal power at the output of satellite TWTA of which IBO is 0dB. In this definition of $(C/N)_{dw}$, the actual received C/N at the receive earth station would be changed from the given $(C/N)_{dw}$ according to the IBO of TWTA. The power of inter-modulation noise could be improved as decreasing IBO of TWTA while the desired signal power at the output of TWTA would be reduced. In other words, there is the trade-off between the inter-modulation noise power and the desired signal power according to the value of TWTA IBO. Therefore, the best BER performance could be achieved at the optimum value of TWTA IBO, which is compromised of them. The definition of C/N assumed here is based on the actual satellite communications systems, which are taken

into account the desired signal power at the output of non-linear amplifier, and can evaluate the usage of power efficiency of non-linear amplifier.

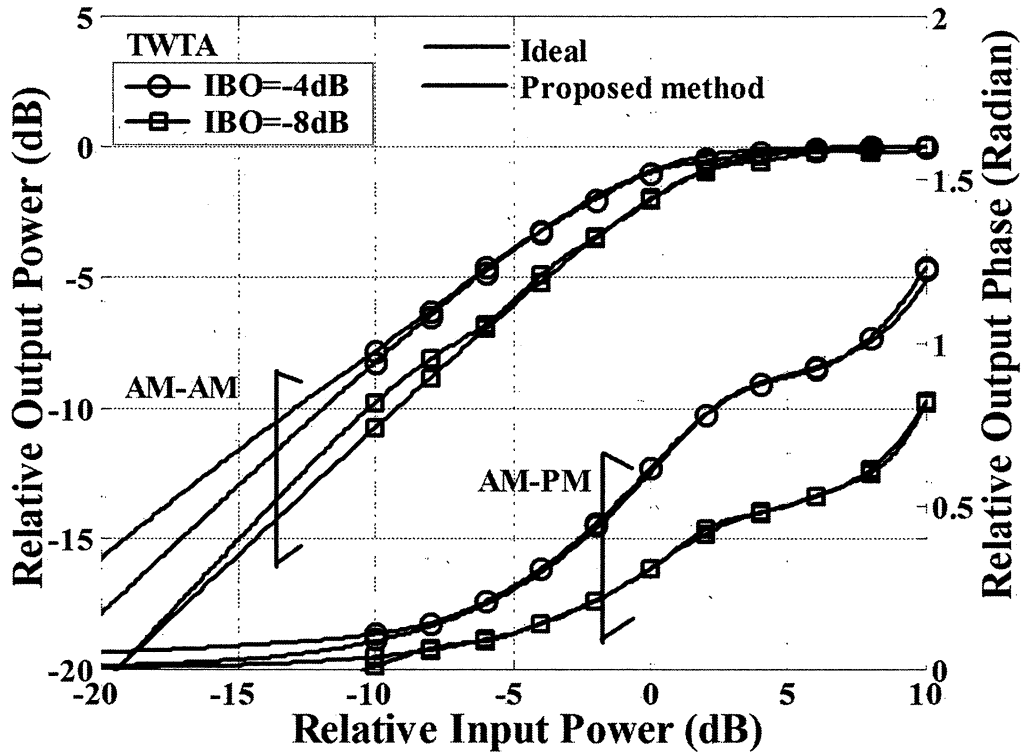

(a) SSPA IBO = -3dB

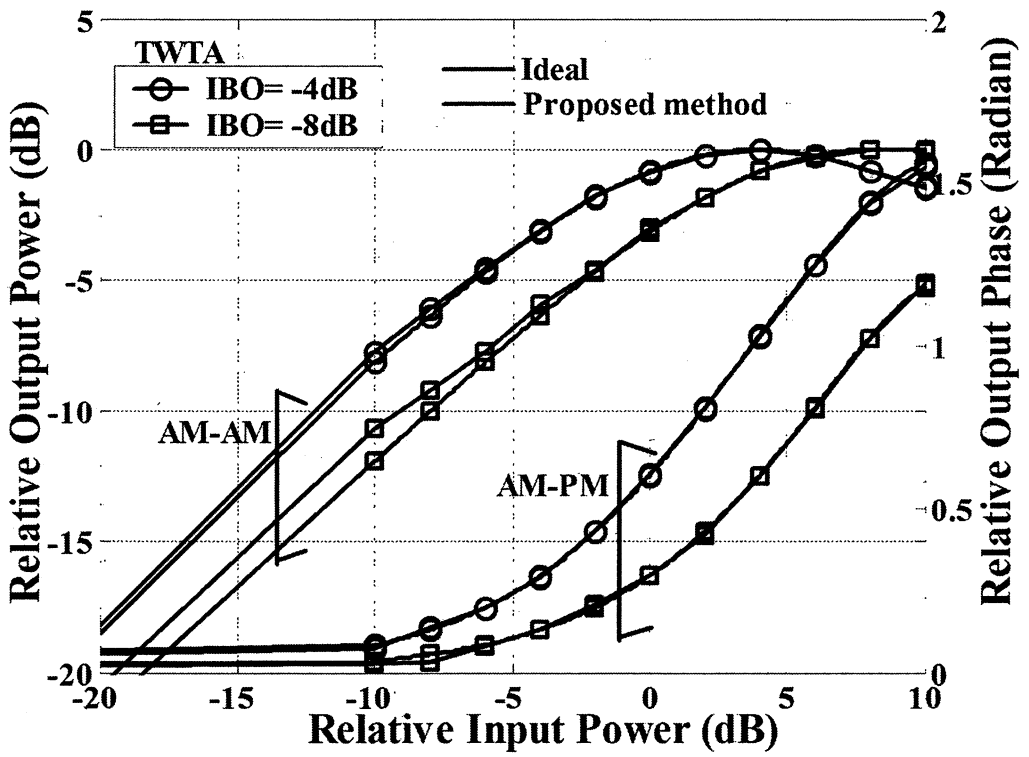

(b) SSPA IBO = -10dB

Fig. 2.10. Estimation accuracy of composite characteristics of SSPA and TWTA.

From the figure, it can be observed that the OFDM-IDAR with proposed estimation method has the optimum TWTA IBO at -4dB, which can achieve the best BER performance, while the optimum TWTA IBO for the conventional SC transmission method is around -8dB. It can be also seen that the proposed method at the optimum TWTA IBO shows much better BER performance than that for the conventional SC method. In other words, the proposed OFDM-IDAR method can operate at the higher TWTA IBO with keeping the better BER performance than that for the conventional SC modulation method. From these results, it can be concluded that the proposed OFDM-IDAR method can achieve the higher usage of non-linear amplifier with keeping the better BER performance.

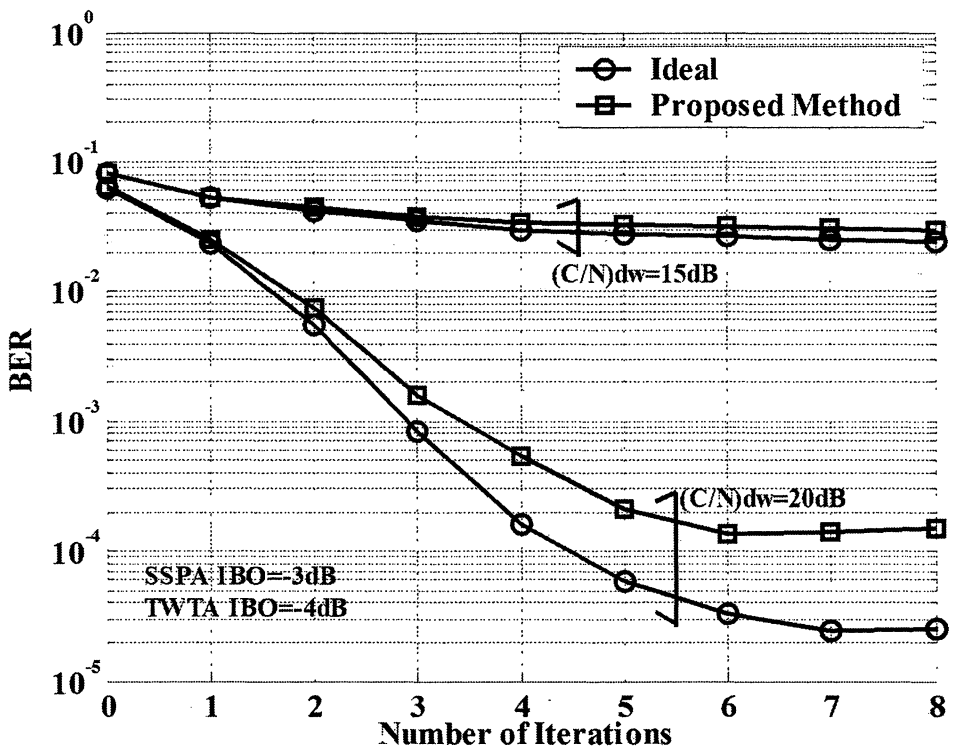

Fig. 2.11. BER performance versus number of iterations.

Figure 2.13 shows the BER performances both for the conventional SC and OFDM-IDAR methods when changing the downlink $(C/N)_{dw}$. In the simulation, the optimum IBO for satellite TWTA are taken by -4dB and -8dB for the proposed and conventional SC methods, respectively based on the results of Fig.2.10. The IBO of earth station SSPA is fixed by -3dB. From the figure, it can be observed that the OFDM-IDAR with the proposed estimation method shows slightly higher BER performance than that for the ideal estimation method. However, the proposed method can achieve much better BER performance than that for the conventional SC transmission method. From these results, it can be concluded that the proposed OFDM-IDAR with the estimation method for non-linear amplifier characteristics

can achieve the higher transmission data rate with keeping the better BER performance than that for the conventional SC transmission method in the non-linear satellite channel

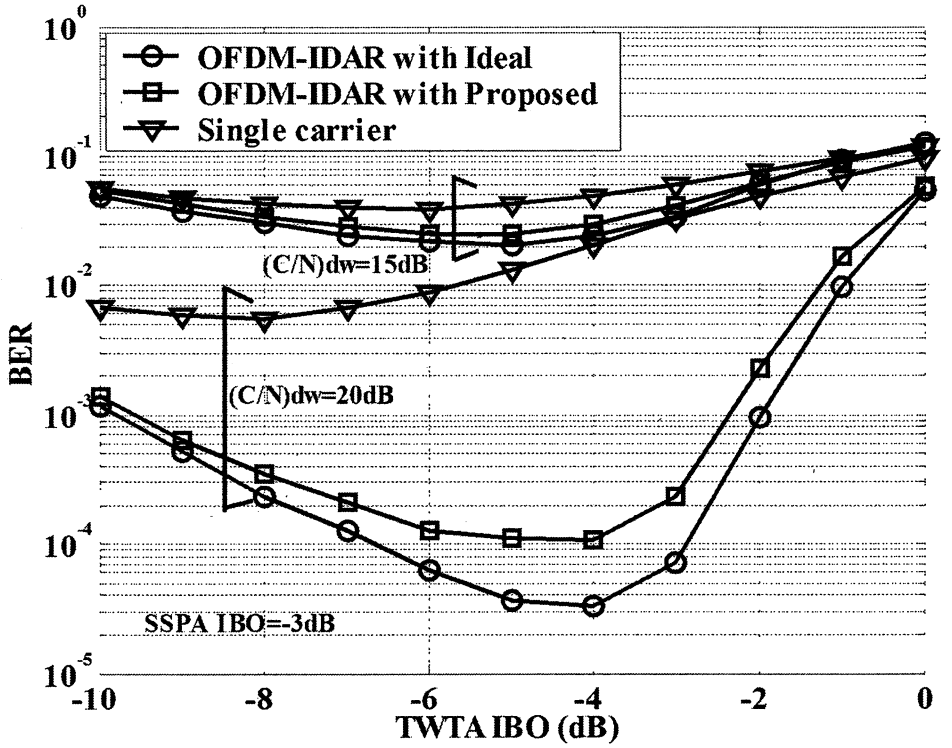

Fig. 2.12. BER performance versus IBO.

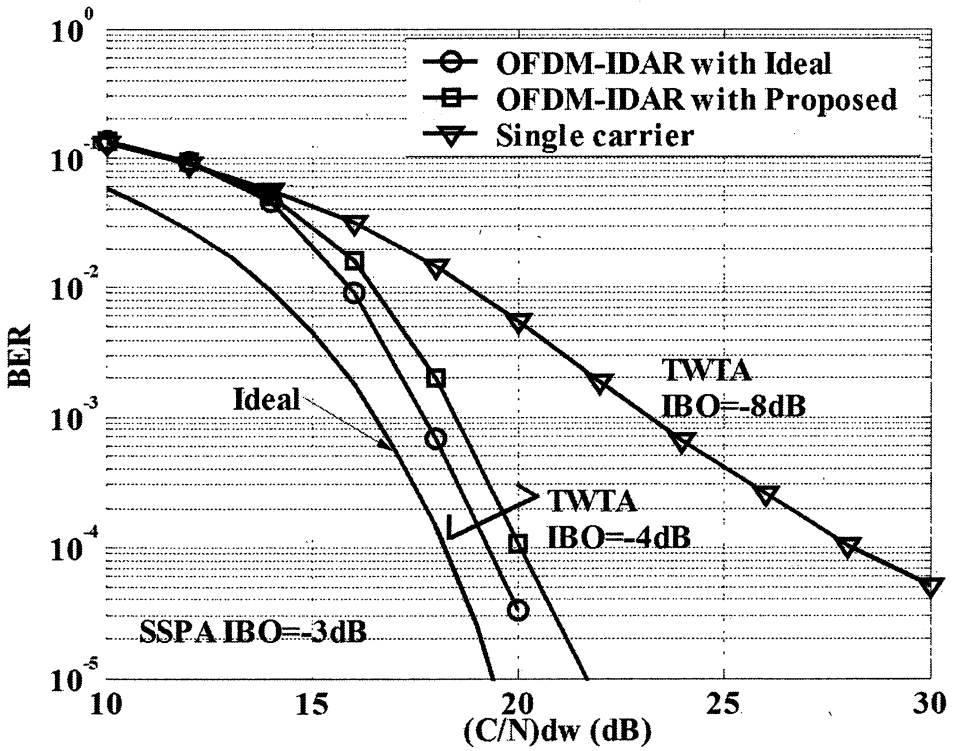

Fig. 2.13. BER performance versus downlink C/N when IBO is selected by optimum.

2.7 Conclusions

This chapter proposed the broadband satellite communication systems by using multi-level QAM-OFDM technique with IDAR method designed for satellite channel. This chapter also proposed estimation method for non-linear satellite amplifiers by using the low PAPR preamble symbols, which is required for the IDAR method. From the computer simulation results, we confirmed that the proposed estimation method for non-linear amplifier characteristics can achieve the better accuracy and can be used in the IDAR method. We also confirmed that the OFDM-IDAR system with the proposed estimation method shows much better BER performance than that for the conventional single carrier transmission method in the non-linear satellite channel. From these results, it could be concluded that the proposed multi-level QAM-OFDM technique with IDAR method can be used in the fixed and broadcasting satellite systems to provide the multimedia broadband satellite services with keeping the better BER performance. This chapter presented the evaluation results only in the AWGN channel assuming the fixed and broadcasting satellite systems. The proposed method could achieve the better BER performance even for the mobile satellite systems including multi-path fading, because the proposed method is based on the OFDM technique.

CHAPTER 3

A NEW WEIGHTING FACTOR OF PTS OFDM WITH LOW COMPLEXITY

Partial Transmit Sequence (PTS) method is a well - known method which can reduce the peak-to-average ratio (PAPR) for an OFDM signal. A major drawback of PTS method is its higher computation complexity due to the necessity of larger number of inverse fast Fourier transforms (IFFT). The PTS method with low computation complexity, called decomposition PTS sub-blocking was proposed [17] which employs the radix-r inverse fast Fourier transform (IFFT) for the signals at the middle stages of an N-point radix-r IFFT and decimation in frequency (DIF) domain. This method (DIF-IFFT) can reduce the computation complexity relatively while providing PAPR reduction similar to other PTS techniques. On the other hand, PTS method can improve PAPR reduction performance very well as increasing a number of weighting factors and clusters. However, the size of side information proportionally increases as increasing the number of weighting factors or/and clutters, which are required to inform the side information to the receiver for recovering the original data. In this chapter, we propose the new weighting factor technique in conjunction with D-PTS sub-blocking technique which can improve both the PAPR performance and computation complexity without any increasing of side information.

3.1. Introduction

The OFDM technique has been received a lot of attentions especially in the field of wireless communications because of its efficient usage of frequency bandwidth and robustness to the multi-path fading. From these advantages, the OFDM has already been adopted as the standard transmission technique in the wireless LAN systems and the terrestrial digital broadcasting system [2-4]. One of the limitations for using OFDM technique is the larger PAPR of its time domain signal. The larger PAPR signal would cause the severe degradation of bit error rate (BER) performance due to the inter-modulation noise occurring in the non-linear amplifier [9].

The PTS approach is well known method as a distortion less technique based on combining signal sub-blocks or clusters, which are multiplied by weighting factors. Although the PAPR performance can be improved by multiplying the optimum weighting factor, the weighting factor employed at the transmitter is required to inform to the receiver as side information. In the PTS method, the PAPR reduction performance can be improved as increasing the number of clusters or weighting factor. However, the computation complexity and the size of side information increase relatively.

To overcome this problem, a PTS method with low complexity was proposed [17]. In this method, called DIF-PTS, the computation complexity is reduced by employing the DIF-IFFT in which an input symbol sequence is partially transformed using the first stages of DIF-IFFT into an intermediate signal sequence and the intermediate signal sequence is partitioned into a number of intermediate signal subsequences. Then, the remaining stages of DIF-IFFT are applied to each of the intermediate signal subsequences and the resulting signal subsequences are summed after being multiplied by each member of a set of rotating vectors to yield distinct OFDM signal sequences. The one with the lowest PAPR among these OFDM signal sequences is selected for transmission. The DIF-PTS method reduces the computational complexity relatively while it shows almost the same performance of PAPR reduction as that of the conventional PTS OFDM scheme.

In this chapter, we propose a new weighting factor technique for the PTS method in conjunction with DIF-PTS method, which can improve both the PAPR performance and computation complexity. The proposed method can show the better PAPR reduction performance than that for the DIF-PTS method without any increasing of the size of side information and computation complexity.

In the following of this chapter, Section 3.2 presents the characteristics of PAPR performance for the OFDM signal. Section 3.3 presents the conventional PTS method. Section 3.4 presents the proposed method and Section 3.5 presents various computer

simulation results to verify the effectiveness of the proposed method as comparing with the conventional PTS method. Some conclusions are given in Section 3.6.

3.2. PAPR Distribution of OFDM Signal

OFDM signal in the time domain is generated by summation of all modulated sub-carriers. Firstly we consider the simple case where all modulated sub-carriers $X(n)$ are independent and identically distributed (i.i.d.) complex Gaussian random variables with zero mean and unit variance. The statistical properties of OFDM signal $x(k)$ in the time domain can be also considered as the i.i.d. Gaussian random variables with zero mean and unit variance. Since the data information prior to the modulation is usually considered as the random pattern, the sub-carriers $X(n)$ modulated with QPSK or multi level-QAM can be approximated as independent discrete uniform random variable. From this fact, the distribution of PAPR for the time domain signal can be considered as i.i.d. Gaussian [32]. This means that the PAPR will be changed according to the pattern of input information data, employed modulation method and the number of sub-carriers.

The number of PAPR values for all kind of data sequences can be given by the following equation which depends on the type of modulation method and the number of sub-carriers.

$$P_{Total} = (Mod)^{M} \tag{3.1}$$

where M is the number of sub-carriers and Mod represents the modulation levels which be decided by the type of modulation method. From (3.1), it can be observed that the possible number of PAPR values becomes huge number. This means that it is very hard to determine the optimum weighting factor in the PTS method which provide the best PAPR performance as increasing the number of sub-carriers. However, the OFDM signal in the time domain has the special characteristics which could be used to determine the optimum weighting factor for the PTS method.

In the following, we show the case of small number of sub-carriers for the purpose of simply explanations. Fig.3.1 shows the relationship between PAPR value and data sequence number. In the figure, the modulation method is QPSK and the number of sub-carrier is 4. The possible data information [0, 1, 2, 3] is mapped into complex number [$1+j$, $1-j$, $-1+j$ and $-1-j$], respectively. By using (3.1), the possible number of PAPR values is given by 256 ($=4^4$). From Fig.3.1, it can be observed that PAPR performance is cyclically changed and the PAPR values for the first and the second are completely the same.

The PTS method is a kind of multiple signal representation in the PAPR reduction method. The conventional PTS method controls the phase of data sub-carriers by multiplying weighting factor and selects the lowest PAPR for the transmitted signal. The weighting factor $e^{j\phi}$ using in the conventional PTS method is usually defined by the following discrete phase.

$$\phi \in \left\{ \frac{2\pi i}{W} \mid i = 0,\ldots,W-1 \right\} \tag{3.2}$$

where W is the number of predetermined discrete phase. When the number of clusters is assumed by 2 and the number of weighting factor W is 2 phases, [0, π], the PAPR value has the same [32] when the first cluster is fixed by one of the weighting factor and the second cluster is changed so as to obtain the lowest PAPR performance. After multiplied the weighting factor, the PAPR performance becomes the same because it's cyclic of PAPR performance as shown in Fig. 3.1. From this reason, the PAPR reduction performance for PTS method can be improved further with less computation complexity. In other words, there is the possibility to improve the PAPR reduction performance by using those characteristics of OFDM signal in the time domain.

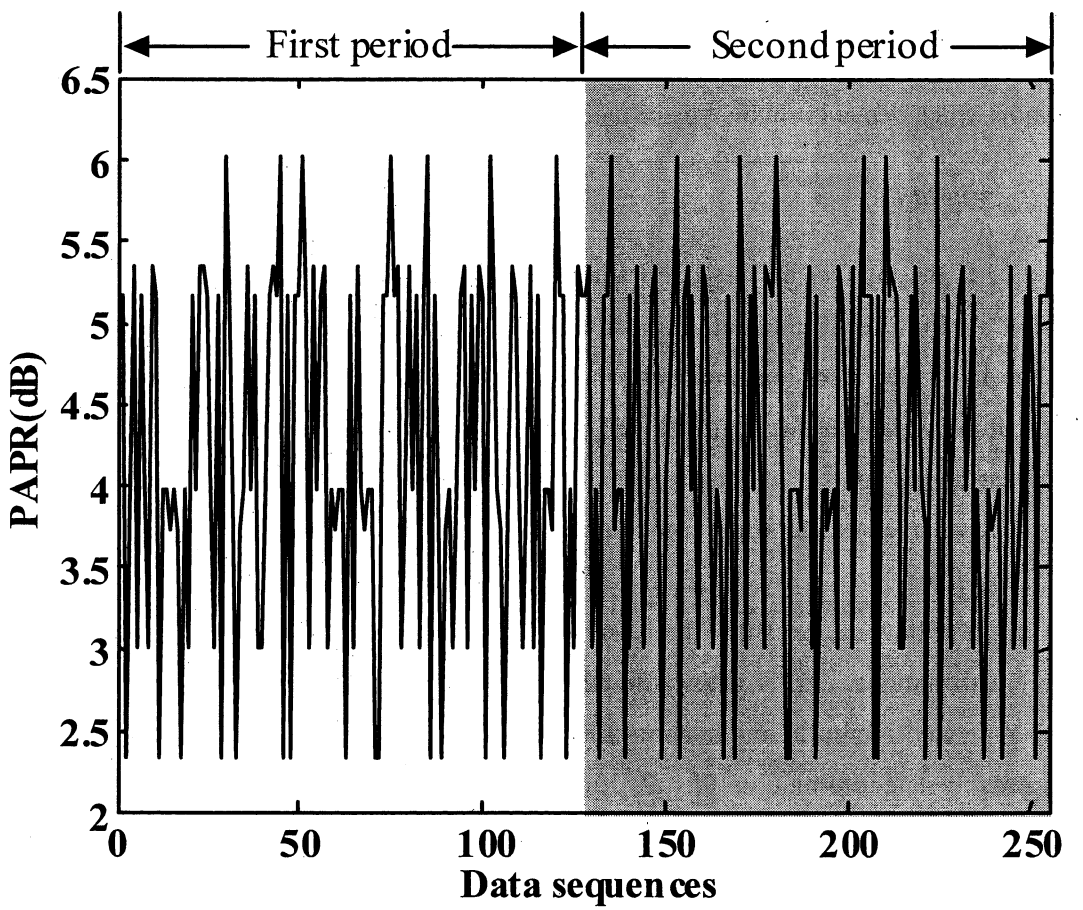

Fig. 3.1. All PAPR performance of OFDM signals in time domain when data sequences are changing.

3.3. Conventional PTS Method

In the PTS method, the data information in the frequency domain $X(n)$ is partitioned into V clusters as $X^{(v)}(n)(1 \le v \le V)$. All sub-carriers for each cluster are multiplied by the weighting factor, $b_n^{(v)} = e^{j\phi_n^{(v)}}$ so as to reduce the PAPR performance. Here, the phase value considered in each cluster is given by the following equation.

$$\phi_n^{(v)} \in \left\{ \frac{2\pi i}{W} \mid i = 0,\ldots,W-1 \right\} \tag{3.3}$$

After multiplying the weighting factor for each cluster, the sub-carrier vector is given by the following equation.

$$Y(n) = \sum_{v=1}^{V} b_n^{(v)} \cdot X^{(v)}(n) \tag{3.4}$$

where $b_n^{(v)}$ is the weighting factors, which are required to inform the receiver as the side information. The set of weighting factor for V clusters are optimized in the time domain so as to achieve the better PAPR performance, by using the following equation.

$$\begin{aligned} y(k) &= \sum_{v=1}^{V} b_n^{(v)} \cdot IFFT\left\{X^{(v)}(n)\right\} \\ &= \sum_{v=1}^{V} b_n^{(v)} \cdot x^{(v)}(k) \end{aligned} \tag{3.5}$$

From (4) and (5), it can be seen that the weighting factor can be multiplied either in the frequency or time domains and the optimized PAPR performance is the same which can be given by the following equation.

$$\tilde{V} = \arg\min_{0 \le w \le W-1} \max_{0 \le k \le N-1} \left| \sum_{v=1}^{V} b_k^v x^v(k) \right| \tag{3.6}$$

where $\tilde{V}$ is optimized argument that can reduce to the lowest PAPR performance. After optimization of phase value for each cluster, the time domain signal after adding the guard interval (GI) is converted to the radio frequency and input to non-linear amplifier of SSPA.

The following shows the problem of conventional PTS method by using the example in Fig. 3.2. When the data sequence is divided into 2 clusters and the number of weighting factor is assumed by 2 phases [0, π], the PAPR performance of initial stage is 6.02dB (A1). After that the PAPR performance is reduced by using PTS method. All possible PAPR performances are [*A1, A2, A3, A4*] as shown in Fig.3.2. The lowest PAPR can be selected from the multiplied weighting factor. From Fig. 3.2, it can be observed that PAPR

performances have the same performance for $A1 = A4$ and $A2=A3$, respectively. From this reason, the calculation of PAPR performance is unnecessary for the second clusters because the PAPR value of second period is the same as the PAPR of first period. This means that there is the possibility to improve the PAPR performance with less computation complexity.

3.4. Proposal of New Weighting Factor with Low Complexity

3.4.1 Proposal of New Weighting Factor with Low Complexity

In the proposed method, the input data block is partitioned into the cluster as the same as conventional PTS method. There are three methods for making the cluster. These three methods include the adjacent partition, interval partition and random partition. The simple explanation of proposed method is we refer to the adjacent partition method. However, the simulation shows the interval method was found to have the better PAPR reduction compared to other methods. The proposed new weighting factor technique can apply to all of these three partition methods. The difference of proposed method as compared with the conventional method is that each cluster is partitioned by first and second parts as shown in Fig. 3.3. The first and second parts of cluster employ the different weighting factor although these two have the predetermined relationship. The frequency domain signal for the proposed method can be given by,

$$Y(n)=\sum_{v=1}^{V}\left(b_n^{\prime v}X^{\prime v}(n)+b_n^{\prime\prime v}X^{\prime\prime v}(n)\right) \tag{3.7}$$

where $b^{\prime v}$ and $b^{\prime\prime v}$ are weighting factors for the first and second parts at the *v-th* cluster, respectively. $X^{\prime v}(n)$ and $X^{\prime\prime v}(n)$ are the data sub-carriers of first and second parts at the *v-th* cluster, respectively. The weighting factor of proposed method for both parts can be defined by $e^{j\phi_n^{\prime v}}$ and $e^{j\phi_n^{\prime\prime v}}$, respectively which are given by the following equation.

$$\begin{aligned}\phi_n' &= \phi_n''/2\\ \phi_n'' &\in \left\{\frac{2\pi i}{W} \mid i=0,\ldots,W-1\right\}\end{aligned} \tag{3.8}$$

where ϕ' is the phase coefficient for the first part of clusters, and ϕ'' is the phase coefficient for the second parts. From (3.3) and (3.8), it can be seen that the conventional and proposed PTS methods have the same number of weighting factor *W*. All possible PAPR performances of proposed method can be given by [*B1, B2, B3* and *B4*] as shown in Fig.3.2. From the figure, it can be seen that the proposed PTS method has more chance to reduce the PAPR performance in the first period and they are not repeating like the conventional PTS method (*A1-A4*). In the assumed example, the B2 sequence will be transmitted as the best PAPR performance. From this fact, the proposed method shows better PAPR performance than conventional PTS method with keeping the same size of side information as the conventional PTS method.

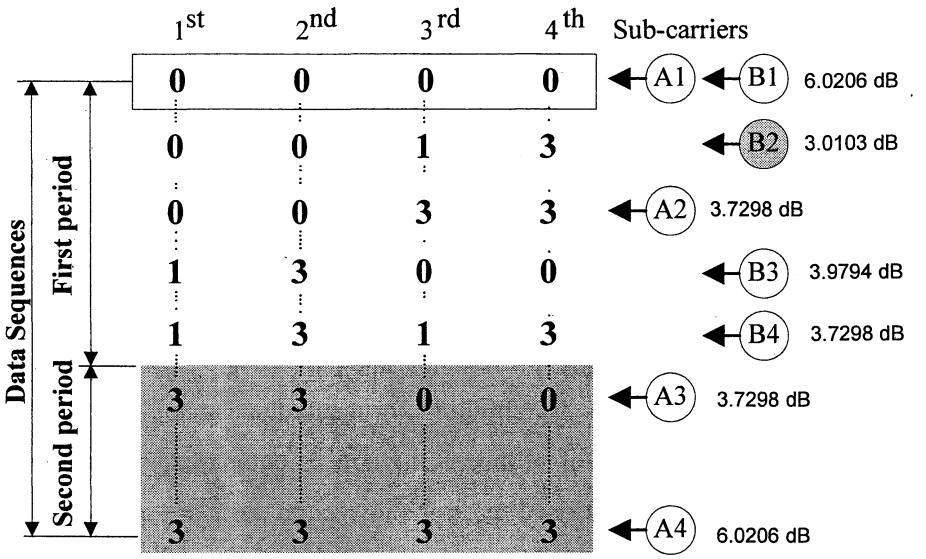

	Conventional PTS				Proposed Method			
Sub-carrier	1st	2nd	3rd	4th	1st	2nd	3rd	4th
Cluster	1st cluster		2nd cluster		1st cluster		2nd cluster	
Part					1st	2nd	1st	2nd
Selected Pattern	Weighting Factor							
A1 and B1	0	0	0	0	0	0	0	0
A2 and B2	0	0	π	π	0	0	π/2	π
A3 and B3	π	π	0	0	π/2	π	0	0
A4 and B4	π	π	π	π	π/2	π	π/2	π

Fig. 3.2. PAPR performance of proposed PTS and conventional PTS methods.

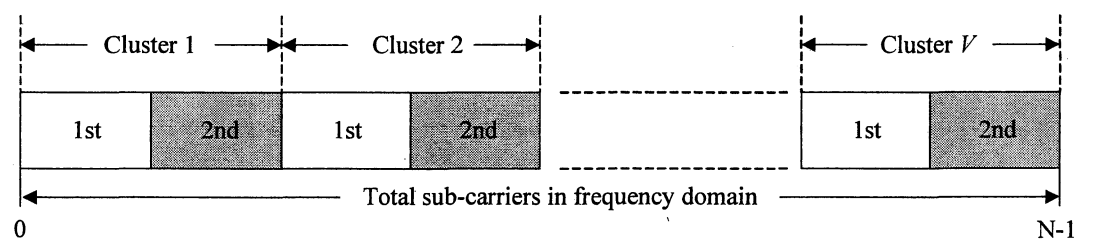

Fig. 3.3. Structure of OFDM symbol for proposed method in the frequency domain.

3.4.2 PTS-Base Radix Technique

The discrete Fourier transform (DFT) of an N-point sequence can be directly computed as,

$$X(n)=\sum_{k=0}^{N-1}x(k)T_N^{nk},\ k=0,1,...,N-1\ \ n=0,1,...,N-1 \tag{3.9}$$

3.4. Proposal of New Weighting Factor with Low Complexity

As the IDFT can be computed by taking the complex conjugate of the input and output sequences while using the same DFT parameters, we need only consider the DFT calculation. Thus, we only use the corresponding FFT computation in the following.

An FFT algorithm recursively converts the DFT computation to $r \times N/r$-point DFTs recurring through $m = \log_r N$ stages. The value of r corresponds to a radix-r FFT algorithm. The DIF radix-r FFT of (9) is given by

$$X(rn+n_o) = \sum_{k=0}^{N/r-1} \left(\left(\sum_{i=0}^{r-1} x\left(k + \tfrac{N}{r} i\right) T_r^{ik_o} \right) T_N^{kn_o} \right) T_{N/r}^{nk} \tag{3.10}$$

where $n_o = 0,1,...,r-1$ is the index of the butterfly outputs. As we consider the inputs to q stage for PTS sub-blocking, symbols and indices are represented with subscript $q: x_q$ and n_q for an input and time index n, respectively, and X_q and k_q for an output X and frequency index k, respectively. Considering the form of (10), the butterfly outputs at q stage are given by

$$X_q(rn+n_o) = \left(\sum_{i=0}^{r-1} x_q\left(k_q + \tfrac{N}{r^q} i\right) T_r^{in_o} \right) T_{N/r^{q-1}}^{k_q n_o} \tag{3.11}$$

where $k_q = 0,1,...,(N/r^q)-1$, $n_q = 0,1,...,(N/r^q)-1, \eta = 1,2,...,r^{q-1}$ and $q = 1,2,...,m$, denotes a particular N/r^{q-1}-point DFT at stage q. Fig. 4 shows the recursive reduction of the η-th N/r^{q-1}-point DFT to N/r^q-point DFTs with DIF radix-r at stage q. Hence, there are $r^{q-1} \times N/r^{q-1}$-point DFTs at stage q. It is assumed that the input sequence is in normal order, and the output is in digit-reversed order. Similarity, we can obtain the butterfly outputs at stage q for DIT.

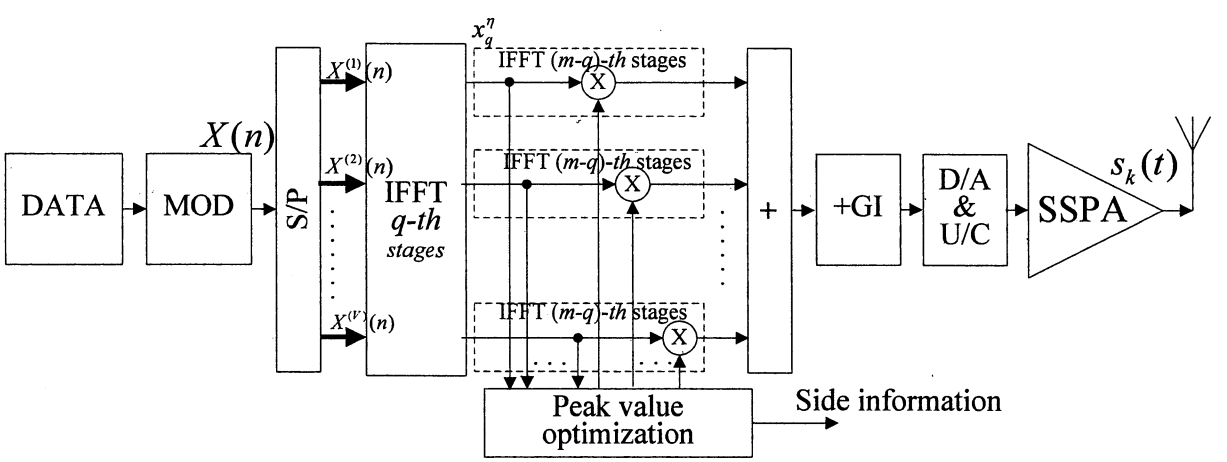

Fig. 3.4. Structure of OFDM transmitter with a low complexity PTS method.

3.4. Proposal of New Weighting Factor with Low Complexity

The inputs $x_q^{\eta}(n_q + (N/r^q)i)$ at stage q are used for cluster partitioning in the proposed PTS technique and the remaining $m-q$ stages are used to compute the multiple transforms as shown in Fig. 3.5.

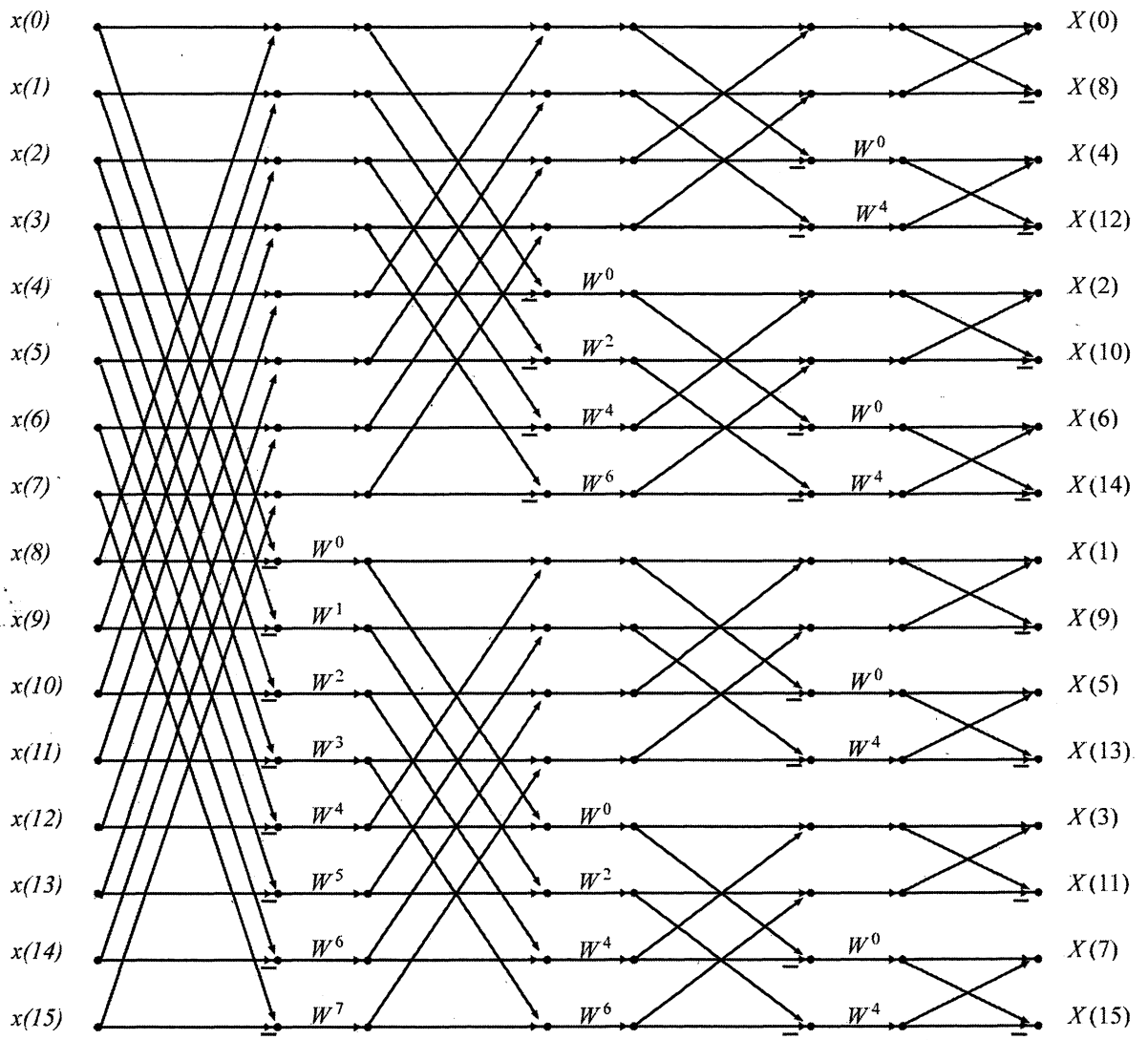

Fig. 3.5. Radix-2 FFT algorithm with length 16.

3.5. Performance Evaluation

This section presents the various computer simulation results to verify the performance of proposed method. The receiver is coherent detector. The side information for both PTS methods assumes to be known at the receiver. The transmitted signal is taken over sampling by a factor of 4 (L=4). The simulation parameters to be used in the following evaluations are shown in Table 3.1.

Figure 3.6 shows the PAPR reduction performance for both the conventional PTS and proposed PTS method with proposed new weighting factor technique when changing the number of clusters and weighting factors of discrete phases. From the figure, it can be observed that the proposed PTS method shows the better PAPR reduction performance than the conventional PTS method.

Table 3.1 Simulation Parameters.

A. Modulation	QPSK
B. Demodulation	Coherent
Allocated bandwidth	5MHz
C. Number of FFT points	256
Number of sub-carriers	64
Number of cluster (V)	4
Number of discrete phase (W)	2 and 4
Symbol duration	12.8us
Guard interval	1.28us

Figure 3.7 shows the PAPR performance for the conventional OFDM, DIF-PTS and the proposed weighting factor technique with DIF-PTS. From the figure, it can be observed that the proposed method shows the better PAPR performance than the conventional OFDM and DIF-PTS method.

Table II shows the comparisons for PAPR performance and computation complexity for the Conventional OFDM, conventional PTS, DIF-PTS [17] and proposed method with DIF-PTS methods. The computation complexity is evaluated by the reduction of complexity as compared with the conventional PTS. From Table II, it can be observed that the proposed method can achieve the best PAPR performance and the same computation complexity as the DIF-PTS method.

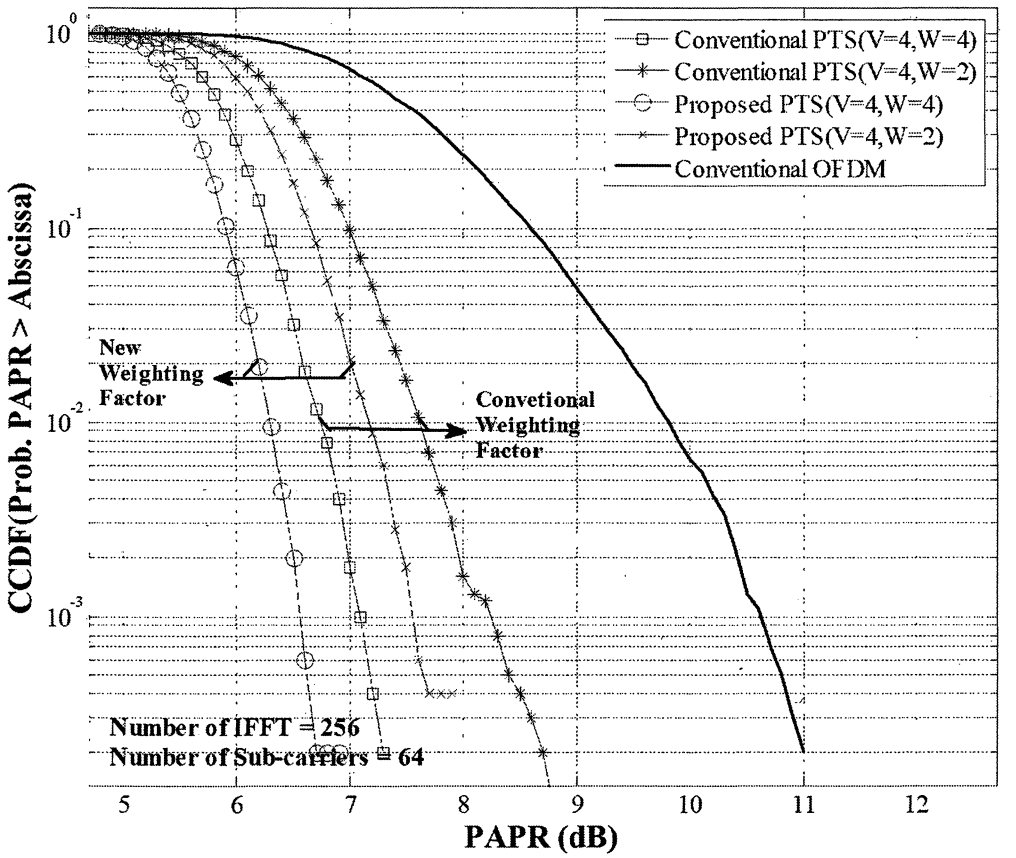

Fig. 3.6. Comparison of PAPR reduction performance with difference number of clusters and phase.

Table 3.2 Comparison of performances for various methods.

	PAPR performance at 10^{-2} of CCDF			Computation Complexity		
	(m-q=4)	(m-q=3)	(m-q=2)	(m-q=4)	(m-q=3)	(m-q=2)
Conventional OFDM	9.8dB	9.8 dB	9.8 dB	NA	NA	NA
Conventional PTS	6.75 dB	6.75 dB	6.75 dB	100%	100%	100%
DIF-PTS[1]	6.75 dB	6.75 dB	8.3 dB	63%	55%	48%
Proposed method with DIF-PTS [1]	6.25 dB	6.25 dB	7.3 dB	63%	55%	48%

3.6. Conclusions

In this chapter, we proposed the new weighting factor technique for the PTS method in conjunction with DIF-PTS method. The feature of proposed new weighting factor technique is to employ the special characteristics of OFDM signal of which PAPR value is changed cyclically according to the pattern of input data sequence. By using this fact, we proposed the new weighting factor technique in which each cluster is divided two parts. The weighting factors for the 1st and 2nd parts have the predetermined relationship so as to keep the same size of side information. To reduce the computation complexity required in the selection of optimum weighting factor for each cluster, this chapter employs the DIF-PTS [17] method. From the various computer simulation results, we confirmed that the proposed method shows the better PAPR performance and the same computation complexity with keeping the same size of side information as compared with the DIF-PTS method.

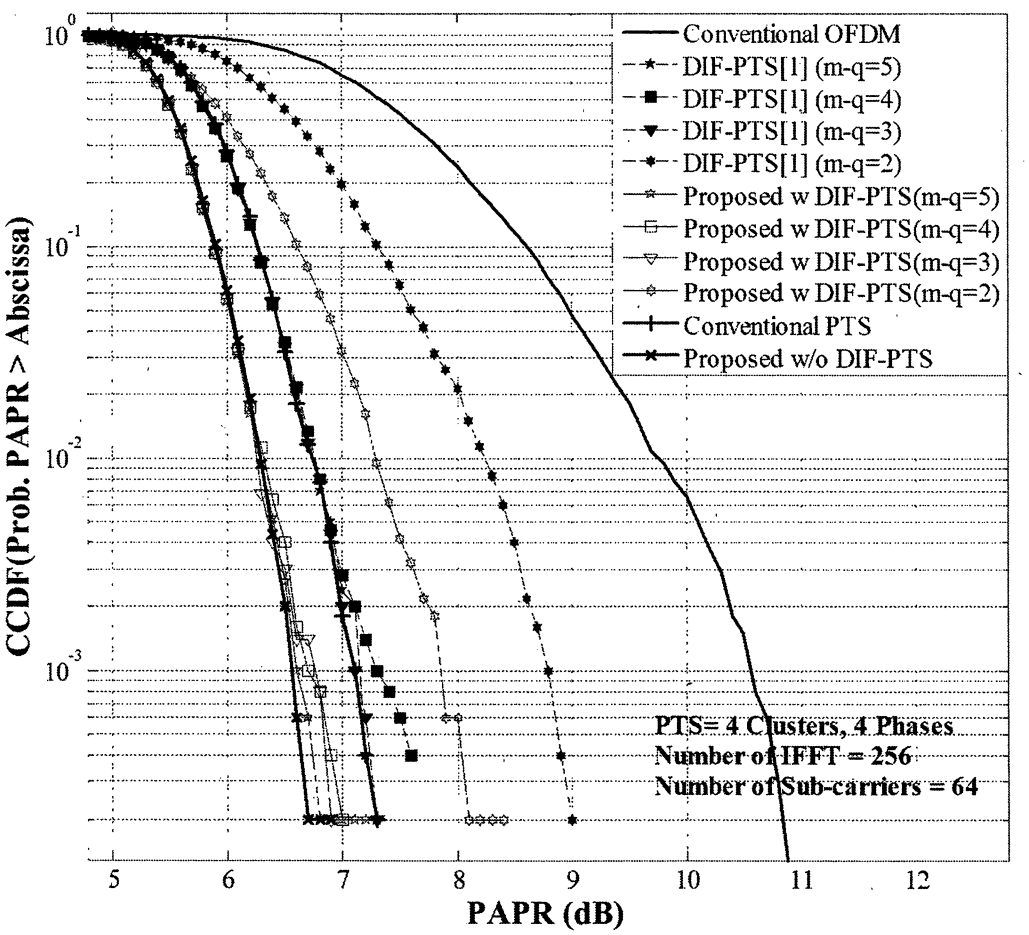

Fig. 3.7 Comparison of PAPR reduction performance between conventional PTS and proposed new PTS method.

CHAPTER 4

PTS OFDM WITH LOW COMPLEXITY BASED ON RADIX-R IFFT ALGORITHMS

The Partial Transmit Sequence (PTS) method with low computation complexity, called decomposition PTS sub-blocking was proposed which employs the radix-2 inverse fast Fourier transform (IFFT) for the signals at the middle stages of an N-point radix-2 IFFT and decimation in frequency (DIF) domain. This method (DIF-PTS) can reduce the computation complexity relatively with keeping the same peak to averaged power ratio (PAPR) performance as that for the conventional PTS techniques. To improve the computation complexity further for the PTS method, the Radix-4, Split-Radix and Extended Split-Radix inverse fast Fourier transforms which can reduce the number of complex computation were proposed. However, the PAPR reduction performance is the same as that for the radix-2 method. In this chapter, we propose a new weighting factor technique in conjunction with DIF-PTS sub-blocking based on Radix-4, Split-Radix and Extended Split-Radix IFFT technique called Improve PTS (I-PTS) which can improve both the PAPR performance and computation complexity without any increasing of side information. This chapter presents the various computer simulation results to verifier the effectiveness of proposed method.

4.1 Introduction

The Orthogonal Frequency Division Multiplexing (OFDM) technique has been received a lot of attentions especially in the field of wireless communications because of its efficient usage of frequency bandwidth and robustness to the multi-path fading. From these advantages, the OFDM technique has already been adopted as the standard transmission techniques in the Wireless Local Area Network (WLAN) systems and the next generation of mobile communications systems [69]. One of the limitations of using OFDM technique is the larger peak to averaged power ratio (PAPR) of its time domain signal. The higher PAPR leads the fatal degradation of OFDM performance in the nonlinear power amplifier located at the transmitter [17].

Partial transmit sequence (PTS) method [27-29] is proposed as one of the distortion-less PAPR reduction methods. However, the computation complexity and the size of side information would increase as increasing the number of clusters and weighting factors. To reduce this computation complexity, DIF-PTS (Decimation in Frequency–PTS) method was proposed [41] in which the intermediate signals are employed within the IFFT and used the radix-2 decimation in the frequency domain (DIF) to obtain the PTS sub-blocks. Multiple IFFTs are then applied to the remaining stages. The PTS sub-blocking is performed in the middle stages of the N-point radix FFT DIF algorithm. The DIF-PTS method can reduce the computational complexity relatively while it shows almost the same PAPR reduction performance as that of the conventional PTS OFDM scheme.

In this chapter, we propose a new weighting factor technique for the PTS method in conjunction with DIF-PTS sub-blocking based on the Radix-4, Split-Radix and Extended Split-Radix IFFT technique which can improve both the PAPR performance and computation complexity. The proposed method can achieve the better PAPR reduction performance than that for the DIF-PTS method without any increasing of the size of side information.

In the next section, the PAPR problem and conventional PTS are reviewed briefly. Section 4.3 presents the PTS-Based Different FFT Algorithms and Section 4.4 presents the proposed method based on Radix-4 FFT, Split-Radix FFT and Extended Split-Radix FFT Algorithms. Section 4.4 presents various computer simulation results to verify the effectiveness of the proposed method as comparing with the conventional PTS method. Some conclusions are given in Section 4.5.

4.2 Partial Transmit Sequence Method

4.2.1 PTS-Based Radix Technique

Let $\{X(k)\}_{k=0}^{N-1}$ denotes the frequency-domain signal, where N is the number of FFT/IFFT points and k is the frequency index. The discrete time-domain OFDM signal is obtained by taking an N-point inverse discrete Fourier transform (IDFT) of $X(k)$ as given by the following equation.

$$x(n) = \frac{1}{N}\sum_{k=0}^{N-1} X(k) T_N^{-nk} \tag{4.1}$$

where n is the discrete-time index, $T_N = e^{-j2\pi/N}$ (known as the twiddle factor), and $j^2 = -1$. The frequency-domain signal $X(k)$ would be added constructively and a time domain signal with large peak amplitude would be generated. To evaluate the envelop variations of OFDM time domain signal, the ratio of peak to envelope power of the signal is usually used. The discrete time PAPR can be evaluated precisely by using more than four times oversampling [4], which is given by,

$$PAPR = \frac{\max_{0\le n\le N-1} |x(n)|^2}{E\left[|x(n)|^2\right]} \tag{4.2}$$

In the PAPR reduction method of using the partial transmit sequences (PTSs), the frequency-domain vector $X(k)$ is partitioned into P disjoint sub-blocks as given by,

$$X(k) = \sum_{p=0}^{P-1} X_p(k) \tag{4.3}$$

Let θ_p be the set of weighting factors with $\theta_1 = 0$ which are applied to the sub-blocks $X_p(k)$. The substitute frequency-domain signal is given by [68],

$$X'(k) = \sum_{p=0}^{P-1} e^{j\theta_p} X_p(k) \tag{4.4}$$

Taking the IDFT of (4.4), and using the linearity property of the IDFT, the following equation can be obtained.

$$x'(n) = IDFT(X'(k)) = \sum_{p=0}^{P-1} e^{i\theta_p} IDFT(X_p(k)) \tag{4.5}$$

$$= \sum_{p=0}^{P-1} e^{j\theta_p} x_p(n)$$

where $x_p(n) = IDFT(X_p(k))$ are the *P-th* time-domain PTS. To determine the sequence $x'(n)$ with the smallest PAPR, the following optimization criterion is employed.

$$\left[\theta_1', \theta_2', ..., \theta_{P-1}'\right] = \arg\min_{[\theta_1, \theta_2, ..., \theta_{P-1}]} \left\{ \max_{0 \le n \le N-1} \left| x'(n) \right| \right\} \tag{4.6}$$

In order to recover the data correctly at the receiver, the required side information is $(P-1)\log_2 W$ bits per OFDM symbol where W is the number of weighting factors. According to (4.4), P IDFTs are required to obtain $x'(n)$ which would increase the significant computational complexity.

In order to recover the data correctly at the receiver, the required side information is $(P-1)\log_2 W$ bits per OFDM symbol where W is the number of weighting factors. According to (4.4), P IDFTs are required to obtain $x'(n)$ which can incur significant computational complexity.

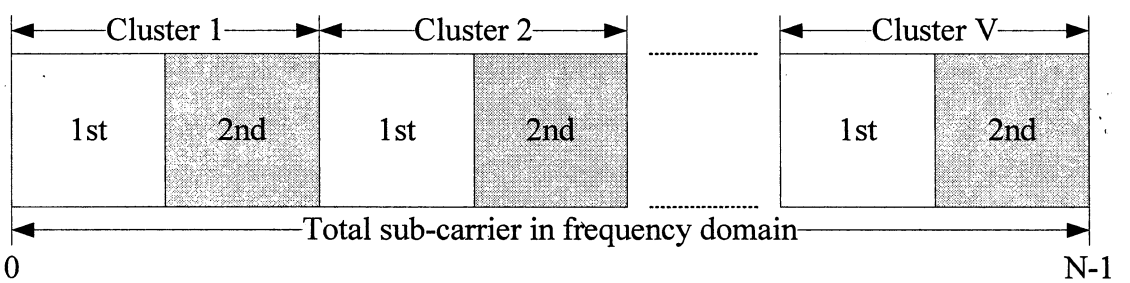

Fig. 4.1. Structure of OFDM symbol for the Improved PTS method.

4.2.2 IPTS-Based Radix Technique

The DFT of an N-point sequence $X(k)$ can be directly computed by using equation (4.1). As the IDFT can be computed by taking the complex conjugate of the input and output sequences while using the same DFT parameters, we need only consider the DFT calculation. Thus, we only use the corresponding FFT computation in the following.

An FFT algorithm recursively converts the DFT computation to $r \times N/r$-point DFTs recurring through $m = \log_r N$ stages. The value of r corresponds to a radix-r FFT algorithm. The DIF radix-r DFT of (1) is given by,

$$X(rk + k_0) = \sum_{n=0}^{N/r-1} \left(\left(\sum_{i=0}^{r-1} x\left(n + \frac{N}{r} i \right) T_r^{ik_0} \right) T_N^{nk_0} \right) T_{N/r}^{kn} \tag{4.7}$$

where $k_0, 0 \le k_0 \le r-1$, is the index of the butterfly outputs. As we consider the inputs to stage q for PTS sub-blocking, symbols and indices are represented with subscript $q: x_q$ and n_q for an input x and time index n, respectively, which X_q and k_q for an output X and frequency index k, respectively. Considering the form of (4.7), the butterfly outputs at stage q are given by,

$$X_q^{\eta}(rk_q + k_0) = \left(\sum_{i=0}^{r-1} x_q^{\eta}\left(n_q + \frac{N}{r^q} i \right) T_r^{ik_0} \right) T_{N/r^{q-1}}^{n_q k_0} \tag{4.8}$$

where k_q=0,1,..., $(N/r^q)-1, n_q$=0,1,..., $(N/r^q)-1$, and η, η =1,2,... r^{q-1}, denotes a particular N/r^{q-1}-point DFT at the stage q. Fig. 3.4 shows the recursive reduction of the η -th N/r^{q-1}-point DFT to N/r^q-point DFTs at stage q. It is assumed that the input sequence is in normal order, and the output is in digit-reversed order. Similarity, we can obtain the butterfly outputs at stage q for decimation in time (DIT) domain.

The inputs $X_q^{\eta}(n_q + (N/r^q)i)$ at stage q are used for cluster partitioning in the proposed PTS technique and the remaining *m-q* stages are used to compute the multiple transforms as shown in Fig. 3.3.

In the Improved PTS method, the input data block is partitioned into the cluster as the same as conventional PTS method. The difference of I-PTS method as compared with the conventional method is that each cluster is partitioned by first and second parts as shown in Fig.3.4. The first and second parts of cluster employ the different weighting factor although these two have the predetermined relationship. The frequency domain signal for the I-PTS method can be given by,

$$x'(n) = \sum_{p=0}^{P-1} \left(e^{j\theta_p'} x_p'(n) + e^{j\theta_p''} x_p''(n) \right) \tag{4.9}$$

where $e^{j\theta_p'}$ and $e^{j\theta_p''}$ are weighting factors for the first and second parts at the *p-th* cluster, respectively. $x_p'(n)$ and $x_p''(n)$ are the data sub-carriers of first and second parts at the *p-th* cluster, respectively. The weighting factors of I-PTS method are given by the following equation.

$$\begin{aligned} \theta_p' &= \chi \theta_p'' \\ \theta_p'' &= \left\{ \frac{2\pi i}{W} \middle| i = 0,1,...,W-1 \right\} \end{aligned} \tag{4.10}$$

where θ_p' is the phase coefficient for the first part of clusters, and θ_p'' is the phase coefficient for the second parts. However, this fact leads other advantage in the computational complexity for the I-PTS method as compared with the case of $\chi = 0.5$. If α is 0, the phase value of

second part of cluster can be obtained by $\phi_2^{(v)} = \alpha\phi_1^{(v)} = 0$ and the weighting factor for the second part of cluster becomes $b_2^{(v)} = e^{j\phi_2^{(v)}} = 1$. This means that the I-PTS method can use the original time domain signal without multiplying the weighting factor for the half part of subcarriers.

From the above results, Fig.4.2 shows the averaged PAPR performance for the I-PTS method when changing χ. The best PAPR performance can be achieved when χ is 0 and the I-PTS method with $\chi = 0$ can reduce the computation complexity. From this fact, the I-PTS method shows better PAPR performance than conventional PTS and DIF-PTS method with keeping the same size of side information and lower computation complexity as the conventional PTS method.

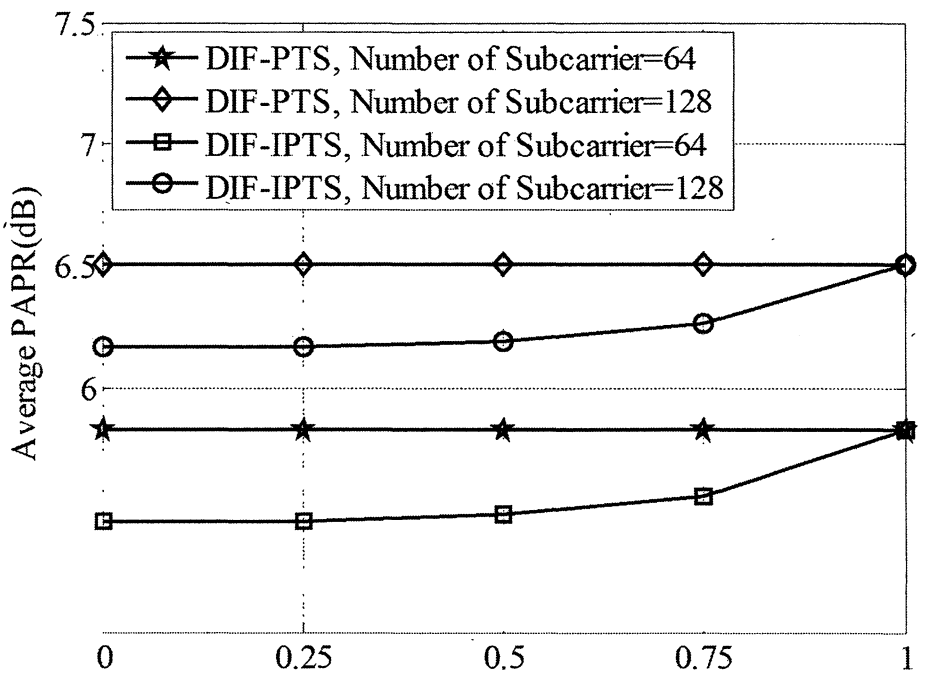

Fig. 4.2. Averaged PAPR Performance for the DIF-IPTS method when changing χ.

4.3 Proposal of New Weighting Factor Based on Various FFT Algorithms

4.3.1 Radix-4 FFT Algorithm

A Radix-2 algorithm diagram can be transformed quite straightforwardly into a Radix-4 algorithm diagram simply by changing the exponents of the twiddle factors. It is quite clear then that at each stage of the algorithm of Radix-4 is better for the odd terms of the DFT and Radix-2 for the even terms of the DFT. So, one might guess that restricting this transformation locally to the lower part of the diagram might improve the algorithm. It turns out that this is indeed the case.

In the proposed method, the input data block is partitioned into the cluster as the same as conventional PTS method. The difference of proposed method as compared with the conventional method is that each cluster is partitioned by first and second parts as shown in Fig. 4.1. The first and second parts of cluster employ the different weighting factor although these two have the predetermined relationship. The frequency domain signal for the proposed method can be given by equation (4.9) And, the weighting factors of proposed method are given by the following equation (4.10).

Computational Complexity Analysis, we define the multiplicative complexity of the DIF IFFT algorithm as the number of complex multiplications by twiddle factors $T_{N/r^{q-1}}^{n_q k_0}$ and $T_r^{ik_0}$ .The twiddle factors $T_r^{ik_0}$ are trivial (± 1 and $\pm j$), if we consider only radix-2 and radix-4 and so they do not introduce any multiplicative complexity. The number of twiddle factors $T_{N/r^{q-1}}^{n_q k_0}$ and $T_r^{ik_0}$ at stage q for the DIF algorithm from (4.8) is

$$\alpha_q^{DIF} = r^{q-1}\left(\frac{N}{r^q}-1\right)\left[(r-1)+(r-2)+(r-1)^2-1\right] \tag{4.11}$$

Which clearly shows that $\alpha_{q+1}^{DIF} < \alpha_q^{DIF}$ .thus, α_q^{DIF} decreases through successive stages.

The number of additions at stage q can be obtained from (4.8) as below, where Nr is the number of r corresponding to a radix-r FFT algorithm.

$$A_q = Nr(r-1) \tag{4.12}$$

In the order to compare the multiplicative complexity between two PAPR techniques, we define the reduction ratios as below. Where M_{total}^1 and M_{total}^2 are multiplication of first and second PAPR techniques respectively.

$$R^{mul} = 1 - (M^1_{total} / M^2_{total}) \tag{4.13}$$

where the overall multiplicative complexity for the PTS-base radix-r FFT technique is given by

$$M_{total} = \sum_{i=1}^{q-1} \alpha_q + P \sum_{i=q}^{m} \alpha_q \tag{4.14}$$

Higher radix algorithms have more twiddle factors per stage but fewer nontrivial multiplications compared to lower radix algorithms. Consequently, the multiplicative complexity is reduced for the remaining stages by using a high radix algorithm. This is confirmed in Section 4.5.

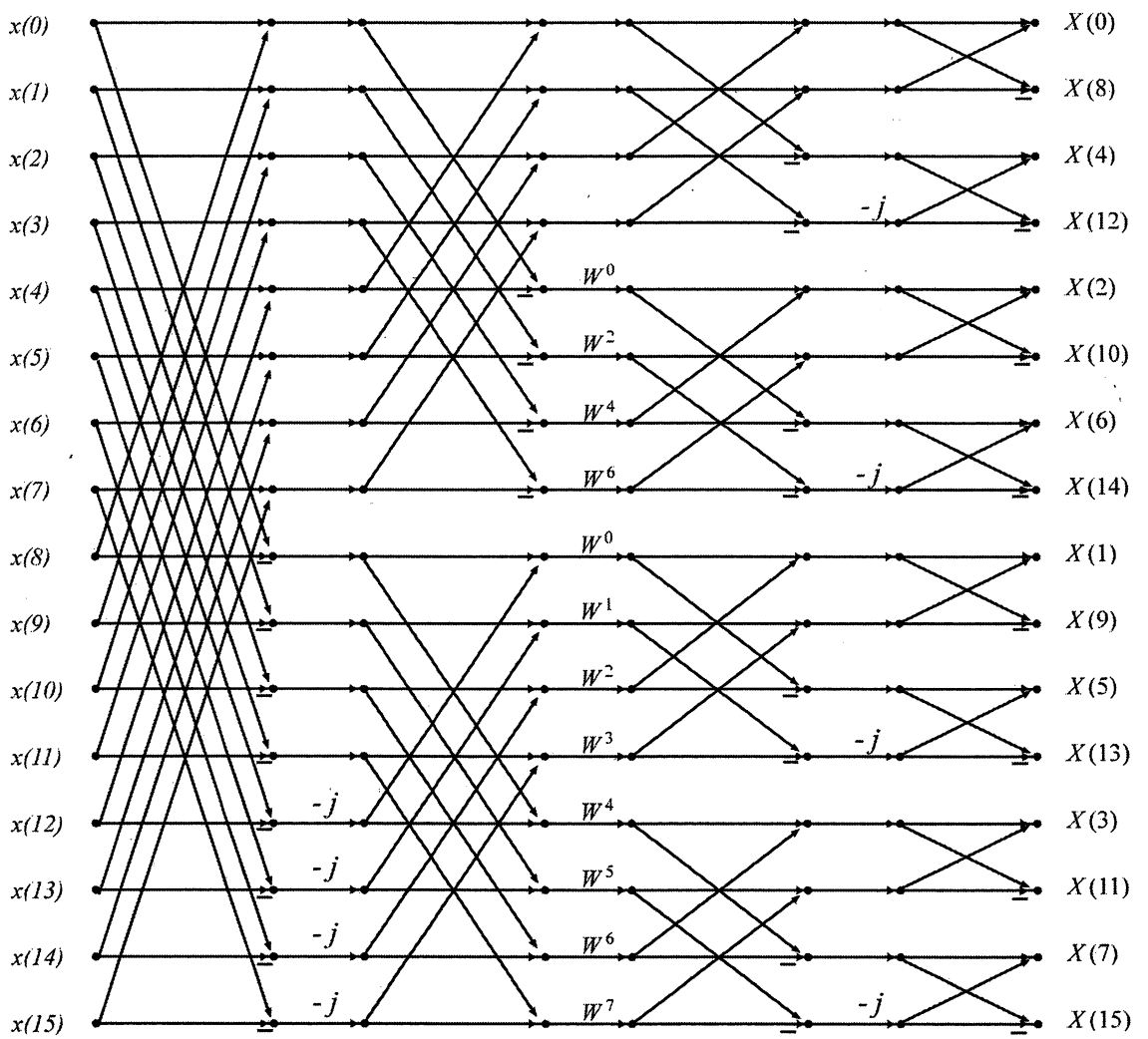

Fig. 4.3. Radix-4 FFT algorithm with length 16.

4.3.2 Split-Radix FFT Algorithm

A Radix-2 or Radix-4 algorithm diagram can be transformed quite straightforwardly into a Split-Radix algorithm diagram simply by changing the exponents of the twiddle factors. It is quite clear then that at each stage of the algorithm of Split-Radix is better for the odd terms of the DFT and Radix-2 or Radix-4 for the even terms of the DFT. So, one might guess that restricting this transformation locally to the lower part of the diagram might improve the algorithm. It turns out that this is indeed the case.

The Split-Radix algorithm is then based on the following decomposition [40].

$$X_k = \sum_{n=0}^{N-1} x_n T_N^{nk} \tag{4.15}$$

$$\text{where} \left(T_N = \cos\frac{2\pi}{N} - j\sin\frac{2\pi}{N} \right)$$

and it is decomposed into,

$$X_{2k} = \sum_{n=0}^{N/2-1} (x_n + x_{n+(N/2)}) T_N^{2nk}$$

$$X_{4k+1} = \sum_{n=0}^{N/4-1} (x_n - x_{n+(N/2)})$$

$$X_{4k+1} = \sum_{n=0}^{N/4-1} (x_n - x_{n+(N/2)}) - j(x_{n+(N/4)} - x_{n+3(N/4)}) T_N^n T_N^{4nk} \tag{4.16}$$

$$X_{4k+3} = \sum_{n=0}^{N/4-1} (x_n - x_{n+(N/2)}) + j(x_{n+(N/4)} - x_{n+3(N/4)}) T_N^{3n} T_N^{4nk}$$

The first stage of a Split-Radix decimation in the frequency decomposition then replaces a DFT of length N by one DFT of length $N/2$ and two DFT's of length $N/4$ at the cost of ($N/2$-4) general complex multiplications (3 real multiplications + 3 additions), and 2 multiplications by the eighth root of unity (2 real multiplications + 2 additions).

The length-N DFT is then obtained by successive use of such decompositions, up to the last stage where some usual radix-2 butterflies (without twiddle factors) are needed as shown in Fig.4.3 for a length 16-Split-Radix FFT.

The DFT of an N-point sequence $X(k)$ can be directly computed by using (4.1). As the IDFT can be computed by taking the complex conjugate of the input and output sequences

while using the same DFT parameters, we need only consider the DFT calculation. Thus, we only use the corresponding FFT computation in the following.

An FFT algorithm recursively converts the DFT computation to $r \times N/r$- point DFTs recurring through $m = \log_r N$ stages. The value of r corresponds to a radix-r FFT algorithm. The DIF radix-r DFT of (4.1) is given by,

$$X(rk+k_0) = \sum_{n=0}^{N/r-1} \left(\left(\sum_{i=0}^{r-1} x\left(n+\frac{N}{r}i\right) T_r^{ik_0} \right) T_N^{nk_0} \right) T_{N/r}^{kn} \tag{4.17}$$

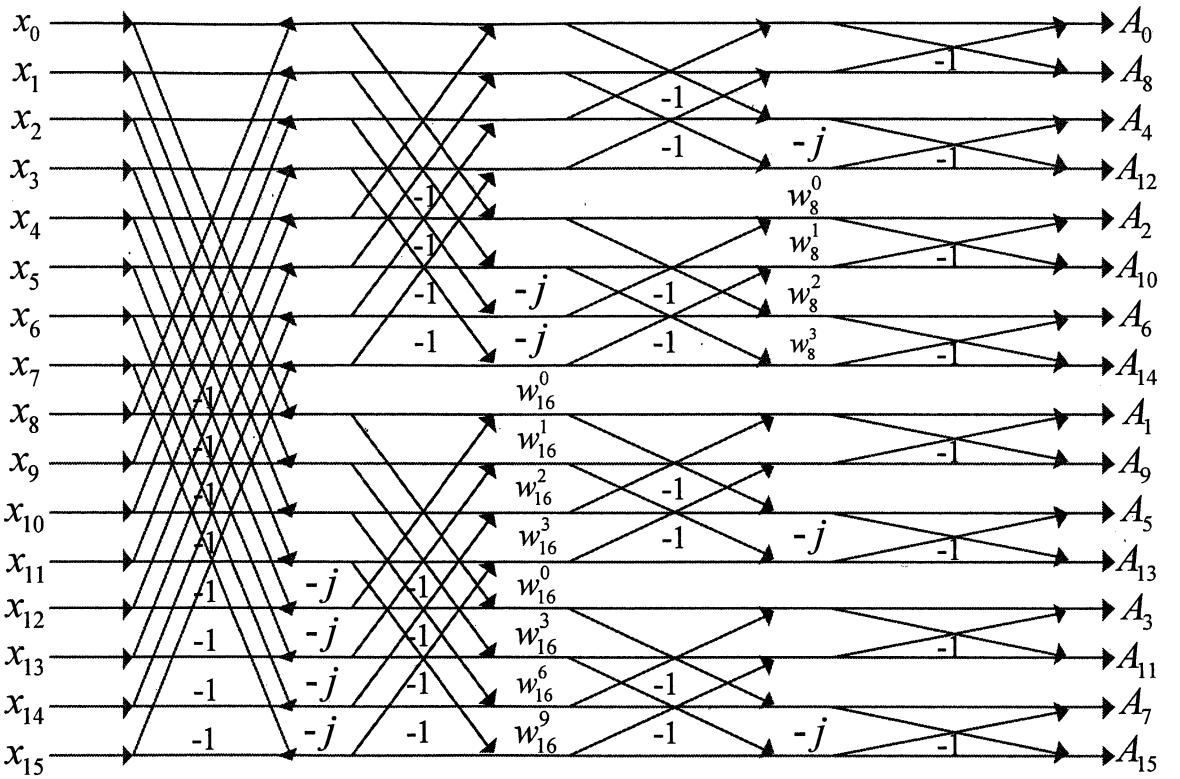

Fig. 4.4. Split-Radix algorithm with length 16.

where $k_0, 0 \le k_0 \le r-1$, is the index of the butterfly outputs. As we consider the inputs to stage q for PTS sub-blocking, symbols and indices are represented with subscript $q: x_q$ and n_q for an input x and time index n, respectively, which X_q and k_q for an output X and frequency index k, respectively. Considering the form of (4.17), the butterfly outputs at stage q are given by,

$$X_q^{\eta}(rk_q+k_0) = \left(\sum_{i=0}^{r-1} x_q^{\eta}\left(n_q+\frac{N}{r^q}i\right) T_r^{ik_0} \right) T_{N/r^{q-1}}^{n_q k_0} \tag{4.18}$$

where k_q =0,1,..., $(N/r^q)-1$, n_q =0,1,..., $(N/r^q)-1$, and η , η =1,2,... r^{q-1} , denotes a particular N/r^{q-1}-point DFT at the stage q. Fig. 4.1 shows the recursive reduction of the η -th

N/r^{q-1}-point DFT to N/r^{q}-point DFTs at stage q. It is assumed that the input sequence is in normal order, and the output is in digit-reversed order. Similarity, we can obtain the butterfly outputs at stage q for decimation in time (DIT) domain.

The inputs $X_q^{\eta}(n_q+(N/r^q)i)$ at stage q are used for cluster partitioning in the proposed PTS technique and the remaining m-q stages are used to compute the multiple transforms as shown in Fig. 3.4.

Computational complexity analyses, we define the multiplicative complexity of the DIF IFFT algorithm as the number of complex multiplications by twiddle factors $T_{N/r^{q-1}}^{n_q k_0}$ and $T_r^{ik_0}$. The twiddle factors $T_r^{ik_0}$ are trivial (± 1 and $\pm j$). Let M_m^c be the number of real multiplications needed to perform a 2^m-complex DFT with the Split-Radix algorithm. By using (4.16), we can obtain the following relationship.

$$M_m^c = M_{m-1}^c + 2M_{m-2}^c + 3\cdot 2^{m-1} - 8 \tag{4.19}$$

And, with the initial conditions $M_1 = 0$, $M_2 = 0$, we obtain,

$$M_m^c = 2^m(m-3)+4 \tag{4.20}$$

Disregarding for a while the number of additions needed to perform the complex multiplications, the remaining ones can easily be evaluated by , since, at each of the m stage, anew point is generated by a complex addition. Then, since the number of real additions needed to compute a complex is equal to the number of multiplications, we have,

$$A_m^c = m\cdot 2^{m+1} + M_m^c \tag{4.21}$$

The Split-Radix algorithm has the lower number of both multiplications and additions than Radix-2 algorithm.

4.3.3 Extended Split-Radix FFT Algorithm

The basic idea of an extended split-radix FFT algorithm is the application of a radix-2 index map to the even-indexed terms and a radix-8 index map to the odd-indexed terms. That is, the extended split-radix FFT algorithm is based on the synthesis of one half-length and four eighth-length DFTs. for the even index terms, and [40]:

$$X_{8k+1} = \sum_{n=0}^{N/8-1}\Big[\{(x_n - x_{n+N/2}) - j(x_{n+N/4} - x_{n+3N/4})\} + \frac{1}{\sqrt{2}}\{(1-j)(x_{n+N/8} - x_{n+5N/8}) - (1+j)(x_{n+3N/8} - x_{n+7N/8})\}\Big]W_N^n W_N^{8nk}$$

$$X_{8k+3} = \sum_{n=0}^{N/8-1}\Big[\{(x_n - x_{n+N/2}) + j(x_{n+N/4} - x_{n+3N/4})\} - \frac{1}{\sqrt{2}}\{(1+j)(x_{n+N/8} - x_{n+5N/8}) - (1-j)(x_{n+3N/8} - x_{n+7N/8})\}\Big]W_N^{3n} W_N^{8nk}$$

$$X_{8k+5} = \sum_{n=0}^{N/8-1} \left[\{(x_n - x_{n+N/2}) - j(x_{n+N/4} - x_{n+3N/4})\} - \frac{1}{\sqrt{2}} \{(1-j)(x_{n+N/8} - x_{n+5N/8}) - (1+j)(x_{n+3N/8} - x_{n+7N/8})\} \right] W_N^{5n} W_N^{8nk} \tag{4.22}$$

$$X_{8k+7} = \sum_{n=0}^{N/8-1} \left[\{(x_n - x_{n+N/2}) + j(x_{n+N/4} - x_{n+3N/4})\} + \frac{1}{\sqrt{2}} \{(1+j)(x_{n+N/8} - x_{n+5N/8}) - (1-j)(x_{n+3N/8} - x_{n+7N/8})\} \right] W_N^{7n} W_N^{8nk}$$

for the odd index terms.

The first stage of an extended split-radix decimation-in-frequency decomposition then replaces a DFT of length by one DFT of length 2 and four DFTs of length 8. The length-DFT is then obtained by successive use of such decompositions up to the last two stages, where some conventional split-radix butterflies (without twiddle factors) are needed, and to the last stage, where some usual radix-2 butterflies (without twiddle factors) are needed. A general elementary butterfly used in the diagram is illustrated in detail in Fig. 4.5.

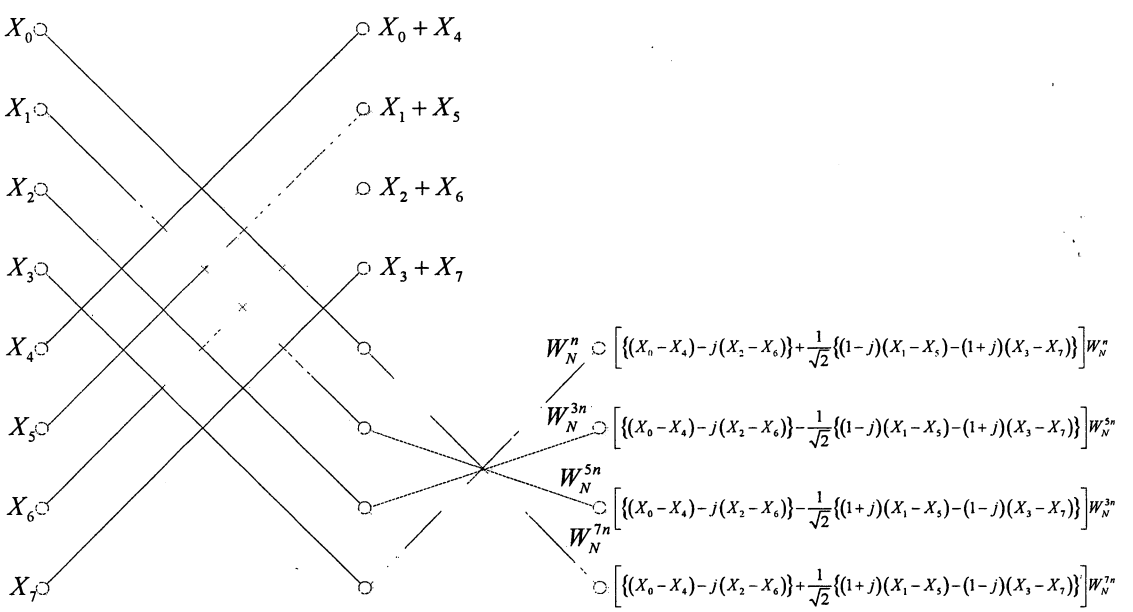

Fig. 4.5. Butterfly used in the graph of a DIF extended split-radix FFT.

We define the multiplicative complexity of the DIF IFFT algorithm as the number of complex multiplications by twiddle factors $T_{N/r^{q-1}}^{n_q k_0}$ and $T_r^{ik_0}$. The twiddle factors $T_r^{ik_0}$ are trivial (± 1 and $\pm j$). Let M_m^c be the number of real multiplications needed to perform a 2^m-complex DFT with the Extended Split-Radix algorithm. By using (4.22), we can obtain the following relationship.

$$M_m^c = M_{m-1}^c + 2M_{m-2}^c + 3 \cdot 2^{m-1} - 8 \tag{4.23}$$

And, with the initial conditions M_1= 0, M_2= 0, we obtain,

$$M_m^c = 2^m (m-3)+4 \tag{4.24}$$

Disregarding for a while the number of additions needed to perform the complex multiplications, the remaining ones can easily be evaluated by $m \cdot 2^{m+1}$, since, at each of the m stage, anew point is generated by a complex addition. Then, since the number of real additions needed to compute a complex is equal to the number of multiplications, we have:

$$A_m^c = m \cdot 2^{m+1} + M_m^c \tag{4.25}$$

The Extended Split-Radix algorithm has the lower number of both multiplications and additions than Radix-2 algorithm.

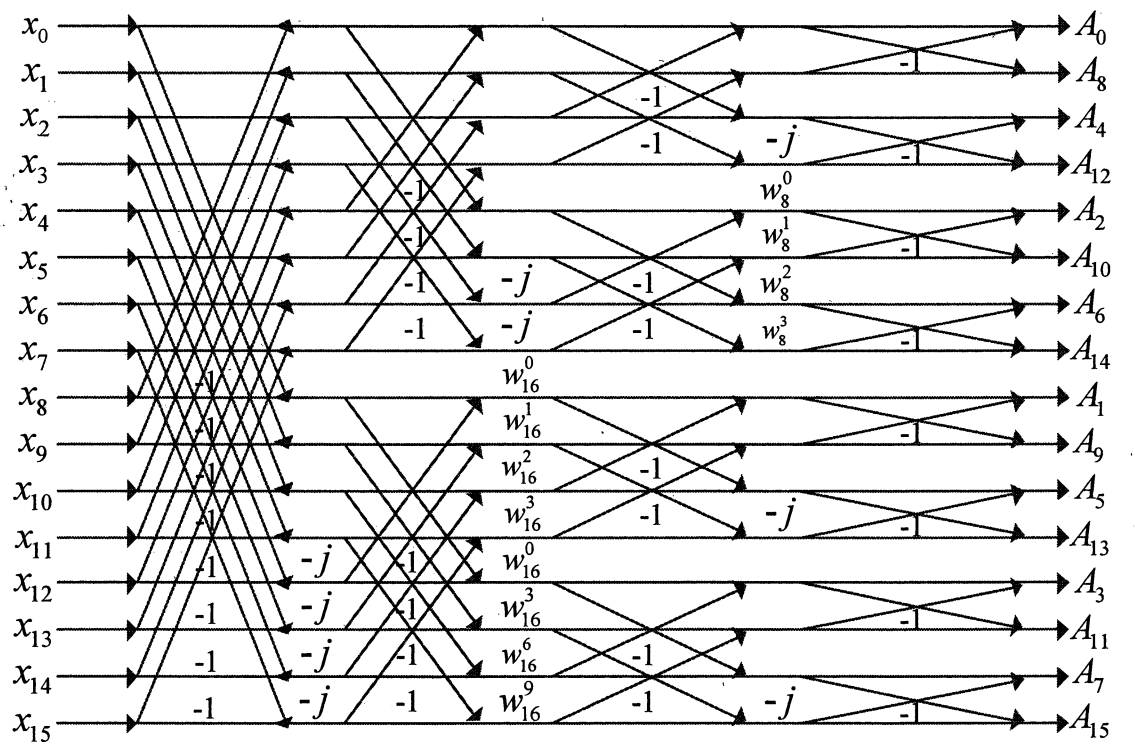

Fig. 4.6. Extended Split-Radix algorithm with length 16.

4.4 Performance Evaluation

4.4.1 Performance of Radix-4 FFT Algorithm

In this section presents the various computer simulation results to verify the performance of proposed method. The receiver is coherent detector. The transmitted signal is taken over sampling by a factor of 4 (L=4). The simulation parameters to be used in the following evaluations are shown in Table I.

Table 4.1 Simulation parameters of Radix-4 FFT algorithms.

Modulation	64QAM
Demodulation	Coherent
Allocated bandwidth	5MHz
Number of FFT points	256
Number of sub-carriers	64
Number of cluster (V)	4
Number of discrete phase (W)	4
Symbol duration	12.8us
Guard interval	1.28us

Figure 4.7 shows the PAPR performance for the conventional OFDM, conventional PTS, DIF-PTS based on radix-2 and radix-4, respectively when the modulation techniques are 64QAM. This figure shows the PAPR reduction performance of DIF PTS method when the radix-2 and redix-4 was employed. The PAPR reduction performance both the DIF-PTS base radix-2 and radix-4 can achieve same as conventional PTS method when middle stages are $(m-q)_{radix-2}=4$ and $(m-q)_{radix-4}=2$, respectively. However, the DIF-PTS can reduce the computation complexity than conventional PTS method.

Table 4.2 shows the comparisons for PAPR performance and computation complexity for the conventional OFDM, conventional PTS, DIF-PTS based on radix-2 and radix-4, respectively. This table shows the comparison computation complexity which refers the conventional PTS. From the table, the DIF-PTS and DIF-IPTS based on radix-2 can reduce the computation complexity 68.76% at $(m-q)_{radix-2}=2$ when compare with conventional PTS. The DIF-IPTS based on radix-4 shows the lower computation complexity which can reduce up to 88.80% at $(m-q)_{radix-4}=1$ when compare with conventional method. We can be conclude that the proposed method can achieve the lower PAPR reduction performance

and reduces the computation complexity compared with the conventional PTS and DIF-PTS based on radix-2.

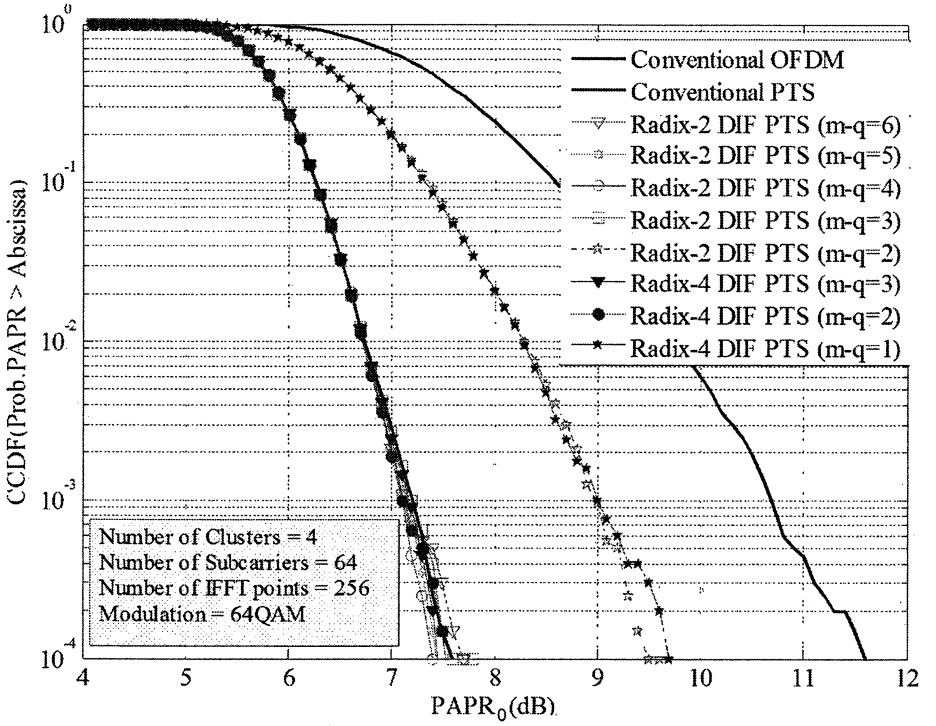

Fig. 4.7. Comparison of PAPR reduction performance among conventional PTS, Radix-2 DIF PTS and Radix-4 DIF PTS.

Table 4.2 Comparison of computation complexity for various methods.

	Computation multiplications Complexity (P=4 and N=256)				
	(m-q=6)	(m-q=5)	(m-q=4)	(m-q=3)	(m-q=2)
Conventional OFDM	NA	NA	NA	NA	NA
Conventional PTS	0%	0%	0%	0%	0%
DIF-PTS [5]	24.68%	36.77%	48.48%	59.40%	68.76%
Radix-2 DIF-IPTS	24.68%	36.77%	48.48%	59.40%	68.76%
Radix-4 DIF-IPTS	51.72%*	-	69.28%*	-	88.80%*

* Radix-4 (m-q = 3, 2, 1) , respectively.

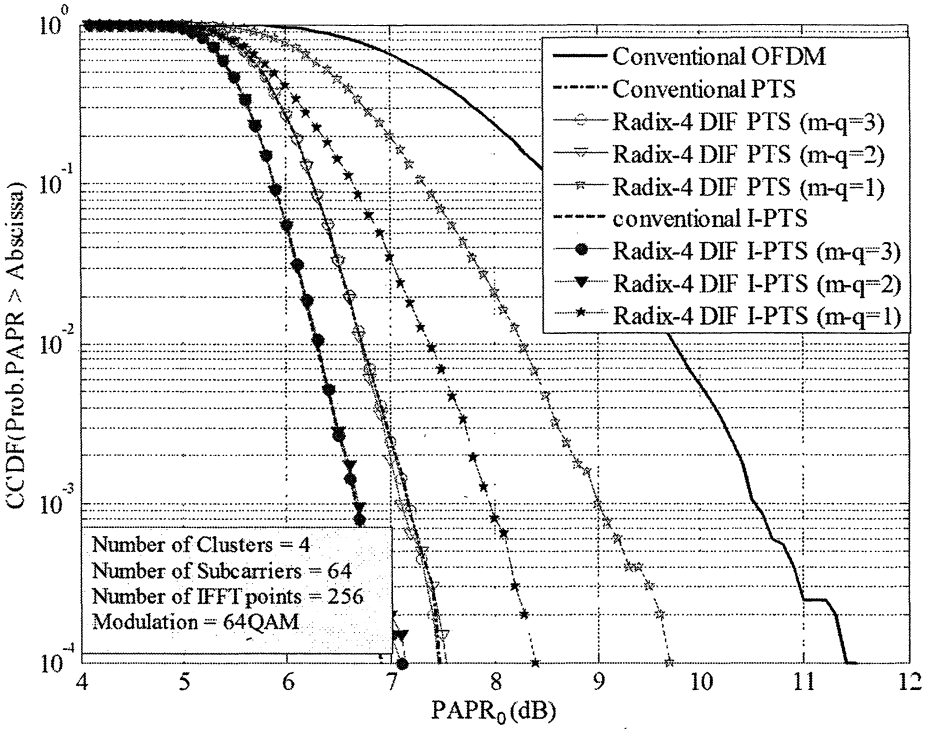

Fig. 4.8. Comparison of PAPR reduction performance among conventional PTS, Radix-4 PTS and Radix-4 DIF IPTS.

Figure 4.8 shows the PAPR performance for the conventional OFDM, conventional PTS, DIF-PTS and DIF-IPTS based on radix-4, respectively when the modulation techniques are 64QAM, number of subcarriers is 64 sub-carriers. This figure shows the PAPR reduction performance of DIF IPTS method based on radix-4 can achieve better PAPR reduction performance when compare with DIF-PTS method based on radix-4. The proposed new weighting factor can achieve the lower computation complex than DIF-IPTS based radix-2.

4.4.2 Performance of Split-Radix FFT Algorithm

This section presents the various computer simulation results to verify the performance of proposed method. The oversampling ratio of transmitted signal is taken by a factor of 4 (L=4). The simulation parameters to be used in the following evaluations are listed in Table 4.3.

Figure 4.9 shows the PAPR performance for the conventional OFDM, conventional PTS, DIF-PTS based on Radix-2 and Split-Radix, respectively when the modulation technique is quadrature phase-shift keying (QPSK). From the figure, we can see the PAPR reduction performance of DIF-PTS method when the Radix-2 and Split-Radix are employed. The PAPR reduction performance both for the DIF-PTS based on Radix-2 and Split-Radix can achieve

the same performance as that for the conventional PTS method when middle stages are $(m-q)_{Radix-2}=4$ and $(m-q)_{Split-Radix}=4$, respectively. However, the DIF-PTS can reduce much more computation complexity than conventional PTS method.

Table 4.3 Simulation parameters of Split-Radix FFT Algorithms.

Parameters	Values
Modulation	QPSK
Demodulation	Coherent
Allocated bandwidth	5MHz
Number of FFT points	256 and 512
Number of sub-carriers	64 and 128
Number of cluster (P)	4
Number of discrete phase (W)	4
Symbol duration	12.8us
Guard interval	1.28us

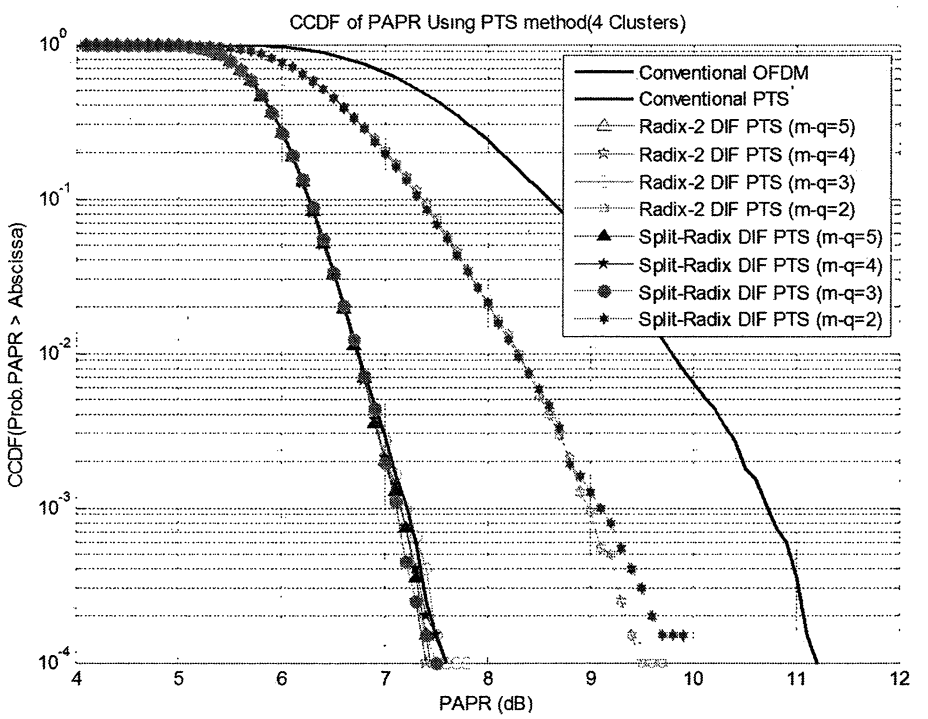

Fig. 4.9. Comparison of PAPR reduction performance for the conventional PTS, Radix-2 DIF PTS and Split-Radix DIF PTS methods.

Table 4.4 shows the comparisons for the computation complexity for the conventional OFDM, conventional PTS, DIF-PTS based on Radix-2 and Split-Radix, respectively. This table shows the comparison computation complexity which refers the conventional PTS.

From the table, the DIF-PTS and DIF-IPTS based on radix-2 can reduce the computation complexity 68.76% at $(m-q)_{Radix-2}=2$ when comparing with conventional PTS. The DIF-IPTS based on Split-Radix shows the lower computation complexity which can reduce up to 81.08% at $(m-q)_{Split-Radix}=2$ when comparing with conventional method.

Table 4.4 Comparisons of computation complexity for difference methods.

	Computation multiplications Complexity (P=4 and N=256)				
	(m-q=6)	(m-q=5)	(m-q=4)	(m-q=3)	(m-q=2)
Conventional OFDM	NA	NA	NA	NA	NA
Conventional PTS	0%	0%	0%	0%	0%
DIF-PTS [4]	24.68%	36.77%	48.48%	59.40%	68.76%
Radix-2 DIF-IPTS	24.68%	36.77%	48.48%	59.40%	68.76%
Split-Radix DIF-IPTS	52.99%	59.04%	67.82%	74.64%	81.08%

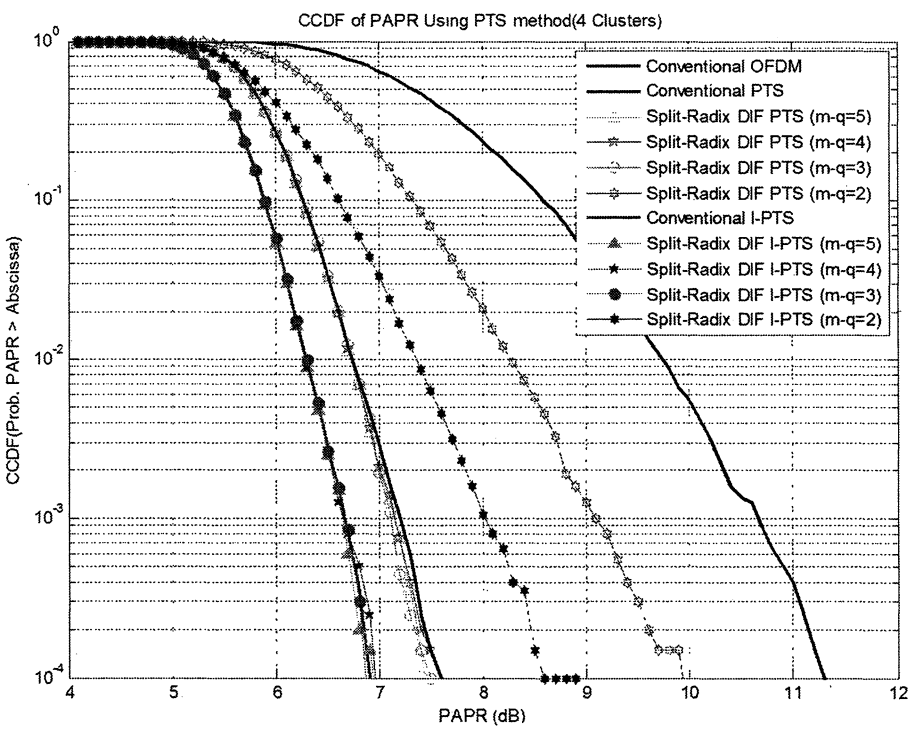

Fig. 4.10. Comparison of PAPR reduction performance between conventional PTS and Split-Radix DIF IPTS methods.

Figure 4.10 shows the PAPR performance for the conventional OFDM, conventional PTS, DIF-PTS and DIF-IPTS based on Split-Radix, respectively when the modulation technique is QPSK, and the number of subcarriers is 64. From the figure, it can be observed that the PAPR reduction performance of DIF-IPTS method based on Split-Radix can achieve better PAPR reduction performance when comparing with DIF-PTS method based on Split-Radix. From the figure, it can be concluded that the proposed new weighting factor can achieve the lower computation complex than DIF-IPTS based Radix-2.

From these results, it can be concluded that the proposed method can achieve the better PAPR reduction performance and the lower computation complexity as compared with the conventional PTS and DIF-PTS based on Radix-2.

4.4.3 Performance of Extended Split-Radix FFT Algorithm

This section presents the various computer simulation results to verify the performance of proposed method. The receiver is coherent detector. The transmitted signal is taken over sampling by a factor of 4 (L=4). The simulation parameters to be used in the following evaluations are listed in Table I.

Table 4.5 Simulation parameters of Extended Split-Radix FFT Algorithms.

Modulation	QPSK
Demodulation	Coherent
Allocated bandwidth	5MHz
Number of FFT points	256 and 512
Number of sub-carriers	64 and 128
Number of cluster (V)	4
Number of discrete phase (W)	4
Symbol duration	12.8us
Guard interval	1.28us

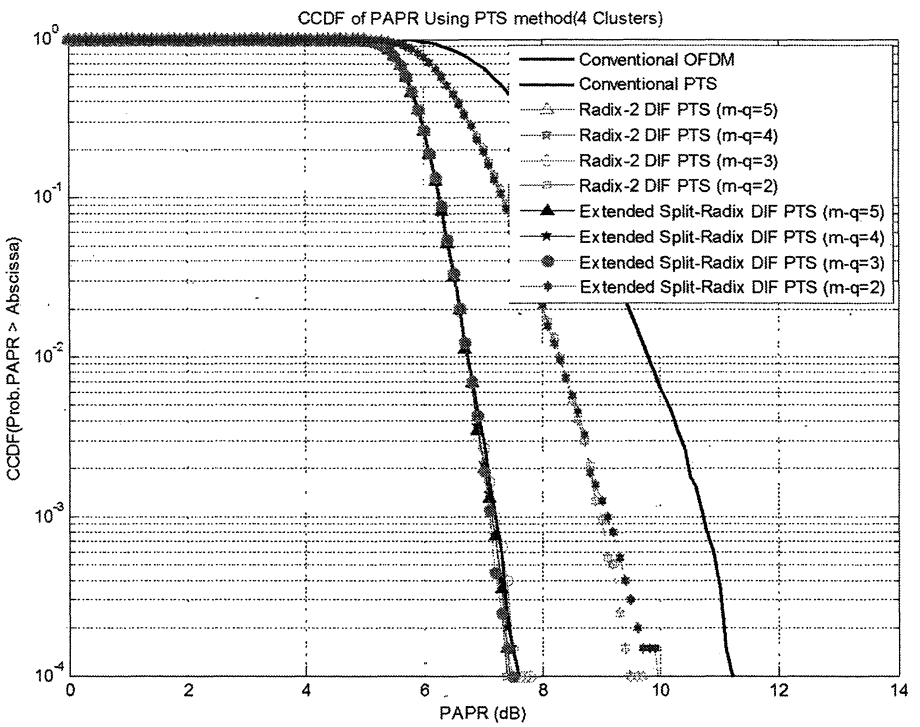

Fig. 4.11. Comparison of PAPR reduction performance for the conventional PTS, Radix-2 DIFPTS and Extended Split-Radix DIF PTS methods.

Figure 4.11 shows the PAPR performance for the conventional OFDM, conventional PTS, DIF-PTS based on Radix-2 and Extended Split-Radix, respectively when the modulation technique is QPSK. This figure shows the PAPR reduction performance of DIF-PTS method when the Radix-2 and Split-Radix are employed. The PAPR reduction performance both for the DIF-PTS base Radix-2 and Extended Split-Radix can achieve same performance as that for the conventional PTS method when middle stages are $(m-q)_{Radix-2}=4$ and $(m-q)_{Split-Radix}=4$ $(m-q)_{Split-Radix}=4$ $(m-q)_{Split-Radix}=4$, respectively. However, the DIF-PTS can reduce much more computation complexity than conventional PTS method.

Table 4.6 shows the comparisons for the PAPR performance and computation complexity for the conventional OFDM, conventional PTS, DIF-PTS based on Radix-2 and Extended Split-Radix, respectively. This table shows the comparison computation complexity which refers the conventional PTS. From the table, the DIF-PTS and DIF-IPTS based on radix-2 can reduce the computation complexity 68.76% at $(m-q)_{Radix-2}=2$ when comparing with conventional PTS. The DIF-IPTS based on Extended Split-Radix shows the lower computation complexity which can reduce up to 76.66% at $(m-q)_{Split-Radix}=2$ when comparing with conventional method. From these results, it can be concluded that the proposed method

can achieve the lower PAPR reduction performance and reduces the computation complexity as compared with the conventional PTS and DIF-PTS based on Radix-2.

Table 4.6 Comparisons of Computation Complexity for Difference Methods.

	Computation multiplications Complexity (P=4 and N=256)				
	(m-q=6)	(m-q=5)	(m-q=4)	(m-q=3)	(m-q=2)
Conventional OFDM	NA	NA	NA	NA	NA
Conventional PTS	0%	0%	0%	0%	0%
DIF-PTS [4]	24.68%	36.77%	48.48%	59.40%	68.76%
Radix-2 DIF-IPTS	24.68%	36.77%	48.48%	59.40%	68.76%
Extended Split-Radix DIF-IPTS	37.65%	47.01%	54.03%	61.45%	76.66%

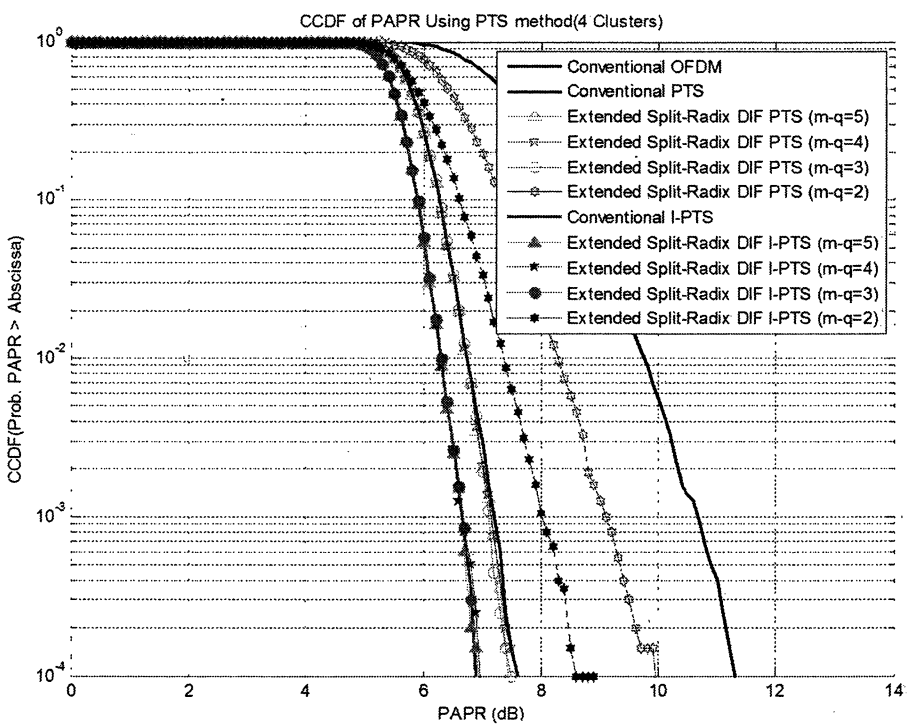

Fig. 4.12. Comparison of PAPR reduction performance between conventional PTS and Extended Split-Radix DIFIPTS methods.

Figure 4.12 shows the PAPR performance for the conventional OFDM, conventional PTS, DIF-PTS and DIF-IPTS based on Extended Split-Radix, respectively when the

modulation technique is QPSK, number of subcarriers is 64. From the figure, it can be observed that the PAPR reduction performance of DIF-IPTS method based on Split-Radix can achieve better PAPR reduction performance when comparing with DIF-PTS method based on Extended Split-Radix. From the figure, it can be concluded that the proposed new weighting factor can achieve the lower computation complex than DIF-IPTS based Radix-2.

4.5 Conclusions

In this chapter, we proposed the new weighting factor technique for the PTS method in conjunction with DIF-PTS method based on the Radix-4, Split-Radix and Extended Split-Radix. The proposed new weighting factors for the 1^{st} and 2^{nd} parts have the predetermined relationship so as to keep the same size of side information. To reduce the computation complexity, we employed the Radix-4, Split-Radix and Extended Split-Radix DIF-IFFT technique. From the computer simulation results, Analysis shows that all methods provide the same PAPR reduction but the computation complexity of I-PTS based radix-4 at middle stage in IFFT shows the better reduction of computation complexity than radix-2, Split-Radix and Extended Split-Radix methods. We confirmed that all the proposed methods showed the better PAPR performance and lower computation complexity with keeping the same size of side information as compared with the conventional DIF-PTS method.

CHAPTER 5

PROPOSAL OF NEW PAPR REDUCTION METHOD FOR OFDM SIGNAL BY USING PERMUTATION SEQUENCES

Many PAPR reduction techniques for OFDM signal have been proposed up to today, which can be classified into two major methods as the distortion and distortion-less methods. The most of distortion-less methods show better PAPR performance without degradation of BER performance. This chapter proposes a novel distortion-less PAPR reduction method which employs the permutation sequence in the frequency domain with embedded side information. The feature of proposed method is to achieve the better PAPR performance with very few side information for the correct demodulation of data information at the receiver. This chapter presents various computer simulation results to verify the effectiveness of proposed method as comparing with the conventional OFDM method in the non-linear channel.

5.1 Introduction

The Orthogonal Frequency Division Multiplexing (OFDM) technique has been received a lot of attentions especially in the field of wireless communications because of its efficient usage of frequency bandwidth and robustness to the multi-path fading. From these advantages, the OFDM technique has already been adopted as the standard transmission technique in the wireless LAN systems and the terrestrial digital TV broadcasting systems. The OFDM technique is also employed in the next generation of mobile communication system (LTE). One of the limitations of using OFDM technique is the larger peak to average power ratio (PAPR) of its time domain signal [17] [9]. The larger PAPR signal would cause the severe degradation of bit error rate (BER) performance due to the inter-modulation noise occurring in the non-linear amplifier.

Many PAPR reduction techniques have been proposed to overcome the PAPR problem up to today. These techniques can be categorized into two major methods as distortion and distortion-less methods. The distortion techniques include the clipping and filtering method [21][22]. Although this method can improve the PAPR performance relatively, it leads the degradation of BER performance and undesirable spectrum re-growth to the adjacent channel. The distortion-less techniques [23],[26],[27],[29],[31],[34],[64] include the coding, tone reservation (TR), tone injection (TI), active constellation extension (ACE), and multiple signal representation techniques such as partial transmit sequence (PTS) and selected mapping (SLM). These techniques can achieve better PAPR performance without degradation of BER performance. However these methods improve the PAPR performance at the cost of transmission efficiency, higher computational complexity, larger memory size, and requirement of separate channel for informing the side information to the receiver. In this chapter, we propose a novel distortion-less PAPR reduction method with permutation of data sequence in the frequency domain. The proposed method also employs a few dummy and parity subcarriers as the embedded side information in the data subcarriers which is used for the demodulation of data information at the receiver. The proposed method can achieve the better PAPR performance with higher transmission efficiency.

In the following of this chapter, Section 5.2 presents the system model of OFDM method in the non-linear channel. Section 5.3 presents the proposed PS method. Section 5.4 presents the various computer simulation results to verify the performance of proposed PS method, and Section 5.5 concludes the chapter.

5.2 System Model

Figure 5.1 shows the block diagram of OFDM system to be used in the following evaluation. In the figure, X_n is the modulated signal at the *n-th* sub-carrier in the frequency domain and x_k is the time domain signal at *k-th* sample point, which is converted from the frequency domain data by using IFFT. The time domain sampled OFDM signal y_k after adding guard interval (GI) to x_k will be converted to the analogue signal by the digital-analogue converter (D/A) and then converted to the radio frequency (RF) by the frequency up-converter (U/C) as shown in Fig.5.1. The output signal of U/C is inputted to the non-linear amplifier and transmitted to the channel. The output signal of non-linear amplifier can be expressed by the following equation

$$s(t) = F[|y(t)|]e^{j\{\arg[y(t)]+\Phi[|y(t)|]\}} \tag{5.1}$$

where, *y(t)* and *s(t)* are the input and output RF signal of non-linear amplifier, and F and Φ represent the AM/AM and AM/PM conversion characteristics of non-linear amplifier. The non-linear amplifier assumed in this chapter is the Solid State Power Amplifier (SSPA) of which AM/AM and AM/PM conversion characteristics are modeled by the following equations (1.44) and (1.45), respectively. In the following evaluations, the values for these parameters are assumed by $A=1$, $r=2$ and $\alpha_\phi = 0.01$ of which these parameters can approximate the typical SSPA [13].

In the OFDM system, M frequency domain data symbols$\{X_n, n = 0,1,\ldots, M\text{-}1\}$ which correspond to subcarriers, are modulated with a set of orthogonal frequency $\{f_n , n = 0,1,\ldots, M\text{-}1\}$. The frequency of M subcarriers are chosen to be orthogonal, i.e. $f_n = n\Delta f$, where $\Delta f = 1/MT$ and T represents the OFDM data symbol period. The resulting baseband OFDM signal x_k can be expressed by,

$$x_k = \sum_{n=0}^{M-1} X_n e^{j\frac{2\pi nk}{N}} \quad 0 \le k \le N-1. \tag{5.2}$$

where N is the number of IFFT points including zero padding. The PAPR [22] of transmitted time domain OFDM signal is defined by,

$$\text{PAPR} = \frac{\max\limits_{0\le k\le N} |x_k|^2}{E\left[|x_k|^2\right]} \tag{5.3}$$

where E denotes the expected value. To evaluate the PAPR performance for OFDM signal from the statistical point of view, the Complementary Cumulative Distribution Function

(CCDF) given in (5.4) is used to represent the probability of exceeding a given threshold $PAPR_0$.

$$CCDF(PAPR_0) = Pr(PAPR > PAPR_0). \tag{5.4}$$

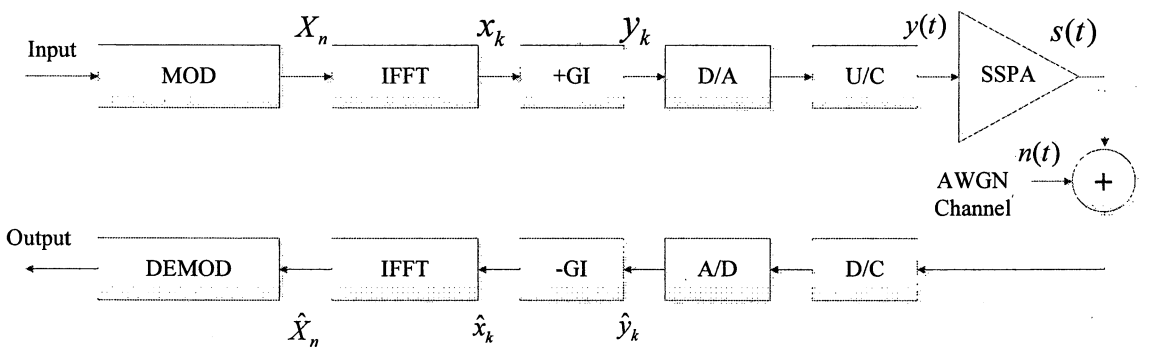

Fig. 5.1. OFDM system model.

5.3 Proposal of PS Method

Figure 5.2 shows the structure of frequency domain OFDM symbol for the proposed PS method. There are two types of permutation methods Type I and Type II as shown in the figure. Type I is to perform the permutation only for the first M/2 subcarriers, while Type II is to perform the permutation both for the first and the last part of M/2 subcarriers. Although the computation complexity for the Type II is larger than Type I, the improvement of PAPR performance for the Type II is better than Type I. For simple explanation, we only give an example explanation for type I in the following. The proposed OFDM symbol consists of (M-3) data sub-carriers, two dummy sub-carriers and one parity sub-carrier which can be expressed by,

$$\boldsymbol{X} = [D_1, D_2, P, X_0, X_1, X_2, \cdots X_{M/2-3}, X_{M/2-2}, \cdots, X_{(M-4)}] \tag{5.5}$$

where D is dummy sub-carriers with power of 0 (Null subcarriers) and P is parity check subcarrier with power of α which power is taken as the same as the averaged power of data subcarriers. The dummy (null subcarriers) and parity subcarriers will be used for the detection of location for the first data subcarrier X_0 at the receiver for the correct demodulation of data information. After the insertion of zero padding, two null sub-carriers and one parity sub-carrier, the new OFDM symbol can be generated by circularly rotation of subcarriers only for the first part of *M/2* subcarriers so as to improve the PAPR performance as shown in Fig.5.2.

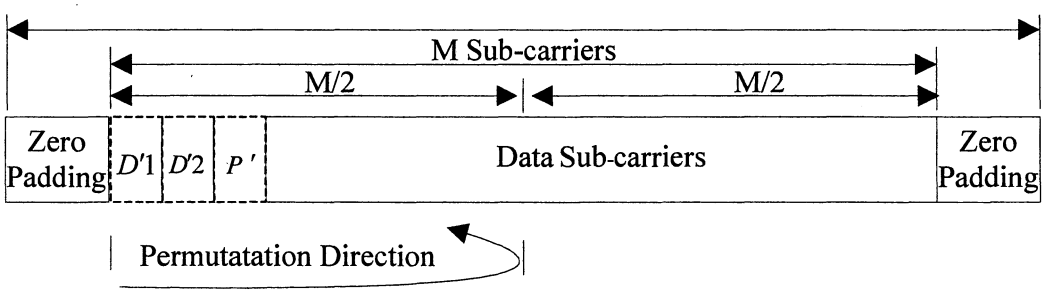

(a) Type I

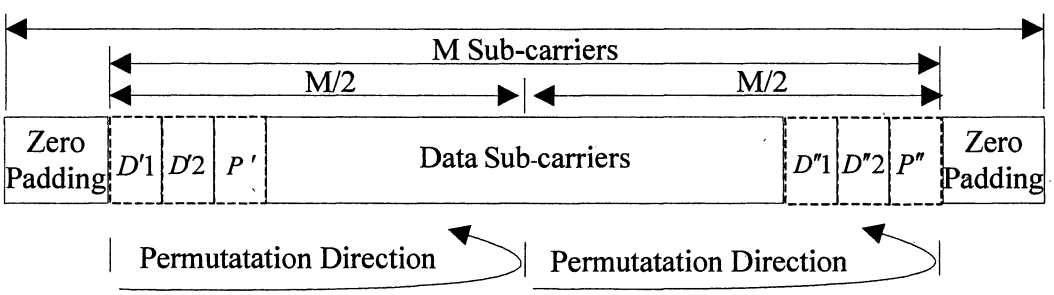

(b) 64QAM

Fig. 5.2. Structure of frequency domain OFDM symbol for proposed PS method.

In the proposed method, the first half of M/2 subcarriers are simply rotated in the frequency domain so as to achieve the better PAPR performance. The number of rotation of subcarriers performed at the transmitter can be detected by using the dummy and parity check subcarriers at the receiver. When the number of rotation for the first M/2 subcarriers is $L=6$ as an example, the resultant ordering of subcarriers is given by,

$$\boldsymbol{X}_{R=6} = [X_2, X_3, \cdots, X_{M/2-3}, D_1, D_2, P, X_0, X_1, X_{M/2-2}, \ldots X_{(M-4)}] \tag{5.6}$$

The example of proposed permutation sequence method for Type I is shown in Fig.5.3

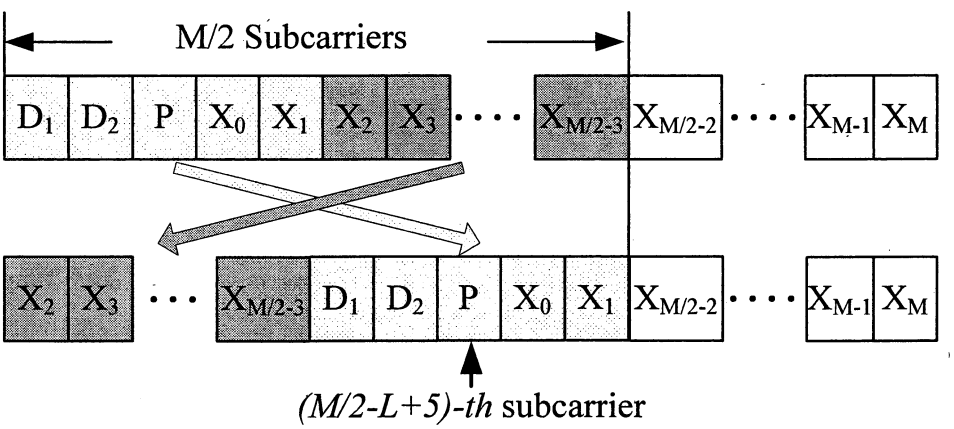

Fig. 5.3. Example of Type I permutation sequence when L=6.

When $L=6$, the location of parity check subcarrier P becomes *(M/2-L+5)-th* subcarrier in the OFDM symbol. In this case, the sign of parity check subcarrier P is set by the following equation in order to detect the number of rotation for the subcarriers with higher accuracy at the receiver.

$$P = (-1)^{(M/2-L+5)} \cdot \alpha \tag{5.7}$$

The permutation for the rotation of the first part of *M/2* subcarriers is taken from *0* to *M/2*. In the proposed method, the best PAPR performance will be selected from among the rotation of subcarriers from *0* to *M/2*. Then the selected ordering of subcarriers with the best PAPR performance will be converted to the time domain signal by using IFFT. The time domain signal can be given by,

$$\tilde{x}_k = \frac{1}{\sqrt{N}} = \sum_{n=0}^{N-1} \widetilde{X}_n \cdot e^{j\frac{2\pi kn}{N}} \tag{5.8}$$

where $\tilde{X}_n$ is the frequency domain signal after performing the permutation of subcarriers rotation and $\tilde{x}_k$ is the time domain signal with low PAPR performance. As for the Type II, the time domain signal with lower PAPR performance can be achieved by using the same procedures as the Type I. Fig. 5.4 shows the structure of proposed transmitter.

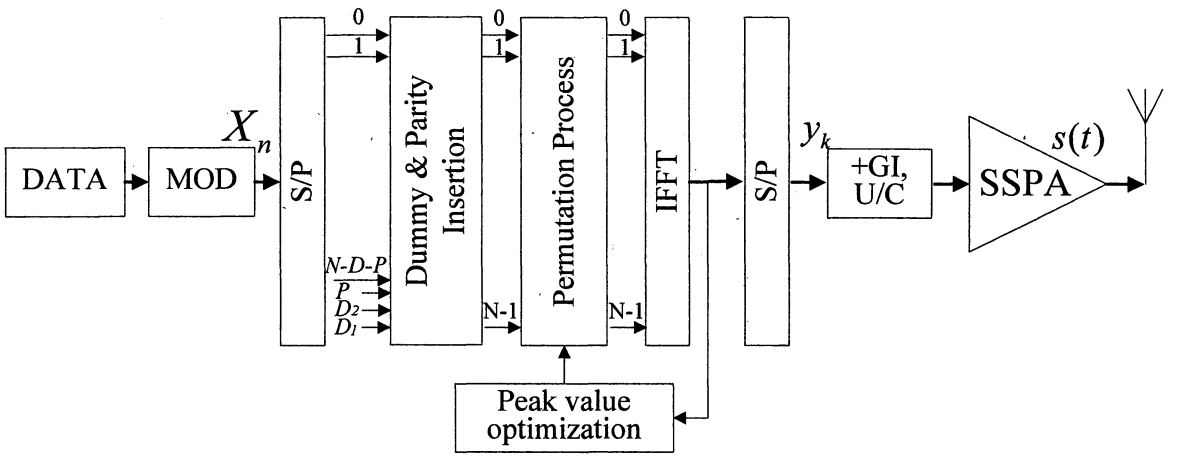

Fig. 5.4. Structure of transmitter for the proposed method.

5.4 Detection method for embedded side information

The first data subcarrier which is moved to the certain subcarrier number after the permutation of subcarriers rotation performed at the transmitter is required to detect at the receiver for the correct demodulation of data information. The position of first data subcarrier can be detected by finding the position of dummy (null subcarriers) and check the sign of parity check sub-carriers.

The proposed detection method is firstly to replace the consecutive two subcarriers to zero from the start of received OFDM signal in the frequency domain and calculate the power of received signal by using the following equation.

$$Power(\ell) = \sum_{n=0}^{M/2} R_n^{(\ell)} \cdot conj(R_n^{(\ell)}) \qquad (5.9)$$
$$\ell = 0, 1, 2, \cdots, M/2-1$$

where $R_n^{(m)}$ is the received frequency domain signal at the *n-th* subcarrier after replacing two subcarriers to zero at $\ell - th$ and $(\ell+1) - th$ subcarriers and *conj* indicates the complex conjugate. From (5.9), the maximum power could be obtained when ℓ is equal to the location of first dummy subcarriers. The detection performance can be improved by checking the sign of the parity check subcarrier P for the next subcarrier of the detected $\ell - th$ and $(\ell+1) - th$ dummy subcarriers with having the maximum power given in (5.9). The sign of parity check subcarrier given by (5.7) can be used for assure the detection of the first data subcarrier X_0. The detection performance can be improved by using two dummy subcarriers and parity check subcarrier. Figs. 5.5 and 5.6 show the detection algorithm for permutation number and the structure of proposed receiver.

By using the above method, the original data sequence can be recovered and the data information can be demodulated correctly. The feature of proposed method is to detect the permutation number precisely by using very few embedded side information.

5.5 Evaluation of Proposed PS Method

This section presents the various computer simulation results to verify the performance of proposed method as comparing with the conventional OFDM. Table 5.1 shows the list of simulation parameters. In the simulations, the number of FFT points $N=256$ is taken by 4 times larger than the number of subcarriers $M=64$ to evaluate the PAPR performance with higher accuracy.

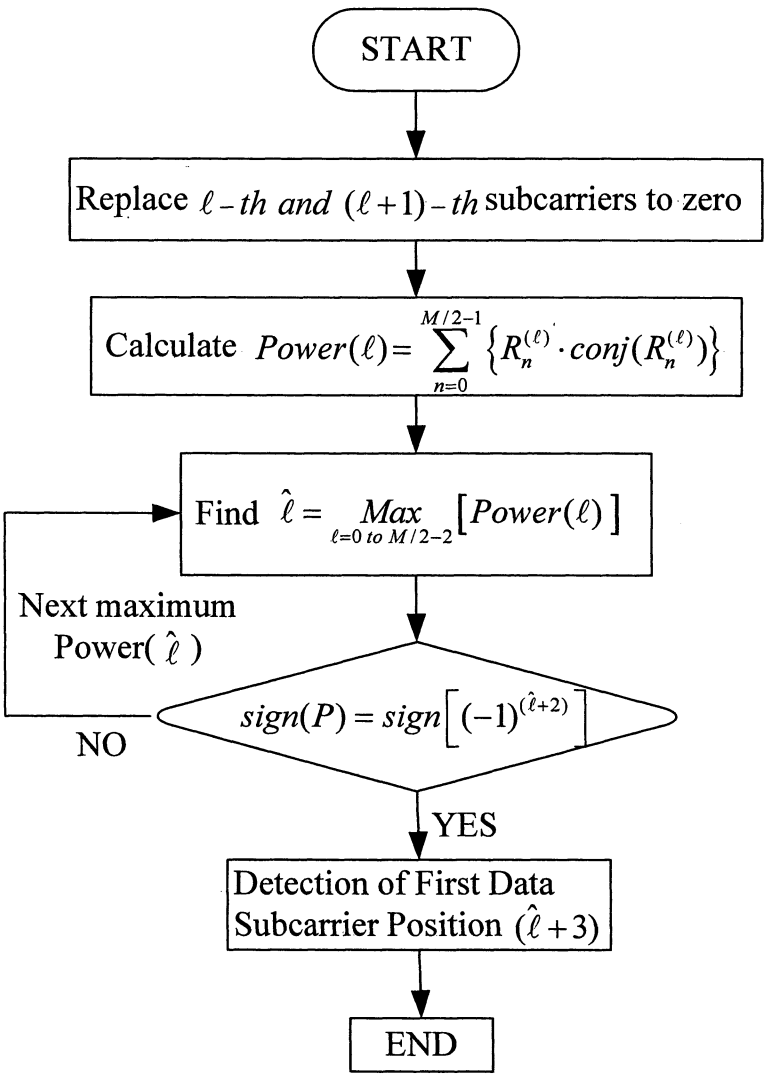

Fig. 5.5. Detection algorithm for permutation number.

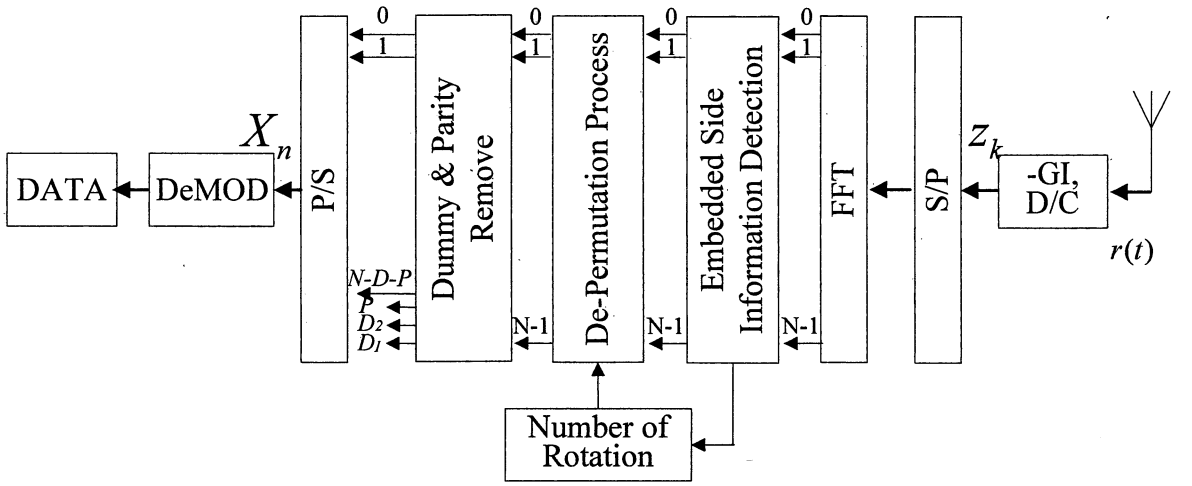

Fig. 5.6. Structure of receiver for the proposed method.

Table 5.1 Simulation parameters.

Modulation method	64QAM
Demodulation method	Coherent
OFDM bandwidth	5 MHz
Number of FFT points (N=Z+M)	256
Number of sub-carriers (M=D+P+K)	64
Number of dummy sub-carriers (D)	2
Number of parity sub-carriers (P)	1
Number of data sub-carriers (K)	61 for Type I 58 for Type II
Number of zero padding (Z)	192
Symbol duration	12.8 us
Guard interval	1.2 us
Model of non-linear amplifier	SSPA
Non-linear parameter of Eq. (2)	r=2
Channel model	AWGN

Table 5.2 shows the transmission efficiency for the proposed Type I and Type II methods. From the table, it can be observed that the proposed method can achieve the higher transmission efficiency because the number of rotation selected at the transmitter can be detected by using 2 dummy subcarriers and one parity check subcarriers for Type I and 4 dummy subcarriers and 2 parity check subcarriers for Type II at the receiver.

5.5 Evaluation of Proposed Method

Figure 5.7 shows the PAPR performance both for the conventional OFDM and proposed PS methods when the number of sub-carriers (*M*) is 64 including 2 dummy sub-carriers (*D*) and one parity sub-carrier for Type I and 4 and 2 for the Type II, respectively. In the figure, the PAPR performance is evaluated by using the Cumulative Distribution Function (CDF). From the figure, it can be observed that the proposed PS method shows better PAPR performance than that for the conventional OFDM by 2.2dB for type I and 3 dB for Type II at CCDF of 10^{-1}, respectively. Here it should be noted that the degradation of BER performance of OFDM signal in the non-linear channel would be dominated by the PAPR performance at the CCDF higher than 10^{-1}. From these results, it can be expected that the proposed PS method could achieve the better BER performance than that for the conventional OFDM method in the non-linear channel.

Table 5.2 Transmission efficiency for the proposed method.

Number of sub-carriers	Transmission efficiency	
	Type I	Type II
64	61/64 (95.3%)	58/64 (90.6%)
256	253/256 (98.8%)	250/256 (97.7%)
1024	1021/1024 (99.7%)	1018/1024 (99.4%)

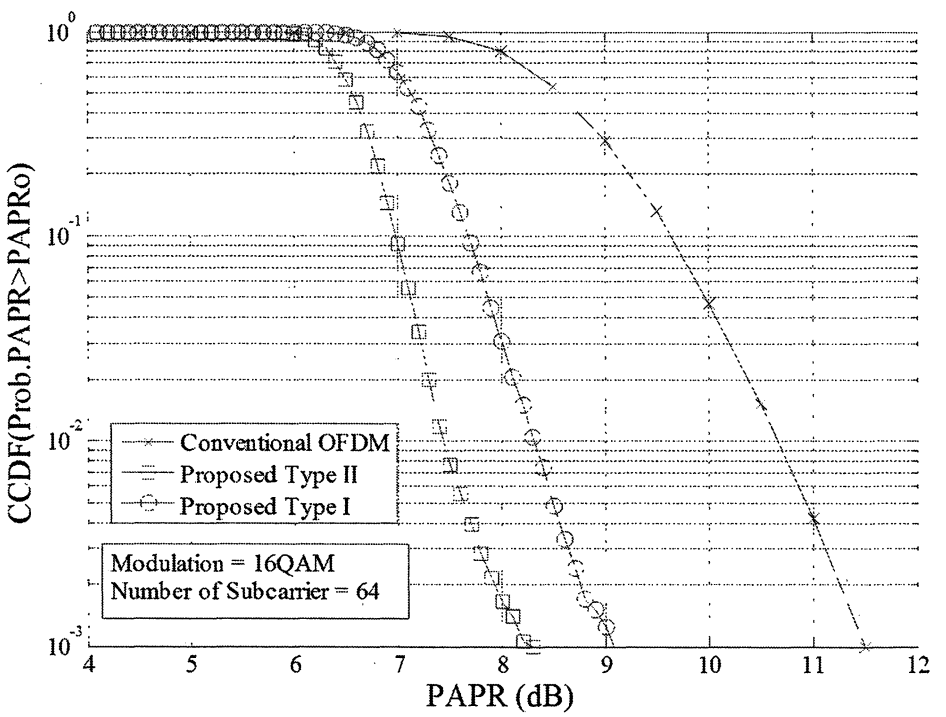

Fig. 5.7. PAPR performance for the proposed method.

Figure 5.8 shows the BER performances in the non-linear channel when changing C/N for the conventional OFDM and the proposed PS method when using 64QAM as modulation method. In the simulation, the number of data subcarriers (K), dummy sub-carriers (D) and parity sub-carrier (P) are taken by 61, 2 and 1 for type I and 58, 4 and 2 for type II, respectively. The input back-off (IBO) of non-linear SSPA amplifier is taken by 0dB, -2dB, -4dB and -6dB, respectively. From the figures, the proposed PS method can achieve much better BER performance than those for the conventional OFDM in the non-linear channel.

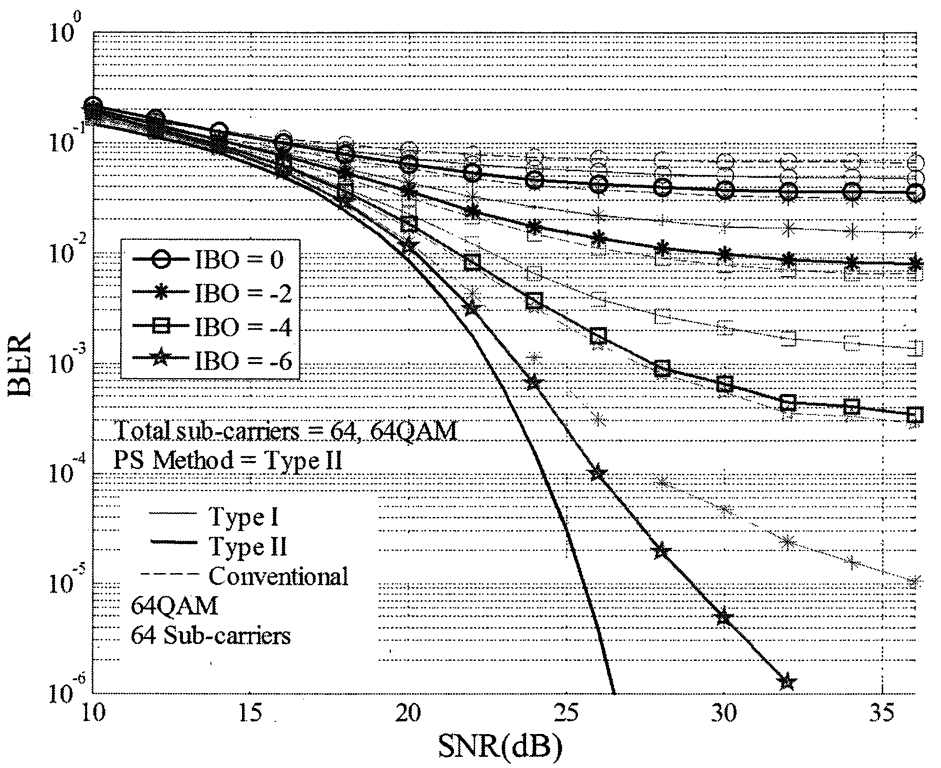

Fig. 5.8. BER performance of proposed method in the non-linear channel.

5.6 Conclusions

This chapter proposed the new PAPR reduction method which can achieve the better PAPR performance. The salient future of proposed method is to rotate the subcarriers in the frequency domain so as to achieve the better PAPR performance. Since the proposed method enables the detection of rotation number precisely selected at the receiver by using the very few dummy subcarriers which is embedded in the OFDM symbol as the side information, the propose method can achieve the higher transmission efficiency. From the computer simulation results, this chapter confirmed that the proposed PS method can achieve the better PAPR performance and better BER performance in the non-linear channel.

CHAPTER 6

CONCLUSIONS

In this thesis, the PAPR in the OFDM modulation technique is studied and evaluated. The OFDM signal with larger PAPR will cause the undesirable spectrum re-growth and the larger degradation of BER performance both due to the inter-modulation products occurring in the non-linear amplifier at the transmitter.

This thesis proposed the solutions for PAPR problems. In this degree thesis, the following two types of methods are proposed to solve the above problems.

1) Non-linear distortion compensation method for OFDM signal
2) PAPR reduction methods for OFDM signal with lower computation complexity

As for the first method, this thesis proposes the Improved DAR (IDAR) method, which can mitigate both the clipping noise and inter-modulation noise. In the proposed IDAR method, the characteristics of non-linear amplifiers are required to be known at the receiver for mitigating the inter-modulation noise. This thesis also proposes the estimation method for AM-AM and AM-PM conversions characteristics of non-linear amplifiers by using low PAPR (Peak to Averaged Power Ratio) preamble symbols.

This thesis demonstrates the effectiveness of proposed IDAR method when applying the satellite communication systems. From the computer simulation results, it is concluded that the proposed IDAR method can achieve the higher transmission data rate and higher efficient usage of non-linear power amplifier with keeping the better BER performance even in the non-linear satellite channel.

As for the second method, this thesis proposes PAPR reduction methods based on PTS technique. The conventional PTS method requires the larger number of clusters and weighting factors to achieve the better PAPR performance which leads larger computation complexity.

5.6 Conclusions

To reduce the computation complexity, DIF-PTS method is proposed which employs the intermediate signals within the IFFT and used radix-2, radix-4, Split-Radix and Extended Split-radix for decimation in the frequency domain (DIF) to obtain the PTS sub-blocks. Multiple IFFTs are then applied to the remaining stages. The PTS sub-blocking is performed in the middle stages of the N-point radix FFT DIF algorithm. The DIF-PTS method can reduce the computational complexity relatively while it shows almost the same PAPR reduction performance as that of the conventional PTS method. To improve the PAPR performance with low computation complexity, this thesis proposes a new weighting factor technique for the PTS method in conjunction with DIF-PTS sub-blocking based on radix-r, Split-Radix and Extended Split-Radix IFFT technique which can improve both the PAPR performance and computation complexity. The proposed method can achieve the better PAPR reduction performance than that for the DIF-PTS method without any increasing of size of side information.

As a conclusion of researches in this thesis, the proposed PAPR reduction methods and mitigation methods of non-linear distortion noise with low computation complexity could provide various practical solutions for next generation of multimedia wireless communications systems employing the OFDM technique.

APPENDIX A

LIST OF PUBLICATIONS

Journal Papers

[1] Pornpawit Boonsrimuang, Pongsathorn Reangsuntea, Pisit Boonsrimuang and Hideo Kobayashi, "Proposal of Improved PTS Method Based on Split-Radix IFFT for OFDM Signal," *David Publishing Journal, Trans on Computer Technology and Application,* Vol. 3, No. 6, pp.425-430, June 2012.

[2] Pornpawit Boonsrimuang, Pisit Boonsrimuang, Tawil Paungma and Hideo Kobayashi, "Proposal of QAM-OFDM System with IDAR Method Designed for Satellite Channel," *ECTI Transactions on Computer and Information Technology*, Vol.6,No.2,pp.108-119,Nov 2012.

[3] Pisit Boonsrimuang, Pornpawit Boonsrimuang, Kazuo Mori, Tawil Paungma and Hideo Kobayashi, "Mitigation of Non-linear Distortion using PTS and IDAR Method for Multi-Level QAM-OFDM system," *ECTI Transactions on Computer and Information Technology*, Vol.1, No.2, pp.84-90, Nov. 2005.

[4] Tanairat Mata, Pornpawit Boonsrimuang, Pisit Boonsrimuang and Hideo Kobayashi, "Proposal of Improved PTS Method for STBC MIMO-OFDM Systems", *IEICE Transactions on Communications*, Vol.E93-B,No.10, pp.2673-2676, Oct. 2010.

[5] Pornpawit Boonsrimuang, Kanchana Limwattanachai, PisitBoonsrimuang and Hideo Kobayashi, "Peak-to-Average Power Ratio Reduction Method for OFDM Signal by Using Permutation Sequences," *ECTI Transactions on Computer and Information Technology* (Under reviewing).

International Conference Articles

[1] Pornpawit Boonsrimuang, Sunisa Sanpan, Pisit Boonsrimuang, Tawil Paungma and Hideo Kobayashi, "Improved PTS Method with New Weighting Factor Technique for OFDM Signal," *Proc. of 69th IEEE Vehicular Technology Conference(VTC2009-Spring)*, April 2009.

[2] Sunisa Sanpan, Pornpawit Boonsrimuang, Pisit Boonsrimuang, Surapol Boonjun and Hideo Kobayashi, "A New Weighting Factor of PTS OFDM with Low Complexity for PAPR Reduction," *Proc. of 6th ECTI Annual Conference (ECTI-CON 2009)*, pp. 958-961, May 2009.

[3] Pornpawit Boonsrimuang, Boonsiri Kriengkriwat, Pisit Boonsrimuang, Tawil Paungma and Hideo Kobayashi, "Proposal of D-PTS Method with Non-Uniform Weighting Factor for PAPR Reduction in OFDM Systems," *Proc. of 6th ECTI Annual Conference (ECTI-CON 2009)*, pp. 954-957, May 2009.

[4] Pornpawit Boonsrimuang, Hideo Kobayashi, Kanchana Limwattanachai and PisitBoonsrimuang, "Peak-to-Average Power Ratio Reduction Method for OFDM Signal by Using Permutation Sequences," *Proc. of IEEE International Symposium on Intelligent Signal Processing and Communication Systems 2011 (ISPACS 2011)*, Dec. 2011.

[5] Pongsathorn Reangsuntea, Pornpawit Boonsrimuang, Pisit Boonsrimuang and Hideo Kobayashi, "A New Weighting Factor of PTS OFDM with Low Complexity Base on Radix-4 IFFT for PAPR Reduction," *Proc. of 1st International Symposium on Technology for Sustainability (ISTS 2011)*, Jan. 2012.

[6] Pornpawit Boonsrimuang, Kanchana Limwattanachai, Pisit Boonsrimuang and Hideo Kobayashi, "Proposal of New PAPR Reduction Method for OFDM Signal by Using Permutation Sequences," *Proc. of 14th International Conference on Advanced Communication Technology 2012* (ICACT2012), Feb. 2012.

[7] Pornpawit Boonsrimuang, Pongsathorn Reangsuntea, Pisit Boonsrimuang and Hideo Kobayashi, "A New Weighting Factor of PTS OFDM with Low Complexity Based on Split-Radix IFFT for PAPR Reduction," *Proc. of 14th International Conference on Advanced Communication Technology 2012* (ICACT2012), Feb. 2012.

[8] Pornpawit Boonsrimuang, Panya Jirajaracheep, Pongsathorn Reangsuntea, Pisit Boonsrimuang and Hideo Kobayashi, "A Low Complexity IPTS-Based Extended Split-Radix IFFT for PAPR Reduction in OFDM Systems," *Proc. of 9th ECTI Annual Conference (ECTI-CON 2012)*, May 2012.

[9] Pongsathorn Reangsuntea, Pisit Boonsrimuang, Tawil Paungma, Pornpawit Boonsrimuang and Hideo Kobayashi, "PAPR Reduction Performance Analysis Base on Partial Transmit Sequence," 2012 *International Conference on Engineering, Applied Sciences, and Technology* (ICEAST 2012), Nov.2012.

Local Conference Articles

[1] Pornpawit Boonsrimuang, Kanchana Limwattanachai, Pisit Boonsrimuang and Hideo Kobayashi, "Peak to Average Power Ratio Reduction Method for OFDM Signal by Using Permutation Sequences," in *Proc. of International Symposium for Sustainability byEngineering at MIU (IS2EMU2011)*, Dec. 2011.

BIBLIOGRAPHY

[1] IEEE Std. 802.11a, High-speed Physical Layer in the 5GHz Band, 1999.

[2] IEEE 802.16 WG, "SC-FDE PHY Layer System Proposal for Sub 11GHz BWA", March 2001.

[3] P. Dambacher, "Digital Terrestrial Television Broadcasting," Springer, 1998.

[4] S. Hara and R. Prasad, "Multicarrier Technoques for 4G Mobile Communications," Artech House, Boston, London, 2003.

[5] J. Proakis, "Digital Communications," McGraw-Hill, 4 edition, Aug. 2000.

[6] J. Barry, E. Lee, D. Messerschmitt, "Digital Communication," Springer; 3 edition, Sept. 2003.

[7] B. Sklar, "Digital Communications: Fundamentals and Applications," Prentice Hall; 2 edition, Jan. 2001.

[8] M. Engels, Wireless OFDM Systems How to make them work?, Kluwer Academic, United States of America, 2002

[9] J. Tellado, "Multicarrier Modulation with Low PAR," Kluwer Academic Publishiers, 2000.

[10] Ahmad R.S. Bahai, Burton R. Saltzberg, "Multi-Carrier Digital Communications Theory and Applications of OFDM", New York, Kluwer academic Pulishers, 2000.

[11] W.W. Lu: "Fourth-Generation Mobile Initiative and Technologies," *IEEE Transactions on Communications,* Vol. 40 No.3, pp104-145, 2002.

[12] Zou W.Y., Yiyan Wu, "COFDM: an overview," *IEEE Transactions on Broadcasting,* vol. COM-29, pp. 1715–1720, Nov. 1981.

[13] C. Rapp, "Effects of HPA-Nonlinearity on a 4-DPSK/OFDM-Signal for a Digitial Sound Broadcasting System," in *Proceedings of the Second European Conference on Satellite Communications*, Liege, Belgium, pp. 179-184, Oct. 22-24, 1991.

[14] A. A. M. Saleh, "Frequency independent and frequency dependent nonlinear model of TWT amplifiers," *IEEE Transactions on Communications,* vol. COM-29, pp. 1715–1720, Nov. 1981.

[15] Seung Hee Han, Jae Hong Lee, "An Overview of Peak-To-Average Power Ratio Reduction Techniques for Multicarrier Transmission," *IEEE Wireless Communications*, pp56-65, April 2005.

[16] C.E. Dimakis, S.S. Kouris and S.A. Kosmopoulos, "Performance Evaluation of 16-QAM Signaling Through Nonlinear Channel in an AWGN and Interference Environment: A Simulation Approach," *IEE Proceedings*, Vol.137, no 5, pp315-322, Oct. 1990.

[17] D Dardari, V. Tralli and A Vaccari, "A Theoretical Characterization of Nonlinear Distortion Effects in OFDM Systems," *IEEE Transactions on Communications,* Vol. 48, no. 10, pp.1775-1764, Oct 2000.

[18] L.J. Cimini, Jr: "Analysis and simulation of a digital mobile channel using orthogonal frequency division multiplexing," *IEEE Transactions on Communications*, Vol. COM-33, pp.665-675, 1985.

[19] Elena Costa and Silvano Pupolin, "M-QAM-OFDM System Performance in the Presence of a Nonlinear Amplifier and Phase Noise," *IEEE Transactions on Communications,* vol.50, pp462-472, March 2002.

[20] R. O'Neill and L. B. Lopes, "Envelope Variations and Spectral Splatter in Clipped Multicarrier Signals," *Proceedings of IEEE International Symposium on Personal Indoor and Mobile Radio Communications (PIMRC'95)*, Toronto, Canada, pp. 71–75, Sept. 1995.

[21] X. Li and L.J. Cimini, "Effects of clipping and filtering on the performance of OFDM," *Proceedings of IEEE Vehicular Technology Conf. (VTC'97)*, pp1634-1638, May 1997.

[22] J. Armstrong, "Peak-to-Average Power Reduction for OFDM by Repeated Clipping and Frequency Domain Filtering," *IEEE Transactions on Electronics Letter*, vol. 38, no. 8, pp. 246–47, Feb. 2002.

[23] A. E. Jones, T. A. Wilkinson, and S. K. Barton, "Block Coding Scheme for Reduction of Peak to Mean Envelope Power Ratio of Multicarrier Transmission Scheme," *IEEE Transactions on Electronics Letter*, vol. 30, no. 22, pp. 2098–99, Dec. 1994.

[24] A. E. Jones and T. A. Wilkinson, "Combined Coding for Error Control and Increased Robustness to System Nonlinearities in OFDM," *Proceedings of IEEE Vehicular Technology Conference (VTC'96)*, Atlanta, GA, pp. 904–08, Apr. –May 1996.

[25] J. A. Davis and J. Jedwab, "Peak-to-Mean Power Control and Error Correction for OFDM Transmission Using Golay Sequences and Reed-Muller Codes," *IEEE Transactions on Electronics Letter*, vol. 33, no. 4, pp. 267–68, Feb. 1997.

[26] B. S. Krongold and D. L. Jones, "PAR Reduction in OFDM via Active Constellation Extension," *IEEE Transactions on Broadcasting*, vol. 49, no. 3, Sept. 2003, pp. 258–68.

[27] S. H. Muller and J. B. Huber, "A Comparison of Peak Power Reduction Schemes for OFDM," *Proceedings of IEEE Global Telecommunications Conference (GLOBECOM '97)*, Phoenix, AZ, pp. 1–5, Nov. 1997.

[28] S. H. Muller and J. B. Huber, "A Novel Peak Power Reduction Scheme for OFDM," *Proceedings of IEEE International Symposium on Personal Indoor and Mobile Radio Communications (PIMRC'97)*, Helsinki, Finland, pp. 1090–94, Sept. 1997.

[29] S. H. Muller and J. B. Huber, "OFDM with reduce peak-to-average power ratio by optimum combination of partial transmit sequences," *IEEE Transactions on Electronics Letter,* vol. 33, no. 5, pp. 368–369, Feb. 1997.

[30] A. D. S. Jayalath and C. Tellambura, "Adaptive PTS Approach for Reduction of Peak-to-Average Power Ratio of OFDM Signal," *IEEE Transactions on Electronics Letter*, vol. 36, no. 14, pp. 1226–28, July 2000.

[31] L.J. Cimini, Jr. and N.R. Sollenberger, "Peak-to-Average Power Ratio Reduction of an OFDM Signal Using Partial Transmit Sequences," *IEEE Transactions on Communications Letter,* Vol. 4, no. 3, pp86-88, March 2000.

[32] C. Tellambura, "Improved Phase Factor Computation for the PAR Reduction of an OFDM Signal Using PTS," *IEEE Transactions on Communications Letter,* Vol. 5, no. 4, pp135-137, March 2001.

[33] Yang L., Chen R.S., Siu Y.M. and Soo K.K., "PAPR reduction of an OFDM signal by use of PTS with low computational complexity," *IEEE Transactions on Broadcasting*, Vol. 52, no. 1, pp83 – 86, March 2006.

[34] R. W. Bäuml, R. F. H. Fisher, and J. B. Huber, "Reducing the Peak-to-Average Power Ratio of Multicarrier Modulation by Selected Mapping," *IEEE Transactions on Communications Letter*, vol. 32, no. 22, pp. 2056–57, Oct. 1996.

[35] H. Breiling, S. H. Müller–Weinfurtner, and J. B. Huber, "SLM Peak-Power Reduction without Explicit Side Information," *IEEE Transactions on Communications Letter*, vol. 5, no. 6, pp. 239–41, June 2001.

[36] M. Friese, "Multitone Signals with Low Crest Factor", *IEEE Transactions on Communications*, vol. 45, pp. 1338–1344, Oct 1977.

[37] E. V. Der Ouderaa, Schoukens and J.Renneboog., "Peak Factor Minimization Using a Time-Frequency Domain Swapping Algorithm," *IEEE Transactions on Instrumentation and Measurement*, vol.37, pp145-147, Mar 1988.

[38] E. V. Der Ouderaa, Schoukens and J.Renneboog., "Peak Factor Minimization of input and Output Signals of Linear Systems," *IEEE Transactions on Instrumentation and Measurement,* vol.37, pp207-212, June 1988.

[39] B. S. Krongold and D. L. Jones, "PAR Reduction in OFDM via Active Constellation Extension," *IEEE Trans. Broadcast.*, vol. 49, no. 3, Sept. 2003, pp. 258–68.

[40] K.R. Rao, Do Nyeon Kim and Jae Jeong Hwang, "Fast Fourier Transform - Algorithms and Applications (Signals and Communication Technology ," Springer; Springer Dordrecht Heidelberg London New York, 2010.

[41] P. Duhamel, "Implementation of "Split-Radix" FFT Algorithms for Complex, Real, and Real-Symmetric Data," *IEEE Trans. on Acoustics, Speech, and Signal Processing.* Vol. ASSP-34, no. 2, pp285-295, April 1986.

[42] Ghassemi, A.; Gulliver, T.A., "A Low-Complexity PTS-Based Radix FFT Method for PAPR Reduction in OFDM Systems," *IEEE Transactions on Signal Processing*, vol.56, no.3, pp.1161-1166, March 2008.

[43] D. Takahashi, "An Extended Split-Radix FFT Algorithm," *IEEE signal processing letters*. Vol. 8, no. 5, pp145-147, May 2001.

[44] C.E. Dimakis, S.S. Kouris and S.A. Kosmopoulos, "Performance Evaluation of 16-QAM Signaling Through Nonlinear Channel in an AWGN and Interference Environment: A Simulation Approach," *IEE Proceedings,* Vol137, no 5, pp315-322, Oct. 1990.

[45] Dukhyn Kim, Gordon L. and Stuber, "Clipping Noise Mitigation for OFDM by Decision-Aided Reconstruction," *IEEE Transactions on Communications Letter,* vol. 3, pp. 4–6, Jan 1999.

[46] H. Saedi, M. Sharif, and F. Marvasti, "Clipping noise cancellation in OFDM systems using oversample signal reconstruction," *IEEE Transactions on Communications Letter*, Vol. 6, pp.73-75, Feb. 2002.

[47] Hideo Kobayashi, Kazuo Mori and Tomataka Nagaosa, "Clipping Noise Mitigation Method for OFDM Transmission Technique," *IEICE Technical Report*, RCS2002-102, pp. 73–78, July 2002.

[48] H. Ochiai and H. Imai, "Performance analysis of deliberately clipped OFDM signals," *IEEE Transactions on Communications*, vol. 50, pp. 89-101, Jan. 2002.

[49] H. Chen and M. Haimovish, "Iterative Estimation and Cancellation of Clipping Noise for OFDM Signals," *IEEE Transactions on Communications Letter*, vol. 7, no. 7, pp. 305–07, July 2003.

[50] Kwangjae Lim, Kunseok Kang and Sooyoung Kim, "Adaptive MC-CDMA for IP-based broadband mobile satellite systems," *Proceedings of IEEE Vehicular Technology Conf. (VTC'03)*, vol.4, pp2731 - 2735, Oct. 2003.

[51] Kang K., Kim S., Ahn D. and Lee H.J., "Efficient PAPR reduction scheme for satellite MC-CDMA systems," *Proceedings of IEE on Communications*, vol.152, no. 5, pp697-703, Oct. 2005.

[52] Fernando W.A.C. and Rajatheva R.M.A.P., "Performance of COFDM for LEO satellite channels in global mobile communications," *Proceedings of IEEE Vehicular Technology Conferrence (VTC'98)*, vol.2, pp1503-1507, May 1998.

[53] H. Ochiai and H. Imai, "On the Distribution of the Peak–to–Average Power Ratio in OFDM Signals," *IEEE Transactions on Communications*, vol. 49, no. 2, pp. 282–89, February 2001.

[54] S. Wei, D. L. Goeckel, and P. E. Kelly, "A Modern Extreme Value Theory Approach to Calculating the Distribution of the PAPR in OFDM Systems," *Proceedingof IEEE ICC* 2002, New York, NY, May 2002, pp. 1686–90.

[55] M. Sharif, M. Gharavi-Alkhansari, and B. H. Khalaj, "On the Peak-to-Average Power of OFDM Signals Based on Oversampling," *IEEE Transactions on Communications*, vol. 51, no. 1, January 2003, pp. 72–78.

[56] G. Wunder and H. Boche, "Upper Bounds on the Statistical Distribution of the Crest-Factor in OFDM Transmission," *IEEE Transactions on Information Theory*, vol. 49, no. 2, Feb. 2003, pp. 488–94.

[57] Van Nee, R.; de Wild, A.; "Reducing The Peak-To-Average Power Ratio of OFDM", Vehicular Technology Conference, 1998. *Proceedings of IEEE Vehicular Technology Conference (VTC'98)*, Vol:3, 18-21 May 1998, pp. 2072-2076.

[58] Farserotu J. and Prasad R., "A survey of future broadband multimedia satellite systems, issues and trends," *IEEE Communications Magazine*, Vol.38, Jun 2000, pp.128-133.

[59] Conforto P., Tocci C., Losquadro G., Sheriff R.E., Chan P.M.L. and Fun Hu Y., "Ubiquitous Internet in An Integrated Satellite-Terrestrial Environment: the SUITED Solution," *IEEE Communications Magazine*, Vol. 40, Jan. 2002, pp.98-107.

[60] Del Re E. and Pierucci L., "Next-generation mobile satellite networks," *IEEE Communications Magazine*, vol. 40, Sept. 2002, pp. 150–159.

[61] Ibnkahla M., Rahman Q. M., Sulyman A. I., Al-asady H. A., Jun Yuan, and Safwat A., " High-Speed Satellite Mobile Communications: Technologies and Challenges," *Proceedings of IEEE*, Vol. 92, No. 2, Feb 2004, pp.312-339.

[62] Evans B., Werner M., Lutz E., Bousquet M., Corazza G.E., Maral G. and Rumeau, R., "Integration of Satellite and Terrestrial Systems in Future Multimedia Communications," *IEEE Transactions on Communications*, Vol. 12, Oct 2005, pp.72-80.

[63] Gouta M.D., Kouris S.S. and Kosmopoulos S.A., "Analytical Expression for the Performance Bounds of 16-QAM Signaling in Non-Gaussian Products Environment," *Proceedings of IEE Radar and Signal Processing*, Vol.135, Jun 1988, pp.265-271.

[64] X.Li and L. J. Cimini, "Effect of clipping and filtering on the performance of OFDMA," *IEEE Commun. Lett.*, vol. 2, no. 5, pp, 131-133, May 1998.

[65] H. G. Ryu, J. E. Lee and J.S. Park, "Dummy Sequence Insertion (DSI) for PAPR Reduction in the OFDM Communication System," *IEEE Transactions on Consumer Electronics,* Vol. 50, No. 1, Feb 2004.

[66] C. Tellambura, "Computation of the continuous-time PAR of an OFDM signal with BPSK subcarriers," *IEEE Trans. on Comm., Lett.* Vol. 5, no. 5, pp185-187, May 2001.

[67] A. D. S. Jayalath, C. Tellambura and H. Wu, "Reduced complexity PTS and new phase sequences for SLM toreduce PAP of an OFDM signal", *IEEE Proc. Vehicular Technology Conference*, pp.1914-1917, 2007.

[68] P.Boonsrimuang, K.Naito, K.Mori, T.Paungma and H.Kobayashi, "Proposal of Clipping and Inter-Modulation Method for OFDM Signal in Non-linear Channel",IEICE Transation on Communication Theory, E88-B(2), pp.427-435, 2005.

[69] P.Boonsrimuang, K.Mori, T.Paungma and H.Kobayashi, "Proposal of Improved PTS Method for OFDM Siganl", The 18th IEEE (PIMRC'07) 2007.

[70] "Universal mobile telecommunications system (UMTS): UMTS terrestrial radio access (UTRA); Concept evaluation," Tech.Rep.,ETSI, TR 101 146, 1997.